CONTROL SYSTEM DESIGN FOR ROBUST STABILITY AND ROBUST PERFORMANCE

Thesis submitted for the degree of
Doctor of Philosophy
at the University of Leicester

by

Jong-Lick Lin, MSc, BSc (Taiwan)
Department of Engineering
University of Leicester

May 1992

Control System Design for
Robust Stability and Robust Performance

by

Jong-Lick Lin

Declaration of Originality:

This thesis is submitted in fulfilment of the requirements for the degree of Doctor of Philosophy in the Department of Engineering, the University of Leicester, U.K. All work recorded in this thesis is original unless otherwise acknowledged in the text or by references. No part of it has been submitted for any other degree, either to the University of Leicester or to any other university.

Jong-Lick Lin

Jong-Lick Lin (林鐘獎)
May 1992

To

my wife Mei-Fei

and

Pei-Hui, Ting-Chieh, Ming-Wei

CONTROL SYSTEM DESIGN FOR ROBUST STABILITY AND ROBUST PERFORMANCE

ABSTRACT

A central problem in control system design is how to design a controller to guarantee that the closed-loop system is robustly stable and that performance requirements are satisfied despite the presence of model uncertainties and exogenous disturbance signals. The analysis problem, that is the assessment of control systems with respect to robust stability and robust performance, can be adequately solved using the structured singular value μ as introduced by Doyle. The corresponding design problem (how to choose a controller K to minimize μ) is still largely unsolved, but an approximate solution can be found using Doyle's $D-K$ iteration. In this thesis we present an alternative algorithm, called $\mu - K$ iteration, which works by flattening the structured singular value μ over frequency. As a prelude to this a classical loop shaping approach to robust performance is presented for $SISO$ systems, and is also based on flattening μ.

In μ-synthesis it is often the case that real uncertainties are modelled as complex perturbations but the conservatism so introduced can be severe. On the other hand, if real uncertainties are modelled as real perturbations then $D-K$ iteration is not relevant. It is shown that $\mu - K$ iteration still works for real perturbations. In addition, a geometric approach for computing the structured singular value for a scalar problem with respect to real and/or complex uncertainty is described. This provides insight into the relationship between real μ and complex μ.

A robust performance problem is considered for a 2-input 2-output high purity distillation column which is an ill-conditioned plant. Analysis reveals the potentially damaging effects on robustness of ill-conditioning. A design is carried out using $\mu - K$ iteration and the "optimum" μ compared with that obtained by Doyle and by Freudenberg for the same problem.

ACKNOWLEDGEMENTS

Firstly, I would like to express my deepest gratitude to Professor Ian Postlethwaite, my supervisor, for his guidance and encouragement throughout the course of this research. His thorough reading of this thesis, his constructive suggestions for its improvement and his patience and concern are gratefully acknowledged.

I would also like to thank Dr. Da-Wei Gu for many helpful discussion over the past two years. I have also benefited greatly from many conversations in our research group. Especially, I am grateful to E.J.M. Geddes and J.F. Whidborne for their help in overcoming problems I faced in using the computer facility.

I gratefully acknowledge financial support from the National Cheng-Kung University and the National Science Council, Taiwan, the Republic of China, and from the committee of Vice-Chancellors and Principals of the Universities of the United Kingdom for an Overseas Research Student Award.

Finally, I would like to express my gratitude to my wife, Mei-Fei, for her love and encouragement throughout the years of my research.

Contents

List of Figures

Chapter 1

INTRODUCTION

1.1 Motivation

Feedback control mechanisms have been used for millenia, and are crucially important to reduce the effects of plant uncertainties and to attenuate system response to external disturbances. Plant uncertainty is always present since no mathematical system can exactly model a physical system. Actual systems will suffer from parameter variations affecting low frequency behaviour and unmodelled dynamics at high frequencies. And if the feedback is badly designed these modelling errors might adversely affect the stability and performance of a control system. In addition to plant uncertainties, the performance of a closed-loop system can also be compromised by exogenous disturbances acting on the system. Typically these disturbances are caused by environmental effects. Disturbances result in regulation and tracking error, and performance can degrade to the point of unacceptability. Therefore, in control engineering a central problem is to design a control system which remains stable and maintains at least minimum performance levels despite the presence of model uncertainties and disturbance signals. Performance levels concern such important objectives as command following, disturbance rejection, noise attenuation, sensitivity reduction, etc. Yet this generic design problem is still largely unsolved. The *RSRP* problem, as we shall call it, is to design an optimal controller $K(s)$ for robust stability (RS) and robust performance (RP).

1.2 Related Work

It is well known that for a plant with structured uncertainty, the singular value approach for robust stability analysis can sometimes give conservative results. To remedy this conservatism, in 1982, Doyle proposed and developed the concept of the structured singular value (SSV) which is a less conservative indicator of stability robustness [Doy82]. A major advantage arising from this work was that robust $\mathcal{H}^\infty$ performance tests could be expressed as a robust stability test in the presence of a fictitious perturbation representing performance uncertainty. A general framework for analyzing robust performance using the structured singular value μ as a measure of performance was introduced by Doyle who proposed a controller synthesis procedure, called μ-synthesis [Doy85]. In this procedure a controller is sought which minimizes μ, or which achieves levels of performance arbitrarily close to the optimum μ by $D-K$ iteration. The $D-K$ iteration algorithm is applicable for a plant with complex uncertainties; it can, however, give arbitrarily conservative results when the uncertainties are real. From an engineering point of view, real parameter variations (called parametric uncertainties) of a plant, which can be caused by movement of the operating point at low frequencies, are a common occurrence. In this thesis, we present an alternative algorithm to $D-K$ iteration, called $\mu-K$ iteration, which can also be applied to real uncertainty without introducing conservatism.

A major theme in this thesis is the use of loop shaping in control system design. Related work in this area can be found in [McG90] [OrL91] [Fre90] [StD88]. In [McG90] the open-loop singular values are first shaped by a pre and/or post compensator to correspond to good performance and robust stability. The loop is closed through a robustly stabilization controller which, if satisfactory, will not change the open-loop singular values significantly. In [OrL91], a classical loop shaping methodology is applied to individual channels of a multivariable system. In [Fre90], a loop shaping technique is used to minimize the structured singular value, μ, for robust performance. In [StD88], the general idea of loop shaping approach to open-loop singular values is discussed. In this thesis we present a new loop shaping approach for minimizing the robustness performance measure μ.

Many authors have worked on the computation of μ, [FaT88] [FTD91] [PFD88] [PaD88] [Hel88]. In this thesis we also give some consideration to this important problem in the particular case of a mixture of real and complex uncertainty blocks.

1.3 Contribution and Organization

The main contributions of this work are considered to be:

- A relationship between a mixed sensitivity $\mathcal{H}^\infty$-optimization problem and classical loop shaping is investigated for $SISO$ systems. This then provides insight into a further development of loop shaping to minimize the structured singular value for robust performance. This work has been published in [PLG91a].

- A new algorithm is developed, called $\mu - K$ iteration, which can be used to design a μ-optimal controller for the $RSRP$ problem when the plant has structured real and/or complex uncertainties. The technique assumes availability of an algorithm for computing μ for a given controller. This work has been accepted for publication in the forthcoming Special Issue of Automatica on Robust Control [LPG91].

- By analyzing an ill-conditioned plant, namely a 2-input 2-output high purity distillation column with a particular structure of controller, we reveal that at low frequencies robust performance is concerned only with the low plant gain (smallest singular value) whereas at high frequencies robust stability is determined only by the high plant gain (largest singular value). In the intermediate frequency range, both the low and high plant gains are coupled and become significant in determining the robustness measure μ. The $\mu - K$ iteration algorithm is applied to the distillation column example and compared with the results of other methods. Some of this work was reported at the 30th IEEE Conference on Decision and Control, Brighton, 1991 [PLG91b].

- For a simple situation (namely one real parameter uncertainty and one complex fictitious perturbation representing performance uncertainty), the circle-invariant property of bilinear maps (linear fractional transformations) is used to derive the structured singular value. From the derivation the relationship between real-μ and complex-μ is more clearly understood.

The thesis is organized into eight chapters which can be summarized as follows:

Chapter 2: Signals and Systems

In this chapter we review the basic concepts concerning signals and systems, concepts on which a theory of robust control can be developed. We introduce appropriate norms for measuring the size of signals and systems. The singular value decomposition, which plays a key role in robustness analysis, is covered in detail. The well-posedness of a system, $BIBO$ stability and internal stability are all defined. A statement of the small gain theorem is given because of its central importance in the derivation of many stability tests using singular values. It is useful because it does not need detailed information about the system and its uncertainties.

Chapter 3: Uncertainties and Robustness

In this chapter we first introduce a linear fractional transformation which can be used to represent all uncertainty models by means of the $(G, \hat{\Delta})$ format illustrated in Figure 1.1. If all the uncertainties occur in different parts of the system and they are lumped into a single uncertainty, then this is the so called unstructured uncertainty. Otherwise, it is said to be structured uncertainty. Some robust stability tests are given for unstructured uncertainty. Two examples are given to illustrate that the singular value approach for robust stability analysis can sometimes give conservative results. To remedy this conservatism, Doyle's structured singular value (SSV) can be used to measure robustness. Some properties of μ and Osborne's method for μ-computation are presented in this chapter.

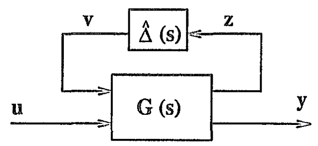

Figure 1.1: $(G, \hat{\Delta})$ format of a perturbed plant.

In reality, all parametric uncertainties in physical systems are structured. The SSV can be used to characterize robust performance as well as robust stability. For structured uncertainties, according to the performance robustness theorem, robust performance is assured if and only if stability robustness is achieved with a fictitious complex-disk-bounded uncertainty introduced to characterize the performance requirements. Doyle's $D-K$ iteration algorithm which can be used to find a controller K to minimize the SSV is reviewed in this chapter.

An example is given to illustrate that a system which is robust with respect to individual uncertainties can be destabilized by small simultaneous uncertainties. Finally, for the disturbance rejection problem (minimum sensitivity problem) it is shown that multiplicative input uncertainty of the plant causes more robust performance problems than multiplicative output uncertainty when either the plant or the controller is ill-conditioned.

Chapter 4: A Loop Shaping Approach to Robust Performance for SISO Systems

This chapter presents a procedure for solving a robust performance problem for $SISO$ systems using a loop shaping technique which has been published in [PLG91a]. Firstly the relationship between a mixed sensitivity $\mathcal{H}^{\infty}$-optimization problem and classical loop shaping is investigated. It is shown how classical loop shaping can be used to minimize the $\mathcal{H}^{\infty}$ cost function. This then provides insight into a further development of loop shaping to minimize the structured singular value for robust performance. The approach is demonstrated by its application to the control of a robot arm whose moment of inertia varies considerably with angle.

Chapter 5: $\mu-K$ Iteration: A New Algorithm for μ-Synthesis

In this chapter we present an alternative algorithm to $D-K$ iteration for solving robust performance problems by μ-synthesis. Convergence properties of the new algorithm are considered and demonstrated by examples. The algorithm, called $\mu-K$ iteration, works by flattening the structured singular value μ over frequency. Two examples are given to illustrate the method.

Chapter 6: Robust Control of a Distillation Column

The purpose of this chapter is to give insight into the problems associated with the control of ill-conditioned plants, and to illustrate the usefulness of μ-synthesis by $\mu - K$ iteration. As in [SMD88] we focus on the control of a high purity distillation column, and use the same linear plant model given by Skogestad et al. (1988).

By analyzing a particular controller structure and design strategy, the potentially damaging effects of an ill-conditioned plant on robust stability and robust performance are revealed. The structured singular value μ, used to measure robustness, is shown to be determined at high frequencies by high plant gain (largest singular value) and at low frequencies by low plant gain (smallest singular value). This is as one might expect since small loop gain is typically required at high frequencies for robust stability, while large loop gain is usually required at low frequencies for robust performance. In the intermediate frequency range both the low and high plant gains are significant in determining μ.

A μ-synthesis design is carried out for the distillation column using the $\mu - K$ iteration algorithm proposed by Lin et al. (1991). The design example addresses the same μ-optimal control problem considered by Skogestad et al. (1988) using the $D - K$ iteration algorithm, and by Freudenberg (1989) using a loop shaping method.

Chapter 7: μ-Optimal Controller Design for Real Uncertainty by $\mu - K$ Iteration

This chapter presents a geometric approach for calculating the structured singular value with respect to complex uncertainties or mixed real (parametric uncertainty) and complex (fictitious performance) uncertainties. With an algorithm for calculating μ, the μ-optimal controller can then be derived by $\mu - K$ iteration.

A robust performance problem is considered when the plant has one real parametric uncertainty and performance is characterized by a fictitious uncertainty which must be complex. The approach is demonstrated by its application to a $SISO$ example. The controller obtained is just a cascaded combination of a phase lead and a phase lag network, it is stable and has only 2 states compared with 2 for the nominal plant. Doyle's $D - K$ iteration algorithm is not appropriate in this case unless one models the real uncertainty to be a complex uncertainty and then the results are conservative. For the complex-μ controller and the real-μ controller (obtained by $\mu - K$ iteration), the curves of $\mu_{\mathcal{C}}(M)$ and $\mu_{\mathcal{R}}(M)$ are coincident in both the low and high frequency ranges. However they are quite different in the intermediate frequency range.

The circle-invariant property of a bilinear mapping (linear fractional transformation) is seen to be useful in deriving the SSV and reveals an interesting geometric relationship between complex-μ and real-μ.

Chapter 8: Conclusions and Further Work

This chapter contains concluding remarks and suggestions for further research.

1.4 Notation and Abbreviations

The following conventions will be adopted. The figures and equations are numbered consecutively within each chapter. The examples, lemmas, theorems and corollaries are numbered consecutively within each section. Thus, for example, Theorem 1 of Section 2.7 will be referred to as Theorem 2.7-1.

Notation

$a \in S$	a is an element of set S; a belongs to S
$\exists a \in S$	there exists an element a of set S
$\forall a \in S$	for every element a of set S
ϕ	the empty set
$S_1 \cap S_2$	intersection of sets S_1 and S_2
$S_1 \cup S_2$	union of sets S_1 and S_2
$S_1 \subset S_2$	set S_1 is contained in set S_2
$p \Longrightarrow q$	p implies q
$p \Longleftarrow q$	q implies p
$p \Longleftrightarrow q$	p if and only if q; equivalently, p implies q and q implies p
$A := B$	A is equal to B by definition

$A =: B$	B is equal to A by definition
$a \,//\, b$	curve a is parallel to curve b
$a \ll b$	a is much less than b
$a \gg b$	a is much greater than b
$a \approx b$	a is approximately equal to b
$\forall$	for all
$\ni$	such that
$\mathcal{C}$	space of complex numbers
$\mathcal{R}$	space of real numbers
$\mathcal{C}^n$	space of complex n-vectors
$\mathcal{R}^n$	space of real n-vectors
$\mathcal{C}^{n\times m}$	space of $n \times m$ complex matrices
$\mathcal{R}^{n\times m}$	space of $n \times m$ real matrices
j	$\sqrt{-1}$; sometimes an index, as in x_{ij}
$\Re e(z)$	real part of complex number z
$\mathcal{I}_m(z)$	imaginary part of complex number z
$\bar{z}$	complex-conjugate of complex number z
$\|z\|$	modulus of complex number z
$\angle z$	argument of complex number z
I	identity matrix of unspecified dimension
I_n	$n \times n$ identity matrix
A^{-1}	inverse of the square matrix A
A^T	transpose of the matrix A
A^*	complex-conjugate transpose of the matrix A
$\|A\|$	nonnegative matrix; comprising the moduli of the entries of the matrix A
$A > 0$	matrix A is positive definite
$A \geq 0$	matrix A is semi-positive definite
A_{ij}	the (i,j) element of the matrix A
$\mathrm{diag}\,[x_1, x_2, \cdots]$	diagonal matrix with diagonal elements $x_1, x_2, \cdots$

$\det(A)$	determinant of the square matrix A
$\mathrm{tr}\,(A)$	trace of the square matrix A
$\mathrm{cond}\,(A)$	condition number of the matrix A
$\rho(A)$	spectral radius of the square matrix A
$\lambda_i(A)$	ith eigenvalue of the square matrix A
$\bar{\lambda}(A)$	maximum eigenvalue of the square matrix A
$\underline{\lambda}(A)$	minimum eigenvalue of the square matrix A
$\sigma_i(A)$	ith singular value of the matrix A
$\bar{\sigma}(A)$	maximum singular value of the matrix A
$\underline{\sigma}(A)$	minimum singular value of the matrix A
$\mu_{\mathbf{\Delta}}(M)$	structured singular value of the matrix M with respect to $\mathbf{\Delta}$
$\mathbf{\Delta}$	set of possible block diagonal perturbations
$\mathbf{B\Delta}$	$:= \{\Delta : \bar{\sigma}(\Delta) \leq 1, \ \ \Delta \in \mathbf{\Delta}\}$
$\mathbf{U}$	$:= \{U : \ U = \mathrm{diag}\,[U_1, U_2, \cdots, U_n]\,, \ U_i^* U_i = I, \ U \in \mathbf{\Delta}\}$
$\mathbf{D}$	set of block diagonal scaling matrices conformed with $\mathbf{\Delta}$
$\Vert M \Vert_\mu$	$:= \sup_{\omega \in \mathcal{R}} \mu_{\mathbf{\Delta}}\,[M(j\omega)]$
Δ	model uncertainty
Δ_p	fictitious performance uncertainty
$\tilde{\Delta}$	$:= \mathrm{diag}\,\{\Delta, \Delta_p\}$, augmented block diagonal uncertainty
$\mu_{\mathcal{C}}(M)$	structured singular value of the matrix M with respect to the complex modelling and fictitious performance uncertainties
$\mu_{\mathcal{R}}(M)$	structured singular value of the matrix M with respect to the real parametric modelling uncertainty and complex fictitious performance uncertainty
ess sup	essential supremum
sup	supremum, i.e. least upper bound (*l.u.b.*)
inf	infimum, i.e. greatest lower bound (*g.l.b.*)
max	maximum
min	minimum
$\arg\inf_x F(x)$	that value of x which minimizes $F(x)$

$\mathcal{L}[g(t)]$	Laplace transform of $g(t)$
$\mathcal{F}[g(t)]$	Fourier transform of $g(t)$
$\mathcal{F}^{-1}[G(j\omega)]$	inverse Fourier transform of $G(j\omega)$
$g \overset{\mathcal{F}}{\longmapsto} G$	$G(j\omega) := \mathcal{F}[g(t)]$
$\|x\|$	norm of the vector x
$\|x\|_p$	p-norm of the vector x, $1 \le p < \infty$
$\|x\|_\infty$	∞-norm of the vector x
$L^p(\mathcal{R})$	set of measurable functions whose pth powers are absolutely integrable over $\mathcal{R}$
$L^\infty(\mathcal{R})$	set of essentially bounded measurable functions
$T : A \longrightarrow B$	T is an operator (or a function) mapping from A to B
$\|T\|$	norm of the operator T
$\|T\|_i$	induced norm of the operator T
$\|T\|_{i1}$	induced 1-norm of the operator T
$\|T\|_{i2}$	induced 2-norm of the operator T
$\|T\|_{i\infty}$	induced ∞-norm of the operator T
$\|M\|_F$	Frobenius norm of the matrix M
$\|G\|_\infty$	$:= \sup_{\omega\in\mathcal{R}} \bar{\sigma}\,[G(j\omega)] = \|T\|_{i2}$, the ∞-norm of the transfer function matrix $G(s)$ of the system operator T
$\mathcal{H}^\infty$	set of stable matrix-valued functions $G(s)$ with $\|G\|_\infty < \infty$
$\mathcal{RH}^\infty$	set of real-rational functions in $\mathcal{H}^\infty$
$\mathbf{B}\mathcal{RH}^\infty$	$:= \{\Delta(s) :\ \Delta \in \mathcal{RH}^\infty,\ \Delta(s_0) \in \mathbf{B}\boldsymbol{\Delta},\ \forall s_0 \ni \Re e(s_0) \ge 0\}$
$F_l(M, \Delta)$	lower linear fractional transformation on M by Δ
$F_u(M, \Delta)$	upper linear fractional transformation on M by Δ
$\dot{x}(t)$	$:= \frac{dx(t)}{dt}$
$\frac{\mathrm{d}}{\mathrm{d}r}$	the differentiation with respect to r
$\mathrm{dist}\,(P, Q)$	distance between points P and Q
$K_\infty(s)$	$\mathcal{H}^\infty$-optimal controller
$K_\mu(s)$	μ-optimal controller

Abbreviations

cltf	closed-loop transfer function
e.g.	for example
i.e.	that is
oltf	open-loop transfer function
resp.	respectively
r.m.s.	root-mean-square
BIBO	Bounded-Input Bounded-Output
CRHP	Closed Right-Half Plane
CRM	Causality Recovery Methodology
FDLTI	Finite-Dimensional, Linear and Time-Invariant
I/O	Input-Output
LFT	Linear Fractional Transformation
LHP	Left-Half Plane
LLFT	Lower Linear Fractional Transformation
MIMO	Multi-Input Multi-Output
NP	Nominal Performance
NS	Nominal Stability
PID	Proportional plus Integral plus Derivative
PM	Phase Margin
RHP	Right-Half Plane
RP	Robust Performance
RS	Robust Stability
RSRP	Robust Stability and Robust Performance
SCC	Standard Compensation Configuration
SISO	Single-Input Single-Output
SSV	Structured Singular Value
SVD	Singular Value Decomposition
ULFT	Upper Linear Fractional Transformation

Chapter 2

SIGNALS AND SYSTEMS

2.1 Introduction

In this chapter we review the basic concepts concerning signals and systems on which a theory of robust control can be developed. From a system analysis point of view a control system is a closed-loop system which interacts with its environment through command signals, disturbance signals and noise signals. Tracking error signals and actuator driving signals are also important in control system design. It is essential for analysis and design that we have appropriate measures for the size of these signals. These are given by suitably defined norms. From these signal norms, we can define induced norms to measure the "gain" of linear operators representing systems.

In Section 2.2, we introduce several norms for vectors and signals. Based on these some useful operator norms are given in Section 2.3 which generalize the scalar idea of system gain. The singular value decomposition, which plays a key role in robustness analysis, is covered in Section 2.4. In Section 2.5 well posedness is discussed since not all interconnections of subsystems are well-defined. What we mean by stability ($BIBO$ and internal) is defined in Section 2.6, while important stability tests are given in Section 2.7.

2.2 Norms for Vectors and Signals

Let X be a linear space over the field F (typically, F is the field of real numbers $\mathcal{R}$, or complex numbers $\mathcal{C}$). Then a function

$$\|\circ\| : X \longrightarrow \mathcal{R}$$

that maps X into the real numbers $\mathcal{R}$ is a norm on X *iff*

$$(1) \quad \|x\| \geq 0, \quad \forall x \in X \quad \text{(nonnegativity)} \tag{2.1}$$

$$(2) \quad \|x\| = 0 \Longleftrightarrow x = 0 \quad \text{(positive-definiteness)} \tag{2.2}$$

$$(3) \quad \|\lambda x\| = |\lambda| \cdot \|x\|, \ \forall \lambda \in F, \forall x \in X \text{(homogeneity with respect to } \lambda\text{)} \tag{2.3}$$

$$(4) \quad \|x + y\| \leq \|x\| + \|y\|, \quad \forall x, y \in X \text{ (triangle inequality)} \tag{2.4}$$

Given a linear space X there might be many possible norms on X. For a given norm $\|\circ\|$ on X, the pair $(X, \|\circ\|)$ is called a normed space.

Norms of Vectors in $\mathcal{C}^m$: Let the linear space X be $\mathcal{C}^m$. More precisely, $x \in \mathcal{C}^m$ means that $x = [x_1, x_2, \cdots, x_m]^T$ with $x_i \in \mathcal{C}$, where superscript T denotes the transpose of a vector. Then the p-norm of a vector x is defined by

$$\textbf{1-norm.} \quad \|x\|_1 := \sum_{i=1}^{m} |x_i|, \qquad \text{for } p = 1 \tag{2.5}$$

$$p\textbf{-norm.} \quad \|x\|_p := \left(\sum_{i=1}^{m} |x_i|^p \right)^{1/p}, \quad \text{for } 1 < p < \infty \tag{2.6}$$

$$\infty\textbf{-norm.} \quad \|x\|_\infty := \max_{1 \leq i \leq m} |x_i|, \qquad \text{for } p = \infty \tag{2.7}$$

where $\|x\|_2$ is the familiar Euclidean norm.

Norms of Signals: Let the linear space X be continuous or piecewise continuous time scalar-valued signals $x(t)$, $t \in \mathcal{R}$. The p-norm of a signal x is defined by

$$\textbf{1-norm.} \quad \|x\|_1 := \int_{-\infty}^{\infty} |x(t)| \, dt, \qquad \text{for } p = 1 \tag{2.8}$$

$$p\textbf{-norm.} \quad \|x\|_p := \left(\int_{-\infty}^{\infty} |x(t)|^p \, dt \right)^{1/p}, \quad \text{for } 1 < p < \infty \tag{2.9}$$

$$\infty\textbf{-norm.} \quad \|x\|_\infty := \operatorname*{ess\,sup}_{t \in \mathcal{R}} |x(t)|, \qquad \text{for } p = \infty \tag{2.10}$$

where

$$\operatorname*{ess\,sup}_{t\in\mathcal{R}} |x(t)| := \inf\{a \in \mathcal{R} : \nu\left[\{t : |x(t)| > a\}\right] = 0\} \tag{2.11}$$

and $\nu[A]$ denotes the Lebesgue measure of set A. The corresponding normed spaces are called, respectively, $L^1(\mathcal{R})$, $L^p(\mathcal{R})$ and $L^\infty(\mathcal{R})$. More precisely, let $x(t)$ be a function on $(-\infty, \infty)$ of the signal spaces, then

$$L^1(\mathcal{R}) := \left\{ x(t) : \|x\|_1 = \int_{-\infty}^{\infty} |x(t)| dt < \infty, \text{ convolution kernel} \right\} \tag{2.12}$$

$$L^2(\mathcal{R}) := \left\{ x(t) : \|x\|_2 = \left(\int_{-\infty}^{\infty} |x(t)|^2 dt \right)^{\frac{1}{2}} < \infty, \text{ finite energy} \right\} \tag{2.13}$$

$$L^\infty(\mathcal{R}) := \left\{ x(t) : \|x\|_\infty = \operatorname*{ess\,sup}_{t\in\mathcal{R}} |x(t)| < \infty, \text{ bounded signal} \right\} \tag{2.14}$$

From a signal point of view the 1-norm, $\|x\|_1$, of the signal $x(t)$ is the integral of its absolute value. The square $\|x\|_2^2$ of the 2-norm is often called the energy of the signal $x(t)$ since that is what it is when $x(t)$ is the current through a $1-\Omega$ resistor. Finally the ∞-norm, $\|x\|_\infty$ is its amplitude or peak value.

Remark: Let X be a linear space of continuous or piecewise continuous *vector-valued* functions of the form $x(t) = [x_1(t), x_2(t), \cdots, x_m(t)]^T$, $t \in \mathcal{R}$, then

$$L^p_m(\mathcal{R}) := \left\{ x(t) : \|x\|_p = \left(\int_{-\infty}^{\infty} \|x(t)\|_p^p dt \right)^{\frac{1}{p}} < \infty, \text{ for } 1 \le p < \infty \right\} \tag{2.15}$$

$$L^\infty_m(\mathcal{R}) := \left\{ x(t) : \|x\|_\infty = \operatorname*{ess\,sup}_{t\in\mathcal{R}} \|x(t)\|_\infty < \infty \right\} \tag{2.16}$$

Power Signals: Some signals are useful for stochastic control system analysis. For example, the sinusoidal signal, $x(t) = A\sin(\omega t + \phi)$, $t \in \mathcal{R}$, is not a 2-norm signal. However the average power of $x(t)$

$$\lim_{T\to\infty} \frac{1}{2T} \int_{-T}^{T} x(t)^2 dt \tag{2.17}$$

exists. The signal $x(t)$ will be called a power signal if the above limit exists. The square root of expression (2.17) is well-known as the r.m.s. (root-mean-square) value of $x(t)$. Unfortunately a nonzero signal can have zero average power, so expression (2.17) is not a norm. It does, however, have all the properties of a norm, except property (2).

2.3 Norms for Linear Operators and Systems

We next turn to a discussion of the gain of a system, which is mathematically defined as the norm of an operator. Figure 2.1 illustrates an input-output mapping system. The system operator T maps the input signal $x(t)$ into the output signal $y(t)$, where $x \in (X, \|\circ\|_X)$, $y \in (Y, \|\circ\|_Y)$. Suppose that T is a linear and bounded map

$$T : (X, \|\circ\|_X) \longrightarrow (Y, \|\circ\|_Y) \tag{2.18}$$

Then the norm, maximum system gain, of the operator T is defined as

$$\|T\| := \sup_{x \neq 0} \frac{\|Tx\|_Y}{\|x\|_X} \tag{2.19}$$

Obviously

$$\|Tx\|_Y \leq \|T\| \cdot \|x\|_X \tag{2.20}$$

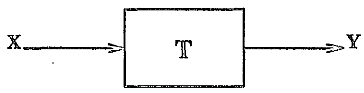

Figure 2.1: Input-output mapping system.

Facts:

- Definition (2.19) is equivalent to

$$\|T\| = \sup_{\|x\|_X = 1} \|Tx\|_Y = \sup_{\|x\|_X \leq 1} \|Tx\|_Y \tag{2.21}$$

- $\|T\|$ is called the induced norm of the linear map T or operator norm induced by the vector norms $\|\circ\|_X$ and $\|\circ\|_Y$.

- An operator T is called linear, if for any x_1, $x_2 \in X$ and any scalar $\alpha \in F$,

$$T(x_1 + x_2) = Tx_1 + Tx_2 \tag{2.22}$$

$$T(\alpha x) = \alpha \cdot Tx \tag{2.23}$$

that is, T is additive and homogeneous.

- An operator T is called bounded, if for any $x \in X$, there exists a finite constant M such that

$$\|Tx\|_Y \leq M \cdot \|x\|_X \tag{2.24}$$

It is obvious that $\|T\| \leq M$ by (2.19).

- If T_1 and T_2 are two linear bounded operators, then

$$\|T_1T_2x\| = \|T_1(T_2x)\| \leq \|T_1\| \cdot \|T_2x\| \leq \|T_1\| \cdot \|T_2\| \cdot \|x\| \tag{2.25}$$

implies

$$\|T_1T_2\| \leq \|T_1\| \cdot \|T_2\| \tag{2.26}$$

Linear operators can be represented by matrices with respect to a specific basis, so that (2.19) may be used to define the norms of matrices. Consider the $n \times m$ complex-valued matrix M as a linear map from $X := \mathcal{C}^m$ to $Y := \mathcal{C}^n$ defined by $y = Mx$. Then depending on the norms defined on X and Y, we obtain different matrix norms [LaT85] for $M \in \mathcal{C}^{n\times m}$.

Norms of Matrices:

1. If the 1-norm is defined on both X and Y, then

$$\|M\|_1 = \max_{1\leq j\leq m} \sum_{i=1}^{n} |m_{ij}|, \qquad \text{(column sums)} \tag{2.27}$$

2. If the 2-norm is defined on both X and Y, then

$$\|M\|_2 = \max_{1\leq i\leq m} [\lambda_i(M^*M)]^{\frac{1}{2}} \tag{2.28}$$

Where $\lambda_i(A)$ denotes the ith eigenvalue of matrix A and the superscript $*$ is the complex-conjugate transpose. This matrix norm induced by the Euclidean vector norm is known as the spectral norm, and it is probably the most widely used norm in matrix analysis.

3. If the ∞-norm is defined on both X and Y, then

$$\|M\|_\infty = \max_{1\leq i\leq n} \sum_{j=1}^{m} |m_{ij}|, \qquad \text{(row sums)} \tag{2.29}$$

4. The Frobenius norm $\|\circ\|_F$ defined as

$$\|M\|_F := \left(\sum_{i=1}^{n}\sum_{j=1}^{m}|m_{ij}|^2\right)^{\frac{1}{2}} = [\mathrm{tr}\,(M^*M)]^{\frac{1}{2}} \tag{2.30}$$

is not an induced norm, but it is compatible with $\|M\|_2$:

$$\frac{1}{\sqrt{n}}\|M\|_F \le \|M\|_2 \le \|M\|_F, \qquad \text{for } n = m \tag{2.31}$$

with $\mathrm{tr}\,(A)$ denoting the trace of matrix A.

Next we will introduce two norms of a causal and $FDLTI$ system, induced by the ∞-norm and 2-norm respectively.

Norms of Linear Systems: In the time-domain an input-output model for a $SISO$ convolution system with impulse response $g(t)$ can be represented as

$$\begin{aligned} y(t) &= \int_{-\infty}^{\infty} g(t-\tau)x(\tau)\,d\tau, \quad t \in \mathcal{R} \\ &=: (Tx)(t) \end{aligned} \tag{2.32}$$

Let the frequency response function $G(j\omega)$ denote the Fourier transform of $g(t)$ (i.e. $G(j\omega) = \mathcal{F}[g(t)]$). Then the norms of a $SISO$ system induced by the signal spaces of ∞-norm and 2-norm are given by the following theorems [DeV75].

Theorem 2.3-1(SISO systems): If the input and output signal spaces are measured with ∞-norm, then $\|T\|_{i\infty}$, the induced norm of the linear map $T : L^\infty(\mathcal{R}) \longrightarrow L^\infty(\mathcal{R})$ is given by

$$\|T\|_{i\infty} = \|g\|_1 = \int_{-\infty}^{\infty} |g(\tau)|\,d\tau \tag{2.33}$$

$\square$

Theorem 2.3-2 (SISO systems): If the input and output signal spaces are measured with 2-norm, and assuming $g \in L^1(\mathcal{R})$, then $\|T\|_{i2}$, the induced norm of the linear map $T : L^2(\mathcal{R}) \longrightarrow L^2(\mathcal{R})$ is given by

$$\|T\|_{i2} = \|G\|_\infty = \sup_{\omega\in\mathcal{R}} |G(j\omega)| \tag{2.34}$$

$\square$

Remark: The impulse response $g(t)$ of a *FDLTI* system should belong to $L^1(\mathcal{R})$ to guarantee the existence of its Fourier transform $G(j\omega)$. Let $g \xrightarrow{\mathcal{F}} G$ denote the Fourier transform $G(j\omega)$ of $g(t)$, which is defined as

$$G(j\omega) = \mathcal{F}[g(t)] := \int_{-\infty}^{\infty} g(t)e^{-j\omega t}dt \tag{2.35}$$

then [DeV75]

$$(a) \quad L^1 \xrightarrow{\mathcal{F}} L^\infty \tag{2.36}$$

$$(b) \quad L^2 \xrightarrow{\mathcal{F}} L^2 \qquad \text{(convergence with respect to } L^2\text{-norm)} \tag{2.37}$$

$$(c) \quad \int_{-\infty}^{\infty} f(t)g(t)dt = \frac{1}{2\pi}\int_{-\infty}^{\infty} F^*(j\omega)G(j\omega)d\omega \quad \text{(Parseval theorem)} \tag{2.38}$$

$$(d) \quad \|g\|_2 = \frac{1}{\sqrt{2\pi}}\|G\|_2 \tag{2.39}$$

Obviously, the definition of a Fourier transform leads to

$$|G(j\omega)| \leq \int_{-\infty}^{\infty} |g(t)| \cdot |e^{-j\omega t}|dt = \int_{-\infty}^{\infty} |g(t)|dt = \|g\|_1 \tag{2.40}$$

then

$$\|G\|_\infty = \sup_{\omega\in\mathcal{R}} |G(j\omega)| \leq \|g\|_1 \tag{2.41}$$

hence

$$\|G\|_\infty \leq \|g\|_1 \tag{2.42}$$

This means that $g \in L^1(\mathcal{R})$ can be used to guarantee the existence of $\|G\|_\infty$.

Furthermore, the norms of a *MIMO* system induced by the ∞-norm and 2-norm on the input and output vector-valued signal spaces are shown in the following theorems [DeV75].

Theorem 2.3-3 (MIMO systems): For the linear and time-invariant *MIMO* system T, $T : L_m^\infty(\mathcal{R}) \longrightarrow L_n^\infty(\mathcal{R})$, with impulse response matrix $g(t)$, the induced norm $\|T\|_{i\infty}$ is given by

$$\|T\|_{i\infty} = \max_{1\leq i\leq n} \sum_{j=1}^{m} \|g_{ij}\|_1, \qquad \text{(row sums)} \tag{2.43}$$

where g_{ij} is the (i, j) element of g. $\square$

Theorem 2.3-4 (MIMO systems): For the linear, time-invariant *MIMO* system T, $T : L_m^1(\mathcal{R}) \longrightarrow L_n^1(\mathcal{R})$, with impulse response matrix $g(t)$, the induced norm $\|T\|_{i1}$ is given by

$$\|T\|_{i1} = \max_{1 \le j \le m} \sum_{i=1}^{n} \|g_{ij}\|_1 \qquad \text{(column sums)}$$

□

Theorem 2.3-5 (MIMO systems): For the linear, time-invariant *MIMO* system T, $T : L_m^2(\mathcal{R}) \longrightarrow L_n^2(\mathcal{R})$, with impulse response matrix $g(t)$, $g_{ij}(\cdot) \in L^1(\mathcal{R})$, $1 \le i \le n$, $1 \le j \le m$, and corresponding frequency response matrix $G(j\omega)$, the induced norm $\|T\|_{i2}$ is given by

$$\|T\|_{i2} = \sup_{\omega \in \mathcal{R}} \|G(j\omega)\|_2 \tag{2.44}$$

□

The induced norm of an operator is equivalent to the maximum system gain which depends on the yardsticks used to measure the size of input and output signals. By definition the induced ∞-norm of the system represents the maximum peak gain. On the other hand, the induced 2-norm of the system describes the maximum energy gain. When the peak values of the signals in a control system are of interest, e.g. actuator input signals, the induced ∞-norm is relevant; this leads to L^1-optimization. In comparison the induced 2-norm which is concerned with energy gain leads to $\mathcal{H}^\infty$-optimization.

2.4 Singular Value Decomposition

The aspects of system specification: stability, performance and robustness are of crucial importance in control system design. By robustness is meant the ability to maintain some specified degree of stability and performance in the face of plant modelling errors and exogenous disturbances. The eigenvalues (characteristic gains) of a loop transfer function are directly related to feedback stability. However they do not give an adequate characterization of closed-loop performance. This is because the eigenvalues do not give a good description of the gain behaviour of a system operator, unless the eigenvectors form an orthonormal set. Consider a transfer function matrix

$$G(s) = \begin{bmatrix} 0 & 0 \\ \frac{1000}{s+10} & 0 \end{bmatrix} \tag{2.45}$$

Both eigenvalues are zero for all s, yet it obviously has a very large gain for certain inputs. Although not relevant to $SISO$ systems, directionality is very important in $MIMO$ systems in addition to frequency considerations.

A convenient way of representing a matrix that exposes its internal structure is known as the singular value decomposition (SVD) which is important in the robustness analysis of the feedback systems. For a matrix $M \in \mathcal{C}^{n \times m}$, the SVD is given by [Ste73] [AmH58]

$$M = U\Sigma V^* = \sum_{i=1}^{k} \sigma_i u_i v_i^*, \quad k := \min\{n, m\} \tag{2.46}$$

where U and V are unitary matrices with column vectors denoted by

$$U = [u_1, u_2, \cdots, u_n] \tag{2.47}$$

$$V = [v_1, v_2, \cdots, v_m] \tag{2.48}$$

and

$$\Sigma = \begin{bmatrix} \Sigma_0 \\ 0 \end{bmatrix}, \qquad n \geq m, \quad \text{or} \tag{2.49}$$

$$\Sigma = [\Sigma_0 \quad 0], \qquad n \leq m \tag{2.50}$$

where

$$\Sigma_0 = \text{diag}\{\sigma_1, \sigma_2, \cdots, \sigma_k\} \tag{2.51}$$

with

$$\bar{\sigma} := \sigma_1 \geq \sigma_2 \geq \cdots \geq \sigma_k =: \underline{\sigma} \geq 0 \tag{2.52}$$

By simple manipulation, (2.46) gives

$$M^*MV = V\Sigma^2 \tag{2.53}$$

and

$$MM^*U = U\Sigma^2 \tag{2.54}$$

It follows that the v_i and u_i are eigenvectors of M^*M and MM^*, respectively, with respect to the eigenvalue σ_i^2. $\{\sigma_i\}_{i=1}^k$ are known as the singular values (or principal gains) of M; $\{v_i\}_{i=1}^m$ and $\{u_i\}_{i=1}^n$ are, respectively, the right and left singular vectors of M.

Facts:

- $\max_{x\neq 0} \dfrac{\|Mx\|_2}{\|x\|_2} = \bar{\sigma}(M) = \|M\|_2$ (2.55)
- $\min_{x\neq 0} \dfrac{\|Mx\|_2}{\|x\|_2} = \underline{\sigma}(M)$ (2.56)
- $U^*U = UU^* = I \Longrightarrow \bar{\sigma}(UM) = \bar{\sigma}(M), \quad \bar{\sigma}(MU) = \bar{\sigma}(M)$ (2.57)
- $\max_{\|y\|_2=\|x\|_2=1} |y^*Mx| = \bar{\sigma}(M)$ (2.58)
- $\underline{\sigma}(M) \leq |\lambda_i(M)| \leq \bar{\sigma}(M)$ (2.59)
- $M \in \mathcal{C}^{n\times n} \Longrightarrow \prod_{i=1}^{n} |\lambda_i(M)| = \prod_{i=1}^{n} \sigma_i(M)$ (2.60)
- $MM^* = M^*M \Longrightarrow \sigma_i(M) = |\lambda_i(M)|$ (2.61)
- $\det(M) \neq 0 \Longrightarrow M^{-1} = V\Sigma^{-1}U^*, \text{ and } \bar{\sigma}(M^{-1}) = \dfrac{1}{\underline{\sigma}(M)}$ (2.62)
- $\|M\|_F^2 = \operatorname{tr}(M^*M) = \sum_{i=1}^{k} \sigma_i(M)^2$ (2.63)

Let $\bar{u} := u_1,\ \underline{u} := u_n,\ \bar{v} := v_1$, and $\underline{v} := v_m$, then it is clear that

$$M\bar{v} = \bar{\sigma}(M)\bar{u} \tag{2.64}$$

$$M\underline{v} = \underline{\sigma}(M)\underline{u} \tag{2.65}$$

From the system point of view, the vector $\bar{v}$ ($\underline{v}$) corresponds to the highest (lowest) gain input direction; and $\bar{u}$ ($\underline{u}$) corresponds to highest (lowest) gain output direction. For a $MIMO$ system with transfer function $M(s)$, the gain of the system depends on the frequency and direction of the input vector, $x(t) = ve^{j\omega t}$.

It is well-known that an ill-conditioned plant $M(s)$ can be difficult to control. By ill-conditioned we mean that the gain of the plant is strongly dependent on the input direction, or equivalently that the plant has a high condition number at some frequency. The condition number of $M(j\omega)$ is defined as

$$\operatorname{cond}[M(j\omega)] := \frac{\bar{\sigma}[M(j\omega)]}{\underline{\sigma}[M(j\omega)]} \tag{2.66}$$

Thus an ill-conditioned plant is characterized by strong "directionality". For tight control of ill-conditioned plants the controller must compensate for strong directionality by applying high gain in the plant low-gain direction. This forces the controller to be similar to $G(s)^{-1}$ in directionality, where $G(s)$ is the transfer function of the plant. However, due to plant uncertainty, the high gain direction of the controller will not exactly match the low-gain direction of the plant. This leads to poor performance or instability.

Facts: The following are some inequalities which are useful for robustness analysis, provided the dimension of the matrices involved are compatible.

- $\underline{\sigma}(A)\underline{\sigma}(B) \leq \underline{\sigma}(AB) \leq \bar{\sigma}(A)\underline{\sigma}(B) \leq \bar{\sigma}(AB) \leq \bar{\sigma}(A)\bar{\sigma}(B)$ (2.67)
- $|\bar{\sigma}(A) - \bar{\sigma}(B)| \leq \bar{\sigma}(A+B) \leq \bar{\sigma}(A) + \bar{\sigma}(B)$ (2.68)
- $\underline{\sigma}(A) - \bar{\sigma}(B) \leq \underline{\sigma}(A+B) \leq \underline{\sigma}(A) + \bar{\sigma}(B)$ (2.69)
- $|1 - \bar{\sigma}(Q)| \leq \bar{\sigma}(I+Q) \leq 1 + \bar{\sigma}(Q)$ (2.70)
- $\max\big\{1 - \bar{\sigma}(Q), \underline{\sigma}(Q) - 1\big\} \leq \underline{\sigma}(I+Q) \leq 1 + \underline{\sigma}(Q)$ (2.71)
- $\max\big\{\bar{\sigma}(A), \bar{\sigma}(B)\big\} \leq \bar{\sigma}\big([A\ B]\big) \leq \sqrt{2}\max\big\{\bar{\sigma}(A), \bar{\sigma}(B)\big\}$ (2.72)
- $\det(B + \Delta) = 0 \Longrightarrow \underline{\sigma}(B) \leq \bar{\sigma}(\Delta)$ (2.73)

2.5 Well-Posedness

Generally speaking, a system consists of interconnections of several subsystems. There are three interconnections which interest us here: series, parallel and feedback. All interconnections in a system should be well posed, and behave properly. This leads to the following definition of well-posedness [Che84].

Definition 2.5-1 (Well-Posedness): Let every subsystem of a composite system be described by a rational transfer function. Then the composite system is said to be well posed if

(1) the transfer function of every subsystem is proper; and

(2) the closed-loop transfer function from any chosen input-output pair is well defined (exists) and is proper. □

Examples 2.4-1: The systems shown in Figures 2.2, 2.3, 2.4 and 2.5 are not well posed.

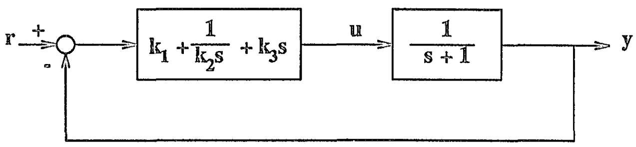

Figure 2.2: PID controller.

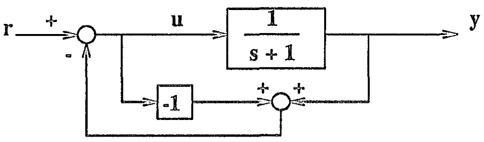

Figure 2.3: Plant I/O configuration.

o *Figure 2.2:* The PID controller subsystem is not proper. Furthermore it is easy to show that the transfer function from r to u is improper. In a practical realization, the differentiator $k_3 s$ could be approximated over any desired frequency range by a proper one, for instance, $\frac{k_3 s}{\tau s+1}$ with $\tau \ll 1$.

o *Figure 2.3:* The transfer function from r to u , i.e.

$$\frac{u(s)}{r(s)} = s + 1$$

is improper. It is interesting to note that it has no state-space representation.

o *Figure 2.4:*

$$G_1(s) = \begin{bmatrix} \frac{-s}{s+1} & \frac{1}{s+2} \\ \frac{1}{s+1} & \frac{-s-1}{s+2} \end{bmatrix}, \quad \text{and } G_2(s) = \begin{bmatrix} 1 & 0 \\ 0 & 1 \end{bmatrix}$$

It can easily be shown that

$$\det[I + G_1(s)G_2(s)] = 0$$

Therefore, the transfer function matrix from r to y, namely

$$y(s) = [I + G_1(s)G_2(s)]^{-1} G_1(s) r(s)$$

is not well defined.

- *Figure 2.5:* Let $w = 0$ and $w_2 = 0$, and

$$P = \begin{bmatrix} 0 & 0 \\ 0 & \frac{s-1}{s+1} \end{bmatrix}, \quad \text{and } K = 1$$

then the transfer function from w_1 to y is not proper.

Remarks: A rational function $g(s)$ is said to be proper if $g(\infty)$ is a finite (zero or nonzero) constant. Otherwise, it is improper. Moreover $g(s)$ is said to be strictly proper if $g(\infty) = 0$. From a system viewpoint, the transfer function of the plant should be strictly proper; and if $MIMO$ this means every transfer function element is strictly proper.

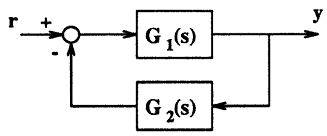

Figure 2.4: Feedback system.

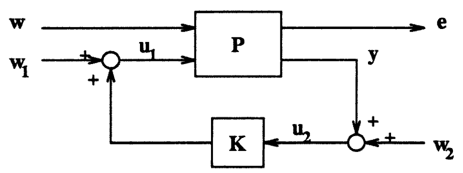

Figure 2.5: Standard compensation configuration (SCC).

In Figure 2.3 the closed-loop transfer function from r to y is equal to 1, which is independent of any stable plant. In other words, the system performance from r to y is completely robust against any plant uncertainty. But as we have already shown the system is not well posed since there exists an input-output pair whose transfer function is improper. An improper transfer function has the effect of differentiation on its input signals. Thus noise injected into the system will be significantly amplified at the output; and might overwhelm the useful signals especially at high frequencies. Furthermore, if the signal contains a discontinuous part, the effect of differentiation might make the system saturate and burn out.

Theorem 2.5-1 (Well-Posedness) [Doy84]: Suppose that $P(s)$ and $K(s)$ are proper in the general interconnection system shown in Figure 2.5. Then the system is well posed *iff*

$$\det[I - P_{22}(\infty)K(\infty)] \neq 0$$

□

To gain insight, consider a $SISO$ system. If $1 - P_{22}(\infty)K(\infty) = 0$, then the closed-loop transfer function has poles at $s = \infty$. This means that the number of zeros is greater than the number of poles.

2.6 BIBO and Internal Stability

The minimum requirement of a system is stability. For an input-output mapping system T, shown in Figure 2.1, the simplest concept of stability is that any bounded input x results in a bounded output $y = Tx$. This leads to the following definition of $BIBO$-stability in the sense of the norms used for the input and output signal spaces [Che84].

Definition 2.6-1 (BIBO Stability): A relaxed system is said to be $BIBO$ (bounded-input bounded-output) stable *iff* for any bounded input, the output is bounded. □

Remark: By this definition, a system with improper transfer function is not $BIBO$ stable, because improper systems might give unbounded outputs with bounded inputs. For instance, a bounded input $x(t) = \sin(\omega t^2)$ produces an unbounded output $y(t) = 2\omega t\cos(\omega t^2)$, if $G(s) = s$.

In the definition, a system is said to be relaxed at time t_0 if the initial conditions at t_0 are zero. For a relaxed system only zero-state responses are considered. Mathematically a relaxed and $FDLTI$ $MIMO$ system $T : x \longrightarrow y$ is $BIBO$ stable, *iff*

$$\forall x \in L_m^\infty(\mathcal{R}) \Longrightarrow Tx = y \in L_n^\infty(\mathcal{R}) \tag{2.74}$$

That is, *iff* the system operator T is bounded, namely $\|T\|_{i\infty} < \infty$. Note that the definition of $BIBO$ stability is suitable for linear, nonlinear, time-varying or time-invariant systems. In particular, for a $FDLTI$ system Theorem 2.3-3 gives the following results:

$$\text{BIBO stable} \iff \|g_{ij}\|_1 < \infty \tag{2.75}$$
$$\iff \int_{-\infty}^{\infty} |g_{ij}(\tau)| d\tau < \infty \tag{2.76}$$

for all (i, j), $1 \le i \le n$, $1 \le j \le m$, where $g_{ij}(t)$ denotes the (i, j) element of the impulse response matrix $g(t)$ of the system; and the corresponding Laplace transform is $G(s)$. Mathematically any time function in the signal space $L^1(\mathcal{R})$ has a Laplace transform in some range of convergence of the complex-frequency domain. Furthermore, Laplace transformation is an isomorphic mapping between the function spaces in the time-domain and in the s-domain. We next present a theorem which is useful in the frequency domain analysis of systems [Che84].

Theorem 2.6-1 (BIBO-Stability for FDLTI Systems):
A relaxed $FDLTI$ system described by a proper rational transfer function matrix $G(s)$ is $BIBO$ stable *iff* there are no poles of $G(s)$ in $\Re e(s) \ge 0$ or, equivalently, all the poles of $G(s)$ have negative real parts, with $\Re e(s)$ denoting the real part of complex frequency s. □

For example a system with transfer function

$$G(s) = \frac{1}{s^2 + \omega_0^2}$$

has poles on the $j\omega$-axis at $s = \pm j\omega_0$. Then the bounded input signal $x(t) = A\cos\omega_0 t$ results in the unbounded output signal $y(t) = \frac{A}{2\omega_0} t \sin\omega_0 t$.

Definition 2.6-2 (Exponential Stability): A rational transfer function matrix is exponentially stable *iff* it is proper and has no poles in $CRHP$. □

Exponential stability is only defined for $FDLTI$ systems and is equivalent to $BIBO$ stability for $FDLTI$ systems. Mathematically it is also equivalent to

$G(s) \in \mathcal{RH}^\infty$, where $\mathcal{RH}^\infty$ is usually referred to as the set of proper and stable matrix-valued real rational functions. In other words

$$G(s) \text{ is BIBO stable} \Longleftrightarrow \|g_{ij}\|_1 < \infty \Longleftrightarrow G(s) \in \mathcal{RH}^\infty \tag{2.77}$$

where $G(s) = \mathcal{L}[g(t)]$ denotes the Laplace transform of $g(t)$.

Let us consider a feedback system shown in Figure 2.6. The system is *BIBO* stable from r to y, but it is not *BIBO* stable from n to y because of the unstable pole-zero cancellation between the compensator and plant. The transfer functions are

$$\begin{aligned} \frac{y(s)}{r(s)} &= \frac{1}{s+3}, \quad \text{and} \\ \frac{y(s)}{n(s)} &= \frac{s+2}{(s+3)(s-1)} \end{aligned}$$

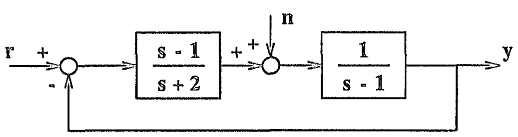

Figure 2.6: A system with unstable pole-zero cancellation.

Thus the system will become unstable due to the noise excitation at the plant input. Therefore, to guarantee stability of the overall system, transfer functions of every input-output pair should be checked to be *BIBO* stable. This leads to the concept of internal stability.

Definition 2.6-3 (Internal Stability): An interconnected system is said to be internally stable *iff* the system is guaranteed to be *BIBO* stable for every input-output pair. □

To illustrate the definition of internal stability we consider the plant I/O (input/output) feedback configuration of Figure 2.7 [Che84]. In order to test for internal stability, we examine the transfer functions between all possible input-output pairs, as shown in Figure 2.8. The system is internally stable if the system with input $(r, n_1, n_2, n_3, n_4, n_5)$ and output $(e, w_1, w_2, w_3, w_4, w_5)$ is *BIBO* stable.

Every n_i, $1 \le i \le 5$, represents a possible exogenous noise signal with bounded magnitude injected into the system. So internal stability guarantees bounded output signals for all bounded exogenous input signals. Needless to say, no unstable pole-zero cancellation can exist in each subsystem. By definition internal stability defined in the s-domain is equivalent to asymptotic stability defined in the time domain.

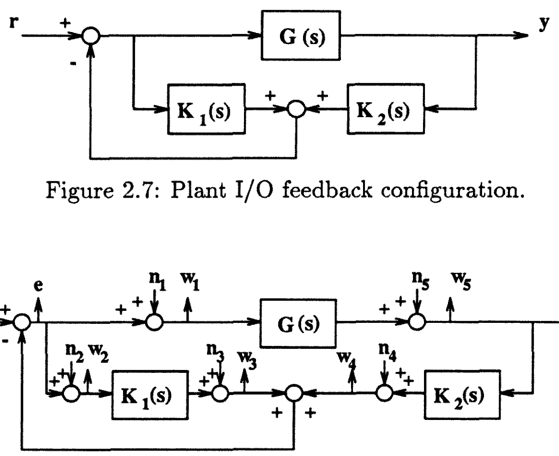

Figure 2.7: Plant I/O feedback configuration.

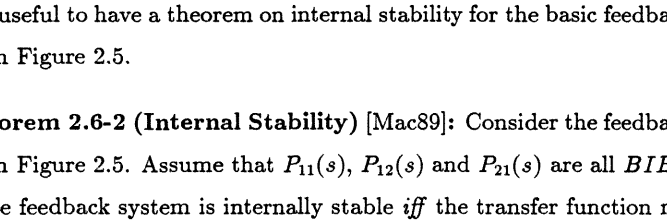

Figure 2.8: With input-output pairs added.

It is useful to have a theorem on internal stability for the basic feedback system shown in Figure 2.5.

Theorem 2.6-2 (Internal Stability) [Mac89]**:** Consider the feedback system shown in Figure 2.5. Assume that $P_{11}(s)$, $P_{12}(s)$ and $P_{21}(s)$ are all $BIBO$ stable. Then the feedback system is internally stable *iff* the transfer function matrix

$$M := \begin{bmatrix} (I - KP_{22})^{-1} & K(I - P_{22}K)^{-1} \\ P_{22}(I - KP_{22})^{-1} & (I - P_{22}K)^{-1} \end{bmatrix}$$

is $BIBO$ stable. Furthermore if $K(s)$ is $BIBO$ stable, then the feedback system is internally stable *iff* $M_{21} = P_{22}(I - KP_{22})^{-1}$ is $BIBO$ stable. ∎

2.7 Small Gain Theorem

The small gain theorem is of central importance in the derivation of many stability tests using singular values. However, it provides only a sufficient condition for stability and is therefore potentially conservative. It is useful because it does not need detailed information about the system.

Consider a *FDLTI* system operator

$$T : L^2_m(\mathcal{R}) \longrightarrow L^2_n(\mathcal{R}) \tag{2.78}$$

with the transfer function matrix $G(s)$. Recall that Theorem 2.3-5 gives the operator gain

$$\|T\|_{i2} = \sup_{\omega \in \mathcal{R}} \|G(j\omega)\|_2 \tag{2.79}$$

when the elements of the impulse response matrix $g(t)$, namely, the $g_{ij}(\cdot)$'s, are in $L^1(\mathcal{R})$, for $1 \leq i \leq n,\ 1 \leq j \leq m$. Moreover (2.28) and (2.55) can be rewritten as

$$\begin{aligned} \|G(j\omega)\|_2 &= \max_{1 \leq i \leq m} \left\{ \lambda_i [G(j\omega)^* G(j\omega)] \right\}^{\frac{1}{2}} \\ &=: \left\{ \bar{\lambda}[G(j\omega)^* G(j\omega)] \right\}^{\frac{1}{2}} \\ &= \bar{\sigma}[G(j\omega)] \end{aligned} \tag{2.80}$$

where $\bar{\lambda}(M)$ denotes the maximum eigenvalue of matrix M. To summarize , we give the following definition.

Definition 2.7-1 (∞-norm of a FDLTI System): The ∞-norm ($\mathcal{H}^\infty$-norm) of an $n \times m$ system matrix $G(s)$ is defined as

$$\|G\|_\infty := \sup_{\omega \in \mathcal{R}} \|G(j\omega)\|_2 \tag{2.81}$$

$$= \sup_{\omega \in \mathcal{R}} \bar{\sigma}[G(j\omega)] \tag{2.82}$$

where $G(j\omega) = \mathcal{F}[g(t)]$ with $g_{ij}(\cdot) \in L^1(\mathcal{R})$, for $1 \leq i \leq n,\ 1 \leq j \leq m$. ◻

Fact:

$$\|G\|_\infty = \|T\|_{i2}\,, \quad \text{if } g_{ij}(\cdot) \in L^1(\mathcal{R}), \text{ for } 1 \leq i \leq n,\ 1 \leq j \leq m \tag{2.83}$$

Remark: By definition we have $\|G\|_\infty = \|T\|_{i2}$, so that the ∞-norm is an operator norm. Therefore

$$\|G_1 G_2\|_\infty \leq \|G_1\|_\infty \cdot \|G_2\|_\infty \tag{2.84}$$

Note that the ∞-norm here is used for a system operator, do not be confused with ∞-norm used in (input or output) function spaces. For *SISO* systems, $\|G\|_\infty$ denotes the maximum value of the Bode plot of magnitude $|G(j\omega)|$.

Figure 2.9: A feedback configuration.

The small gain theorem can be stated as follows.

Theorem 2.7-1 (Small Gain Theorem) [DeV75]**:** Consider a system illustrated in Figure 2.9. Assume that T_1 and T_2 are linear, bounded system operators. Then

$$\|T_1 T_2\| < 1 \text{ and } \|T_2 T_1\| < 1 \Longrightarrow \|w_1\| < \infty \text{ and } \|w_2\| < \infty$$

when $\|n_1\| < \infty$ and $\|n_2\| < \infty$. Furthermore, since $\|T_1 T_2\| \leq \|T_1\| \cdot \|T_2\|$ and $\|T_2 T_1\| \leq \|T_1\| \cdot \|T_2\|$, then

$$\|T_1\| \cdot \|T_2\| < 1 \Longrightarrow \quad \text{the closed-loop is internally stable}$$

where $\|\circ\|$ is taken to be any p-norm, $1 \leq p \leq \infty$, for signals and induced p-norm for system operators. $\square$

Suppose we take the 2-norm, $p = 2$, to measure the size of all signals in a *FDLTI* system and let $G_1(s)$ and $G_2(s)$ describe the transfer function matrices corresponding to the linear bounded system operators T_1 and T_2, respectively. Recall that $\|T\|_{i2} = \|G\|_\infty$. If $G_1(s)$ and $G_2(s)$ are stable and proper (i.e. $G_1 \in \mathcal{RH}^\infty$ and $G_2 \in \mathcal{RH}^\infty$), then by Theorem 2.7-1 we have the following corollary.

Corollary 2.7-1 (Small Gain Theorem in ∞-norm) [DeV75]: For a *FDLTI* system, if $G_1(s)$ and $G_2(s)$ are stable, then

$$\|G_1\|_\infty \cdot \|G_2\|_\infty < 1 \Longrightarrow \quad \text{the closed-loop is internally stable}$$

$\square$

This result is the basis for many singular value robustness tests.

Remark: It is interesting to observe the relationship between the small gain theorem well-known in control theory and the fixed point theorem well-known in Mathematics. The Banach fixed point theorem, applicable in metric spaces [Kre78], gives only a sufficient condition for the existence and uniqueness of a fixed point for a contraction mapping T, (i.e. $\|T\| < 1$ if T is a linear system operator).

Chapter 3

UNCERTAINTIES AND ROBUSTNESS

3.1 Introduction

No mathematical system can exactly model a physical system. Idealized models are simplified representations of physical reality. The actual system will suffer from parameter variations and the model will be inaccurate because of various approximations and uncertainties. The modelling error might adversely affect the stability and performance of a control system. The principal reason for using feedback control as opposed to open-loop control is the presence of model uncertainties and load disturbances. With feedback it is possible to keep the system stable and to maintain performance levels despite uncertainties.

This chapter reviews the singular-value-based methods for modelling uncertainty and for analyzing the robustness of feedback systems. In Section 3.2 a linear fractional transformation (*LFT*) is defined in terms of system components. The *LFT* can be used to simplify a complex system structure, thereby simplifying analysis. In Section 3.3 we consider unstructured uncertainty in which all uncertainties are lumped into one single perturbation Δ for simplicity. There are six kinds of perturbation which are frequently used to describe a perturbed system: additive uncertainty (inverse and non-inverse), multiplicative input uncertainty (inverse and non-inverse) and multiplicative output uncertainty (inverse and non-inverse). The inverse (resp. non-inverse) error models are related to the variation of the poles (resp. zeros) of the perturbed plant. In Section 3.4, all six kinds of perturbation are represented in a common format called $(G, \hat{\Delta})$. It is a generalized uncertainty model described by an *LFT*. Section 3.5 gives a robust stability test for stable unstructured uncertainty. For unstructured uncertainty which is unstable, two theorems are presented in Section 3.6. Two examples are given in Section 3.7 to demonstrate that the singular value approach for robust stability analysis can sometimes give conservative results.

To remedy this conservatism, Doyle's structured singular value (*SSV*) can be used. This is discussed in Section 3.8. In reality, all uncertainties in physical systems are structured. They cannot be lumped into one uncertainty without introducing conservative consequences. In Section 3.9 it is shown how the *SSV* can be used to characterize robust performance as well as robust stability.

To optimize the *SSV*, or μ as it is also called, Doyle has introduced a μ-synthesis procedure called $D - K$ iteration. This is described in Section 3.10. Finally in Section 3.11 an example is used to illustrate how small simultaneous modelling errors can interact to cause instability.

3.2 Linear Fractional Transformation: LFT

The linear fractional transformation of interest can be traced back to circuit theory [Red50] [Red60] in the late 1950's. Some years later in the 1970's Safonov emphasized its role in control theory for modelling uncertainty and parameterizing sets of plants. Figure 3.1 illustrates a system with a component $g_i(s)$ of special concern. From a control point of view, $g_i(s)$ may represent the system uncertainty or the controller to be designed. The general framework to be used is illustrated in the diagram of Figure 3.2.

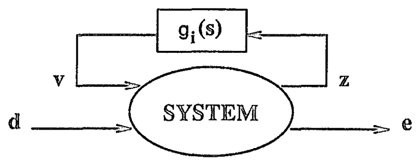

Figure 3.1: A general system with a $g_i(s)$ of interest.

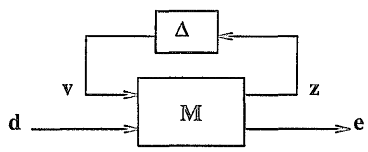

Figure 3.2: $M - \Delta$ structure.

The interconnection matrix M can be partitioned as

$$M = \begin{bmatrix} M_{11} & M_{12} \\ M_{21} & M_{22} \end{bmatrix} \tag{3.1}$$

with M_{11} conforming with Δ. By the signal flow diagram shown in Figure 3.3, Mason's formula gives

$$e = \left[M_{22} + M_{21}\Delta\,(I - M_{11}\Delta)^{-1}\,M_{12}\right] d \tag{3.2}$$

It is easy to see that the expression is well defined *iff* the inverse of $(I - M_{11}\Delta)$ exists. When the inverse exists

$$F_u(M,\Delta) := M_{22} + M_{21}\Delta\,(I - M_{11}\Delta)^{-1}\,M_{12} \tag{3.3}$$

is called an Upper Linear Fractional Transformation ($ULFT$) on M by Δ, where the subscript u on F_u pertains to the "upper" loop of M closed by Δ. On the other hand, in the system illustrated in Figure 3.4, the vectors e and d satisfy $e = F_l(M,\Delta)d$, where

$$F_l(M,\Delta) := M_{11} + M_{12}\Delta\,(I - M_{22}\Delta)^{-1}\,M_{21} \tag{3.4}$$

is called a Lower Linear Fractional Transformation ($LLFT$) on M by Δ, when $(I - M_{22}\Delta)$ is invertible.

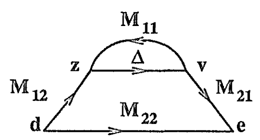

Figure 3.3: Signal flow diagram.

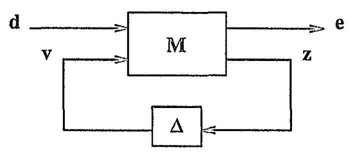

Figure 3.4: $M - \Delta$ structure.

Remark: If M is a 2×2 matrix with scalar elements M_{ij}'s, then (3.3) becomes

$$\begin{aligned} F_u(M, \Delta) &= M_{22} + M_{21}\Delta \frac{1}{1 - M_{11}\Delta} M_{12} \\ &= \frac{M_{22} - (M_{11}M_{22} - M_{21}M_{12})\,\Delta}{1 - M_{11}\Delta} \end{aligned} \tag{3.5}$$

which is a bilinear transformation in Δ. Mathematically a bilinear transformation transforms (generalized) circles into (generalized) circles in the complex plane. This property will be used for robust stability and robust performance analysis in Chapter 7. Let $Q := \Delta(I - M_{11}\Delta)^{-1}$, then (3.3) becomes

$$F_u(M, Q) = M_{22} + M_{21}QM_{12} \tag{3.6}$$

which is an affine transformation of Q, whereas (3.3) is a nonlinear transformation of Δ.

Example 3.2-1: It is interesting to note that a state-space representation can be described by an *LFT*. Consider the state space

$$\begin{aligned} \dot{x} &= Ax + Bu \\ y &= Cx + Du \end{aligned} \tag{3.7}$$

This can be modelled as in Figure 3.2 with

$$y = e, \quad d = u, \quad z = \dot{x}, \quad v = x$$

and

$$M = \begin{bmatrix} A & B \\ C & D \end{bmatrix}, \quad \Delta = \frac{1}{s}$$

Example 3.2-2: An *LFT* can be used to represent a transfer function with uncertainty Δ. Consider the exponential function $e^{-\tau s}$, $0 \le \tau \le 1$ minutes.

$$\begin{aligned} f(s) := e^{-\tau s} &\approx \frac{1 - \frac{\tau s}{2}}{1 + \frac{\tau s}{2}} \text{ (first-order Padé approximation)} \\ &= \frac{\left(1 - \frac{s}{4}\right) - \frac{\Delta s}{2}}{\left(1 + \frac{s}{4}\right) + \frac{\Delta s}{2}} \end{aligned} \tag{3.8}$$

where $\tau = \frac{1}{2} + \Delta$, $|\Delta| \le 0.5$. Note that (1.8) can be represented by an *LFT* because it is a bilinear form in Δ. Simple manipulations yield

$$M = \begin{bmatrix} \frac{-s/2}{1+s/4} & \frac{1}{1+s/4} \\ \frac{-s}{1+s/4} & \frac{1-s/4}{1+s/4} \end{bmatrix}$$

that is

$$e^{-\tau s} \approx F_u(M, \Delta), \quad |\Delta| \le 0.5$$

Remark: Assume $\|M_{11}\| \cdot \|\Delta\| < 1$ in Figure 1.2. Recall from the small gain theorem that this assumption together with the stability of $M_{11}(s)$ and $\Delta(s)$ can be used to guarantee stability of the feedback system. Since $\|M_{11}\| \cdot \|\Delta\| < 1$ implies $\|M_{11}\Delta\| < 1$, it is easy to show that

$$\|M_{11}\Delta\| < 1 \Longrightarrow \left\|(I - M_{11}\Delta)^{-1}\right\| \le (1 - \|M_{11}\Delta\|)^{-1} \tag{3.9}$$

Hence

$$\begin{aligned} \|F_u(M, \Delta)\| &\le \|M_{22}\| + \|M_{21}\| \cdot \|\Delta\| (1 - \|M_{11}\Delta\|)^{-1} \cdot \|M_{12}\| \\ &\le \|M_{22}\| + \|M_{21}\| \cdot \|\Delta\| (1 - \|M_{11}\| \cdot \|\Delta\|)^{-1} \cdot \|M_{12}\| \\ &= F_u(|M|, \|\Delta\|) \end{aligned} \tag{3.10}$$

where

$$|M| := \begin{bmatrix} \|M_{11}\| & \|M_{12}\| \\ \|M_{21}\| & \|M_{22}\| \end{bmatrix} \tag{3.11}$$

is a nonnegative matrix. Inequality (1.10) gives an upper bound on the gain from input d to output e.

3.3 Model Uncertainty Description

In this section, the uncertainties which might occur in different parts of a system are lumped into one single perturbation Δ. We refer to this uncertainty as "unstructured" uncertainty. More precisely, unstructured uncertainty means that several sources of uncertainties, bounded real parameters and unmodelled dynamics are described by a single perturbation Δ which is a full matrix whose dimensions conform with those of the plant. Δ is uncertain, but norm-bounded. It is important to note that robustness analysis will be erroneous if the uncertainty description used is not adequate [Foo85].

Let $G_p(s) \in \prod$ be any member of the set $\prod$ of possible perturbed plants, and let $G_0(s) \in \prod$ denote the nominal model of the plant. To describe unstructured uncertainty the following six perturbations have been proposed:

∘ (a1) additive uncertainty: (Figure 3.5)

$$G_p(s) = G_0(s) + \Delta_a(s), \quad \bar{\sigma}[\Delta_a(j\omega)] \leq \delta_a(\omega) \tag{3.12}$$

∘ (a2) inverse additive uncertainty: (Figure 3.6)

$$G_p(s)^{-1} = G_0(s)^{-1} + \hat{\Delta}_a(s), \quad \bar{\sigma}[\hat{\Delta}_a(j\omega)] \leq \hat{\delta}_a(\omega) \tag{3.13}$$

∘ (b1) multiplicative input uncertainty: (Figure 3.7)

$$G_p(s) = G_0(s)[I + \Delta_i(s)], \quad \bar{\sigma}[\Delta_i(j\omega)] \leq \delta_i(\omega) \tag{3.14}$$

∘ (b2) inverse multiplicative input uncertainty: (Figure 3.8)

$$G_p(s)^{-1} = [I + \hat{\Delta}_i(s)]G_0(s)^{-1}, \quad \bar{\sigma}[\hat{\Delta}_i(j\omega)] \leq \hat{\delta}_i(\omega) \tag{3.15}$$

∘ (c1) multiplicative output uncertainty: (Figure 3.9)

$$G_p(s) = [I + \Delta_o(s)]G_0(s), \quad \bar{\sigma}[\Delta_o(j\omega)] \leq \delta_o(\omega) \tag{3.16}$$

∘ (c2) inverse multiplicative output uncertainty: (Figure 3.10)

$$G_p(s)^{-1} = G_0(s)^{-1}[I + \hat{\Delta}_o(s)], \quad \bar{\sigma}[\hat{\Delta}_o(j\omega)] \leq \hat{\delta}_o(\omega) \tag{3.17}$$

The inverse error models are related to the variation of the poles of the plant in (a2), (b2) and (c2). On the other hand (a1), (b1) and (c1) describe the variation of the zeros of the plant.

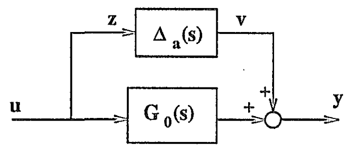

Figure 3.5: Additive uncertainty.

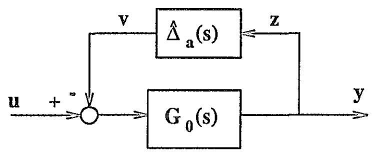

Figure 3.6: Inverse additive uncertainty.

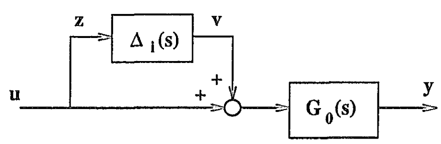

Figure 3.7: Multiplicative input uncertainty.

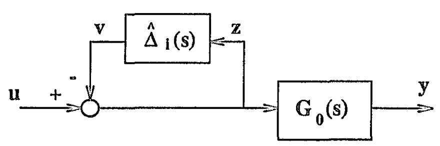

Figure 3.8: Inverse multiplicative input uncertainty.

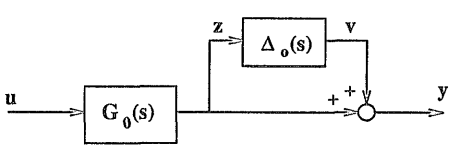

Figure 3.9: Multiplicative output uncertainty.

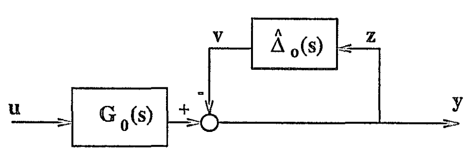

Figure 3.10: Inverse Multiplicative output uncertainty.

3.4 Generalized Uncertainty Model: $(G, \hat{\Delta})$ Format

For the purpose of robustness analysis, the uncertainty models of the preceding section can be unified by an upper *LFT*, called $(G, \hat{\Delta})$ format, as illustrated in Figure 1.11. Let $G_p(s)$ be the transfer function from the actuator input $u(t)$ to the plant output $y(t)$ and let $G(s)$ be an interconnection matrix partitioned to conform with the input vectors v, u and output vectors z, y. Assume $\left[I - G_{11}(s)\hat{\Delta}(s)\right]$ is invertible, then

$$G_p(s) = F_u(G, \hat{\Delta}) \tag{3.18}$$

A bit of thought reveals that

∘ (a1) for additive uncertainty:

$$G = \begin{bmatrix} 0 & I \\ I & G_0 \end{bmatrix}, \quad \bar{\sigma}[\Delta_a(j\omega)] \leq \delta_a(\omega) \tag{3.19}$$

∘ (a2) for inverse additive uncertainty:

$$G = \begin{bmatrix} -G_0 & G_0 \\ -G_0 & G_0 \end{bmatrix}, \quad \bar{\sigma}[\hat{\Delta}_a(j\omega)] \leq \hat{\delta}_a(\omega) \tag{3.20}$$

∘ (b1) for multiplicative input uncertainty:

$$G = \begin{bmatrix} 0 & I \\ G_0 & G_0 \end{bmatrix}, \quad \bar{\sigma}[\Delta_i(j\omega)] \leq \delta_i(\omega) \tag{3.21}$$

∘ (b2) for inverse multiplicative input uncertainty:

$$G = \begin{bmatrix} -I & I \\ -G_0 & G_0 \end{bmatrix}, \quad \bar{\sigma}[\hat{\Delta}_i(j\omega)] \leq \hat{\delta}_i(\omega) \tag{3.22}$$

∘ (c1) for multiplicative output uncertainty:

$$G = \begin{bmatrix} 0 & G_0 \\ I & G_0 \end{bmatrix}, \quad \bar{\sigma}[\Delta_o(j\omega)] \leq \delta_o(\omega) \tag{3.23}$$

∘ (c2) for inverse multiplicative output uncertainty:

$$G = \begin{bmatrix} -I & G_0 \\ -I & G_0 \end{bmatrix}, \quad \bar{\sigma}[\hat{\Delta}_o(j\omega)] \leq \hat{\delta}_o(\omega) \tag{3.24}$$

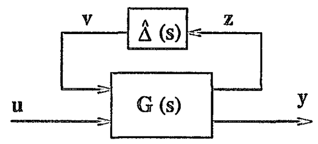

Figure 3.11: $(G, \hat{\Delta})$ format of a perturbed plant.

3.5 Robust Stability: for Stable Unstructured Uncertainty

Let us consider a $FDLTI$ system shown in Figure 1.12, where the perturbed plant is described by the $(G, \hat{\Delta})$ format and the transfer function of controller is given by $K(s)$. Since a plant perturbation can destabilize a nominally stable system, the first issue to be addressed is robust stability (RS). That is, does the closed-loop system remain stable under a given plant perturbation? Stability will be taken to mean that the perturbed system has no $CRHP$ poles.

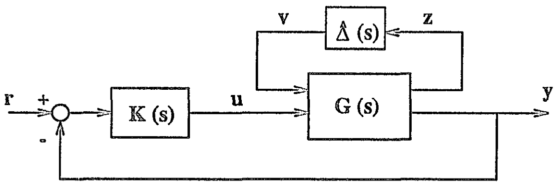

Figure 3.12: A control system with perturbed plant.

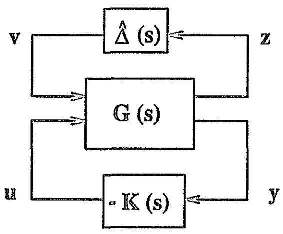

Figure 3.13: Equivalent system, when r=0.

For the purpose of stability analysis, the command signal $r(t)$ can be set to zero and Figure 1.12 redrawn as Figure 1.13. Absorbing $-K(s)$ into $G(s)$ Figure

3.13 can be reduced to 3.14, where matrix $\hat{M}$ is given by

$$\hat{M} := F_l(G, -K) \tag{3.25}$$

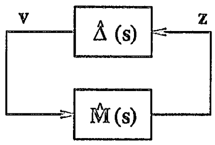

Figure 3.14: General $\hat{M} - \hat{\Delta}$ structure for RS analysis.

By (3.25) and (3.19)-(3.24), we have

o (a1) for additive uncertainty:

$$\hat{M} = -K(I + G_0K)^{-1} \tag{3.26}$$

o (a2) for inverse additive uncertainty:

$$\begin{aligned} \hat{M} &= -G_0 + G_0K(I + G_0K)^{-1}G_0 \\ &= -G_0(I + KG_0)^{-1} \end{aligned} \tag{3.27}$$

o (b1) for multiplicative input uncertainty:

$$\hat{M} = -K(I + G_0K)^{-1}G_0 \tag{3.28}$$

o (b2) for inverse multiplicative input uncertainty:

$$\begin{aligned} \hat{M} &= -I + K(I + G_0K)^{-1}G_0 \\ &= -(I + KG_0)^{-1} \end{aligned} \tag{3.29}$$

o (c1) for multiplicative output uncertainty:

$$\hat{M} = -G_0K(I + G_0K)^{-1} \tag{3.30}$$

o (c2) for inverse multiplicative output uncertainty:

$$\begin{aligned} \hat{M} &= -I + G_0K(I + G_0K)^{-1} \\ &= -(I + G_0K)^{-1} \end{aligned} \tag{3.31}$$

Furthermore, after scaling of $\hat{\Delta}(s)$, it is easy to see that Figure 3.15 is equivalent to Figure 3.14. The perturbation $\hat{\Delta}(s)$ which satisfies

$$\bar{\sigma}[\hat{\Delta}(j\omega)] \leq \alpha(\omega) \tag{3.32}$$

can be normalized by

$$\Delta(s) := \frac{\hat{\Delta}(s)}{\alpha(s)} \tag{3.33}$$

where $\alpha(s)$ denotes a minimum phase, stable rational function which is used to fit the error bounding function $\delta(\omega)$ or $\hat{\delta}(\omega)$. Absorbing the scaling function $\alpha(s)$ into $\hat{M}(s)$, we have the $M - \Delta$ structure shown in Figure 3.15, with

$$M(s) \; := \; \alpha(s)\hat{M}(s), \quad \text{and} \tag{3.34}$$

$$\|\Delta\|_\infty \; \leq \; 1 \tag{3.35}$$

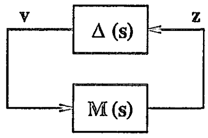

Figure 3.15: General $M - \Delta$ structure with $\|\Delta\|_\infty \leq 1$.

Assume that both $M(s)$ and $\Delta(s)$ are stable, then the following theorem is easily established [CaD91] [MoZ89].

Theorem 3.5-1 (Robust Stability Theorem for Stable Unstructured Perturbation): For a *FDLTI* system shown in Figure 3.15, assume that

(a) $M(s)$ is stable, and

(b) $\Delta(s)$ is stable with $\|\Delta\|_\infty \leq 1$

Then the closed-loop system is internally stable *iff* one of the following conditions is satisfied:

(i) $\det[I - M(j\omega)\Delta(j\omega)] \neq 0, \ \forall \omega \in \mathcal{R}, \ \forall \Delta \ni \|\Delta\|_\infty \leq 1$

(ii) $\|M\|_\infty < 1$ □

Remark: To gain insight, let us consider a *SISO* system shown in Figure 3.15. Theorem 3.5-1 implies that the Nyquist plot of $M(s)$ must be strictly inside a unit circle centred at the origin in the $M(j\omega)$-plane to guarantee robust stability. Otherwise, at some frequency ω_0, the so-called unity-gain frequency of $M(j\omega)$, the Nyquist plot of $M(j\omega)$ crosses the unit circle, as illustrated in Figure 3.16. The phase margin of $M(j\omega)$ is θ_0 , i.e. $M(j\omega_0) = e^{-j(\pi-\theta_0)}$ with $\theta_0 > 0$. If we can properly choose a stable $\Delta(s)$ such that

$$
\begin{aligned}
|\Delta(j\omega_0)| &= 1, \quad \text{and} && (3.36)\\
\angle\Delta(j\omega_0) &= \pi - \theta_0 && (3.37)
\end{aligned}
$$

then clearly $M(j\omega_0)\Delta(j\omega_0) = 1$ and $\det[1 - M(j\omega_0)\Delta(j\omega_0)] = 0$, and the closed-loop system will sustain oscillations at ω_0 and be unstable. Now let us construct a stable transfer function $\Delta(s)$ to satisfy (3.36) and (3.37). A first order all-pass function of $\Delta(s)$ can be chosen as

$$\Delta(s) = \frac{s-a}{s+a}, \quad a > 0 \tag{3.38}$$

Obviously (3.36) is achieved and (3.37) leads to

$$a = \omega_0 \left(\tan\frac{\theta_0}{2}\right)^{-1} \tag{3.39}$$

when $0 \leq \theta_0 \leq \pi$. The equation (3.37) also satisfies the extremal cases that if $\theta_0 = 0$ or $\theta_0 = \pi$, then $\Delta(s) = -1$ or $\Delta(s) = 1$, respectively. Furthermore if the Nyquist plot of $M(j\omega)$ crosses the unit circle in the first or second quadrant, then $\Delta(s)$ can be constructed as

$$\Delta(s) = -\frac{s-a}{s+a}, \quad a > 0 \tag{3.40}$$

when $-\pi \leq \theta_0 \leq 0$.

Remark: For all possible stable unstructured perturbations $\Delta(s)$, $\|\Delta\|_\infty \leq 1$, in Figure 3.15, the application of the small gain theorem does not introduce any conservatism. However, the conservatism might become arbitrarily large if $\Delta(s)$ is structured. To remedy this problem of the singular value approach, the concept of structured singular value will be introduced in Section 3.8.

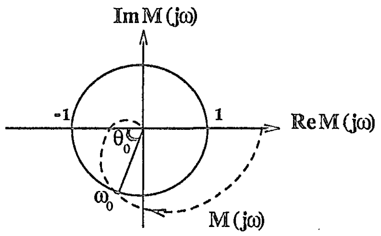

Figure 3.16: Nyquist plot of $M(s)$.

3.6 Robust Stability: for Unstable Unstructured Uncertainty

The derivation of the unstructured robust stability test of Theorem 3.5-1 is based on the small gain theorem under the assumption of stability of the uncertainty model Δ. This might be too restrictive. Much effort has been made to remove the assumption and derive more general stability conditions, e.g. [PoF85] [ChD82]. In this section two theorems are given under the condition that all members G_p of the set $\prod$ of possible plants have the same number of $CRHP$ poles or zeros.

Consider a feedback system of Figure 3.12. Let L and L_0 denote the perturbed and nominal open-loop transfer function matrices, respectively. Clearly, $L_0 = G_0K$, $L = G_pK$ and

$$
\begin{aligned}
I + L &= \left[I + (L - L_0)(I + L_0)^{-1}\right](I + L_0) && (3.41)\\
&=: Q(I + L_0) && (3.42)
\end{aligned}
$$

with $Q := I + (L - L_0)(I + L_0)^{-1} = I + (G_p - G_0)\,K(I + G_0K)^{-1}$.

Furthermore expressions (3.12), (3.14) and (3.16) give

o (a1) additive uncertainty:

$$
\begin{aligned}
Q &= I + \Delta_a K(I + G_0K)^{-1} && (3.43)\\
\det Q &= \det\left[I + K(I + G_0K)^{-1}\Delta_a\right] && (3.44)
\end{aligned}
$$

o (b1) multiplicative input uncertainty:

$$
Q = I + G_0\Delta_i K(I + G_0K)^{-1} \qquad (3.45)
$$

$$\det Q = \det\left[I + K(I+G_0K)^{-1}G_0\Delta_i\right] \tag{3.46}$$

∘ (c1) multiplicative output uncertainty:

$$Q = I + \Delta_o G_0 K(I+G_0K)^{-1} \tag{3.47}$$

$$\det Q = \det\left[I + G_0K(I+G_0K)^{-1}\Delta_o\right] \tag{3.48}$$

The formula $\det(I + AB) = \det(I + BA)$ is used to obtain $\det Q$ in the above equations. Comparing (3.44), (3.46), (3.48) with (3.26), (3.28), (3.30), respectively, it is interesting to note that

$$\det Q = \det\left(I - \hat{M}\hat{\Delta}\right) \tag{3.49}$$

with $\hat{\Delta}$ denoting Δ_a, Δ_i or Δ_o, and $\bar{\sigma}\left[\hat{\Delta}(j\omega)\right] \leq \delta(\omega)$, for additive or multiplicative uncertainty. This leads to the following theorem [Lun89].

Theorem 3.6-1 (for Unstable Additive or Multiplicative Uncertainty): Assume that

(1) the closed-loop system is nominally stable, and

(2) $G_p(s)$ and $G_0(s)$ share the same number of $CRHP$ poles.

Then the closed-loop system is robustly stable *iff*

$$\bar{\sigma}\left[\hat{M}(j\omega)\right] < \frac{1}{\delta(\omega)}, \quad \forall\omega \in \mathcal{R}$$

□

Remark: Mathematically the norm of the operator $\hat{\Delta}(s)$ is infinite because $\hat{\Delta}(s)$ is unstable. However $\bar{\sigma}\left[\hat{\Delta}(j\omega)\right]$ might well exist. For example, if $\hat{\Delta}(s) = \frac{1}{s-1}$, then $\bar{\sigma}\left[\hat{\Delta}(j\omega)\right] = \left(\sqrt{w^2+1}\right)^{-1}$.

We have given a robust stability test for a system with unstable additive or multiplicative uncertainty. Similar tests are also available for unstable inverse additive or inverse multiplicative uncertainty. With open-loop transfer functions L_0 and L at hand, we have the following identities:

$$I + L^{-1} = \left[I + (L^{-1} - L_0^{-1})(I + L_0^{-1})^{-1}\right](I + L_0^{-1}) \tag{3.50}$$

$$=: R(I + L_0^{-1}) \tag{3.51}$$

with

$$\begin{aligned} R &:= I+(L^{-1}-L_0^{-1})(I+L_0^{-1})^{-1} = I+(L^{-1}-L_0^{-1})(I+L_0)^{-1}L_0 \\ &= I+K^{-1}\left(G_p^{-1}-G_0^{-1}\right)(I+G_0K)^{-1}G_0K \end{aligned} \tag{3.52}$$

Then it follows from (3.13), (3.15) and (3.17) that

∘ (a2) inverse additive uncertainty:

$$R = I+K^{-1}\hat{\Delta}_a(I+G_0K)^{-1}G_0K \tag{3.53}$$

$$\begin{aligned} \det R &= \det\left[I+(I+G_0K)^{-1}G_0\hat{\Delta}_a\right] \\ &= \det\left[I+G_0(I+KG_0)^{-1}\hat{\Delta}_a\right] \end{aligned} \tag{3.54}$$

∘ (b2) inverse multiplicative input uncertainty:

$$R = I+K^{-1}\hat{\Delta}_iG_0^{-1}(I+G_0K)^{-1}G_0K \tag{3.55}$$

$$\begin{aligned} \det R &= \det\left[I+G_0^{-1}(I+G_0K)^{-1}G_0\hat{\Delta}_i\right] \\ &= \det\left[I+(I+KG_0)^{-1}\hat{\Delta}_i\right] \end{aligned} \tag{3.56}$$

∘ (c2) inverse multiplicative output uncertainty:

$$R = I+K^{-1}G_0^{-1}\hat{\Delta}_o(I+G_0K)^{-1}G_0K \tag{3.57}$$

$$\det R = \det\left[I+(I+G_0K)^{-1}\hat{\Delta}_o\right] \tag{3.58}$$

Comparing (3.54), (3.56), (3.58) with (3.27), (3.29), (3.31), respectively, it can be seen that

$$\det R = \det\left(I-\hat{M}\hat{\Delta}\right) \tag{3.59}$$

with $\hat{\Delta}$ denoting $\hat{\Delta}_a$, $\hat{\Delta}_i$ or $\hat{\Delta}_o$, and $\bar{\sigma}\left[\hat{\Delta}(j\omega)\right] \leq \hat{\delta}(\omega)$, for inverse additive or inverse multiplicative uncertainty. Then the following theorem is easily established.

Theorem 3.6-2 (for Unstable Inverse Additive or Inverse Multiplicative Uncertainty) [Lun89] **:** Assume that

(1) the closed-loop system is nominally stable, and

(2) $G_p(s)$ and $G_0(s)$ share the same number of $CRHP$ zeros.

Then the closed-loop system is robustly stable *iff*

$$\bar{\sigma}\left[\hat{M}(j\omega)\right] < \frac{1}{\hat{\delta}(\omega)}, \quad \forall\omega \in \mathcal{R}$$

□

3.7 Two Examples

The singular-value approach is very useful for robust stability analysis if the uncertainty of the plant is completely unstructured and norm-bounded. In practice, however, both structured and unstructured information is often available on the plant uncertainty. Consider a process plant with servo-controlled valves [Mac89]. We know that the uncertainty for each valve is not likely to directly affect the others. If there are two such valves, a correct description of the multiplicative input uncertainty of the process plant is

$$\Delta := \begin{bmatrix} \delta_1 & 0 \\ 0 & \delta_2 \end{bmatrix}, \quad |\delta_i| \leq 0.1, \; i = 1, 2$$

But when we write $\bar{\sigma}(\Delta) \leq 0.1$, we lose all the structural information, since this description also allows perturbations such as

$$\Delta = \frac{1}{2}\begin{bmatrix} 0.1 & 0.1 \\ 0.1 & 0.1 \end{bmatrix}$$

and

$$\Delta = \begin{bmatrix} 0 & 0 \\ 0.1 & 0 \end{bmatrix}$$

which do not correspond to any real physical perturbation. Therefore the use of the singular-value approach for robust stability analysis generally leads to compensator designs which are unnecessarily conservative when the plant error model is structured.

Let us consider the following two examples [Lun84].

Example 3.7-1 (A Two Independent Loop System): Consider a perturbed plant which consists of two independent loops, shown in Figure 3.17. The transfer function matrices of nominal plant and controller are

$$G_0(s) = \begin{bmatrix} g_1(s) & 0 \\ 0 & g_2(s) \end{bmatrix}$$

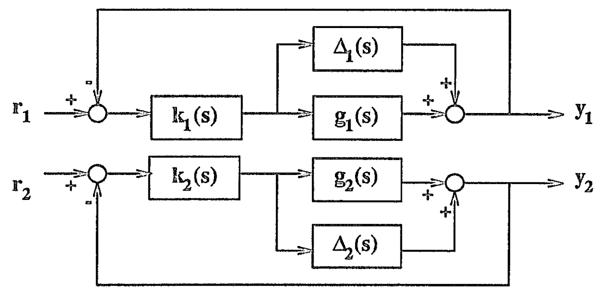

Figure 3.17: Block diagram of a system of two independent loops.

and

$$K(s) = \begin{bmatrix} k_1(s) & 0 \\ 0 & k_2(s) \end{bmatrix}$$

The matrix of stable additive model uncertainties is

$$\Delta(s) = \begin{bmatrix} \Delta_1(s) & 0 \\ 0 & \Delta_2(s) \end{bmatrix}, \quad \bar{\sigma}[\Delta_i(j\omega)] \leq \delta_i(\omega) \ , \quad i = 1,2 \ \ \forall \omega \in \mathcal{R}$$

Assume that the system is nominally stable, then the closed-loop system is robustly stable if the two independent inequalities

$$\left| \frac{k_i}{1 + g_i k_i} \right| < \frac{1}{\delta_i} \ , \quad i = 1,2 \quad \forall \omega \in \mathcal{R}$$

are satisfied for all s in the Nyquist contour.

In contrast to this result the singular-value approach yields

$$M = (I + KG_0)^{-1} K = \begin{bmatrix} \frac{k_1}{1+g_1 k_1} & 0 \\ 0 & \frac{k_2}{1+g_2 k_2} \end{bmatrix}$$

and the sufficient condition

$$\bar{\sigma}[M] < \frac{1}{\bar{\sigma}[\Delta]}, \quad \forall \omega \in \mathcal{R}$$

for robust stability implies

$$\max \left\{ \left| \frac{k_1}{1 + g_1 k_1} \right|, \left| \frac{k_2}{1 + g_2 k_2} \right| \right\} < \frac{1}{\max\{\delta_1, \delta_2\}}, \quad \forall \omega \in \mathcal{R}$$

But this condition might be very conservative for a large value of δ_i !

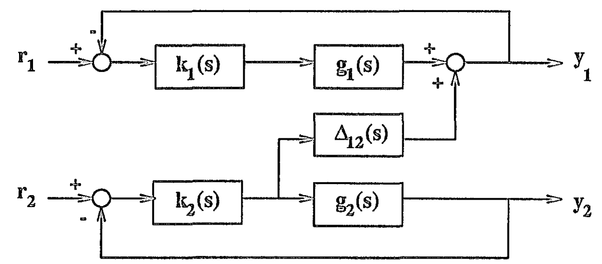

Figure 3.18: A simple coupling system.

Example 3.7-2 (A Simple Coupling System): Consider a closed-loop control system, shown in Figure 3.18, with perturbed plant $G_p(s)$ and controller $K(s)$

$$G_p(s) = \begin{bmatrix} g_1(s) & \Delta_{12}(s) \\ 0 & g_2(s) \end{bmatrix}, \quad \text{with } \bar{\sigma}[\Delta_{12}] \leq \delta, \quad \forall \omega \in \mathcal{R}$$

$$K(s) = \begin{bmatrix} k_1(s) & 0 \\ 0 & k_2(s) \end{bmatrix}$$

Clearly

$$G_0(s) = \begin{bmatrix} g_1(s) & 0 \\ 0 & g_2(s) \end{bmatrix}$$

and

$$\Delta(s) = \begin{bmatrix} 0 & \Delta_{12}(s) \\ 0 & 0 \end{bmatrix}, \quad \bar{\sigma}[\Delta] = \bar{\sigma}[\Delta_{12}] \leq \delta$$

Consider the nominal system

$$M = (I + KG_0)^{-1}K = \begin{bmatrix} \frac{k_1}{1+g_1k_1} & 0 \\ 0 & \frac{k_2}{1+g_2k_2} \end{bmatrix}$$

and assume that $M(s)$ and the perturbation $\Delta(s)$ are stable. Then the sufficient condition

$$\bar{\sigma}[M] < \frac{1}{\bar{\sigma}[\Delta]}, \quad \forall \omega \in \mathcal{R}$$

for robust stability implies

$$\max\left\{\left|\frac{k_1}{1+g_1k_1}\right|,\left|\frac{k_2}{1+g_2k_2}\right|\right\}<\frac{1}{\delta},\quad \forall\omega\in\mathcal{R}$$

This is ridiculous, because from Mason's gain formula the uncertainty $\Delta_{12}(s)$ does not even affect the stability of the closed-loop system. Thus, the degree of conservatism is arbitrarily large !

3.8 Structured Singular Value (SSV)

A real system is always different from its "idealized" mathematical model. This is of crucial significance because modelling errors and exogenous disturbances can seriously affect the stability and performance of a feedback system. Generally speaking, there are two types of uncertainties: unstructured and structured. Unstructured uncertainties include unmodelled or neglected high frequency dynamics (complex uncertainties) in the system, e.g. unmodelled lags, parasitic coupling, hysteresis, resonance, and so on. All uncertainties occurring in different parts of the system which are lumped into one single norm bounded perturbation Δ are also referred to as unstructured uncertainty. On the other hand, some uncertainties affect the low frequency range; for example, sensor or actuator failures, and real parameter variations (called parametric uncertainties) caused by movement of the operating point. Quantitatively these uncertainties might be described by intervals of possible parameter values. From an engineering point of view, structured uncertainties of a plant are the most realistic. Unfortunately, when the plant error model is structured, the standard singular value approach to robust stability analysis may lead to controller designs which are unnecessarily conservative. To remedy this problem, in 1982 Doyle proposed and developed the concept of the structured singular value (SSV) which is a less conservative indicator of stability robustness [Doy82] [DWS82] [Doy84].

Consider the interconnected system shown in Figure 3.19. We can rearrange the block diagram into the standard form of Figure 3.20 , called the $M-\Delta$ structure, by absorbing into M the weighting functions used to model the uncertainty. Δ

is a block diagonal matrix and M is a $FDLTI$ interconnection matrix. Note that M_{22} is the transfer function of nominal performance (with $\Delta = 0$). Figure 3.20 is the format required for μ-analysis. $\Delta_i(s)$ is assumed to be stable with $\bar{\sigma}[\Delta_i(j\omega)] \leq 1$, $\forall i$. For a discussion of situation when an individual perturbation may be unstable see [FoP88].

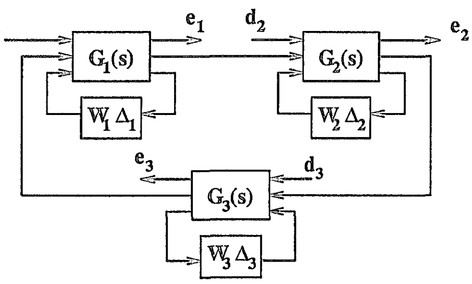

Figure 3.19: An interconnection system.

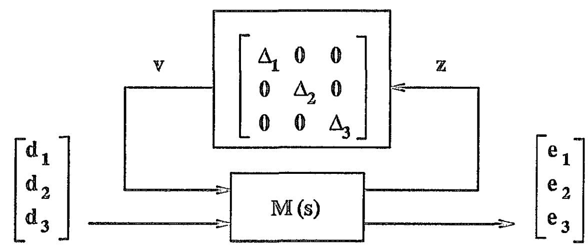

Figure 3.20: $M - \Delta$ structure.

Example 3.8-1: It is interesting to consider an uncertain model of a one-mode flexible structure having the transfer function

$$G(s) = \frac{\omega_n^2}{s^2 + 2\zeta\omega_n s + \omega_n^2} \tag{3.60}$$

where ζ and ω_n are the damping ratio and natural frequency respectively with the parametric uncertainties

$$\zeta = \zeta_o + \Delta_\zeta \tag{3.61}$$

$$\omega_n = \omega_{n_o} + \Delta_{\omega_n} \tag{3.62}$$

ζ_0 and ω_{n_0} represent the nominal values of ζ and ω_n, respectively. From classical control it is not easy to design a proper notch filter to catch up with ω_n because of the uncertainty in ω_n. Therefore the bandwidth of the closed-loop system is restricted to be within $\omega_{n_0}/2$, to roll off the magnitude of the frequency response near ω_{n_0}, when the damping ratio is quite small. Now let us show how to format $G(s)$ into the $M-\Delta$ structure suitable for μ-analysis. A little thought reveals that $G(s)$ is equivalent to the closed-loop transfer function, from input u to output y, of a unity feedback system with forward path transfer function

$$\frac{\omega_n^2}{s(s+2\zeta\omega_n)} \tag{3.63}$$

as shown in Figure 3.21. Moreover Figure 3.21 can be decomposed into Figure 3.22 which is equivalent to Figure 3.23 with parametric uncertainties Δ_ζ and Δ_{ω_n} as in (3.61) and (3.62). Then the block diagram of Figure 3.23 can be rearranged into the standard $M-\Delta$ structure in Figure 3.24 where the block diagonal uncertainty structure is

$$\Delta = \begin{bmatrix} \Delta_{\omega_n} & 0 & 0 \\ 0 & \Delta_{\omega_n} & 0 \\ 0 & 0 & \Delta_\zeta \end{bmatrix} \tag{3.64}$$

and

$$M = \frac{1}{s^2+2\zeta_0\omega_{n_0}s+\omega_{n_0}^2}\begin{bmatrix} -\omega_{n_0} & -s^2 & 2\omega_n s & s^2 \\ 1 & -\omega_{n_0}-2\zeta_0 s & -2s & \omega_{n_0} \\ \omega_{n_0} & 1 & -2\omega_{n_0}s & \omega_{n_0}^2 \\ \omega_{n_0} & 1 & -2\omega_{n_0}s & \omega_{n_0}^2 \end{bmatrix} \tag{3.65}$$

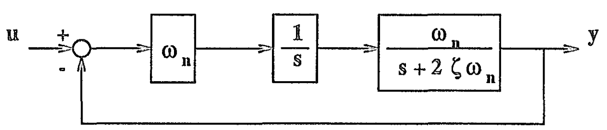

Figure 3.21: A perturbed one-mode flexible structure.

Note that there are two repeated Δ_{ω_n}'s in Δ. This results from the fact that the transfer function $G(s)$ in (3.60) cannot be expressed as a bilinear transformation of ω_n.

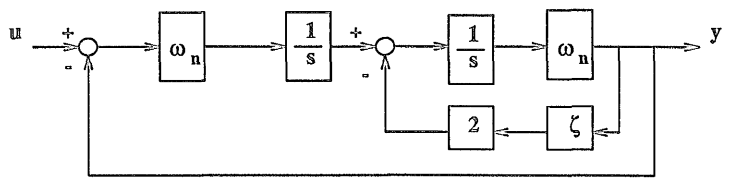

Figure 3.22: An equivalent one-mode flexible structure.

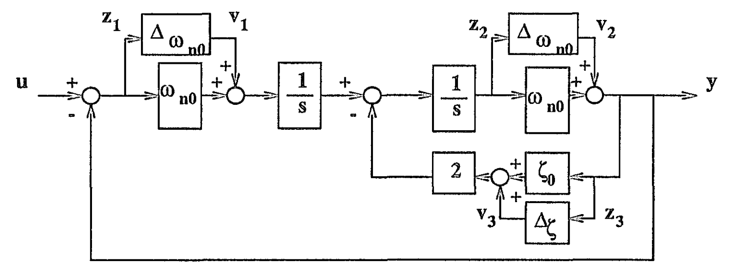

Figure 3.23: An equivalent one-mode flexible structure.

To define the structured singular value $\mu_{\Delta}(M)$, let M be an $n \times n$ complex-valued matrix, $M \in \mathcal{C}^{n \times n}$, and let $\mathbf{\Delta}$ be an underlying structure which involves specifying three things: the type of each block, the total number of blocks and their dimensions. There are two types of blocks: repeated scalar and full blocks. Two integers, s and f, represent the number of repeated scalar blocks and the number of full blocks, respectively. Now we define

$$\mathbf{\Delta} = \left\{ \text{diag}\left[\delta_1 I_{r_1}, \cdots, \delta_s I_{r_s}, \Delta_1, \cdots, \Delta_f\right] : \delta_i \in \mathcal{C},\ \Delta_j \in \mathcal{C}^{m_j \times m_j} \right\} \tag{3.66}$$

and its bounded subset:

$$\mathbf{B\Delta} = \{\Delta : \bar{\sigma}(\Delta) \leq 1,\ \Delta \in \mathbf{\Delta}\}$$

where

$$\sum_{i=1}^{s} r_i + \sum_{j=1}^{f} m_j = n$$

The full blocks in (3.66) do not need to be square, but restricting them as such saves a great deal in terms of notation. The μ-toolbox of MATLAB can handle nonsquare full blocks [BDGPS91].

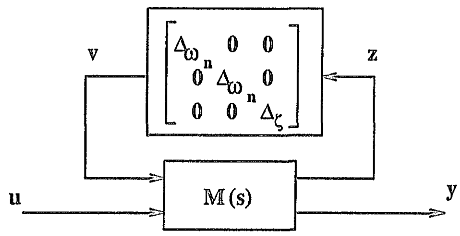

Figure 3.24: $M - \Delta$ structure of Example 3.8-1.

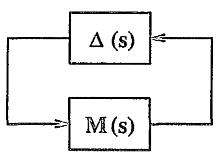

Figure 3.25: $M - \Delta$ structure.

Consider the $M - \Delta$ structure (with zero input) of the feedback system shown in Figure 1.25. Assume $\Delta(s)$ is a stable structured uncertainty and $M(s)$ is a stable nominal system (with $\Delta = 0$). Then it is well known that the stability of the closed-loop system is determined by $\det[I - M(s)\Delta(s)]$. A little thought reveals that as the size of the uncertainty Δ increases, some part of the Nyquist plot of $\det[I - M(s)\Delta(s)]$ might pass through the origin, as s traverses the Nyquist contour. In this situation, there exists some frequency ω_0 such that $\det[I - M(j\omega_0)\Delta(j\omega_0)] = 0$ (i.e. $[I - M(j\omega_0)\Delta(j\omega_0)]$ is singular). This implies that there indeed exists a minimum size $\bar{\sigma}(\Delta)$ of Δ needed to make $[I - M(j\omega_0)\Delta(j\omega_0)]$ singular. Recall that for any fixed frequency ω, $M(j\omega)$ is a complex-value matrix. This motivates the following definition.

Definition 3.8-1 (Structured Singular Value: SSV): For $M \in \mathcal{C}^{n \times n}$, the structured singular value $\mu_\Delta(M)$ of M with respect to $\mathbf{\Delta}$ is the number defined such that $\mu_\Delta^{-1}(M)$ is equal to the smallest $\bar{\sigma}(\Delta)$ needed to make $(I - M\Delta)$ singular. That is

$$\mu_\Delta^{-1}(M) := \min_{\Delta \in \mathbf{\Delta}} \left\{ \bar{\sigma}(\Delta) : \det(I - M\Delta) = 0 \right\} \tag{3.67}$$

If no $\Delta \in \mathbf{\Delta}$ such that $\det(I - M\Delta) = 0$, then $\mu_\Delta(M) := 0$. ◻

Example 3.8-2: Given

$$\begin{aligned} M &= \begin{bmatrix} m_{11} & m_{12} \\ m_{21} & m_{22} \end{bmatrix}, \quad \text{with} \quad \det M = 0, \; M \in C^{2\times 2}; \text{ and} \\ \Delta &= \begin{bmatrix} \Delta_1 & 0 \\ 0 & \Delta_2 \end{bmatrix} \end{aligned}$$

then

$$\det(I - M\Delta) = 1 - m_{11}\Delta_1 - m_{22}\Delta_2$$

and hence

$$\begin{aligned} \det(I - M\Delta) = 0 &\iff 1 - m_{11}\Delta_1 - m_{22}\Delta_2 = 0 \\ &\Longrightarrow |m_{11}| \cdot |\Delta_1| + |m_{22}| \cdot |\Delta_2| \geq 1 \\ &\Longrightarrow \bar{\sigma}(\Delta) = \max\{|\Delta_1|, |\Delta_2|\} \geq \frac{1}{|m_{11}| + |m_{22}|} \qquad (3.68) \\ &\Longrightarrow \frac{1}{|m_{11}| + |m_{22}|} \text{ is a lower bound of } \bar{\sigma}(\Delta) \qquad (3.69) \end{aligned}$$

Inequality (3.68) follows from

$$1 \leq |m_{11}| \cdot |\Delta_1| + |m_{22}| \cdot |\Delta_2| \leq (|m_{11}| + |m_{22}|) \cdot \max\{|\Delta_1|, |\Delta_2|\}$$

Choose

$$\Delta_1 = \frac{e^{-j\angle m_{11}}}{|m_{11}| + |m_{22}|}, \text{ and } \Delta_2 = \frac{e^{-j\angle m_{22}}}{|m_{11}| + |m_{22}|} \qquad (3.70)$$

then

$$\begin{aligned} 1 - m_{11}\Delta_1 - m_{22}\Delta_2 = 0, \quad \text{and} \\ \bar{\sigma}(\Delta) = \max\{|\Delta_1|, |\Delta_2|\} = \frac{1}{|m_{11}| + |m_{22}|} \qquad (3.71) \end{aligned}$$

and combining (3.69) and (3.71) gives

$$\min_{\Delta \in \mathbf{\Delta}} \bar{\sigma}(\Delta) = \frac{1}{|m_{11}| + |m_{22}|}, \quad \text{such that } \det(I - M\Delta) = 0$$

This implies that $\mu_{\mathbf{\Delta}}(M) = |m_{11}| + |m_{22}|$ by the definition of the *SSV*.

In much of what follows we will neglect the subscript $\mathbf{\Delta}$ of $\mu_{\mathbf{\Delta}}(M)$ for brevity.

The reciprocal of the structured singular value is a frequency dependent stability margin, k_m [Saf82] [DeS88], with respect to the uncertainty $\Delta \in \mathbf{\Delta}$, and a nominally stable feedback system will be robustly stable against all uncertainties in the set $\mathbf{B\Delta}$ if and only if $\mu[M(j\omega)] < 1$, $\forall\omega$. This definition tells us that if M is easily destabilized, then $\mu(M)$ is large, and vice-versa. Since M is frequency dependent $\mu(M)$ must be calculated for "each" frequency.

It is clear that for any $\Delta \in \mathbf{\Delta}$, there exists ϵ such that $\Delta = \epsilon\Delta'$, with $\Delta' \in \mathbf{B\Delta}$, namely $\bar{\sigma}(\Delta') \leq 1$. Therefore directly following from the definition of the SSV, an alternative expression for $\mu^{-1}(M)$ is given by

$$\begin{aligned}
\mu^{-1}(M) &= \min\{\bar{\sigma}(\Delta) : \Delta \in \mathbf{\Delta},\ \det(I - M\Delta) = 0\} \\
&= \min\{|\epsilon| : \Delta \in \mathbf{B\Delta},\ \det(I - \epsilon M\Delta) = 0\} \\
&= \min\left\{|\epsilon| : \Delta \in \mathbf{B\Delta},\ \det(\frac{1}{\epsilon}I - M\Delta) = 0\right\} \\
&= \min\left\{|\epsilon| : \Delta \in \mathbf{B\Delta},\ \frac{1}{\epsilon} = \lambda_i(M\Delta)\right\}
\end{aligned}$$

Thus

$$\begin{aligned}
\mu(M) &= \max\left\{\frac{1}{|\epsilon|} : \Delta \in \mathbf{B\Delta},\ \frac{1}{\epsilon} = \lambda_i(M\Delta)\right\} \\
&= \max_{\Delta\in\mathbf{B\Delta}} \max_i \{|\lambda_i(M\Delta)|\} \\
&= \max_{\Delta\in\mathbf{B\Delta}} \rho(M\Delta)
\end{aligned}$$

where $\rho(M\Delta)$ denotes the spectral radius of the square matrix $(M\Delta)$. This leads to the following lemma [BDGPS91].

Lemma 3.8-1: $\mu(M) = \max_{\Delta\in\mathbf{B\Delta}} \rho(M\Delta)$ □

Furthermore the matrix function μ has the following properties:

- $\mu(\alpha M) = |\alpha| \cdot \mu(M)$
- $\det(I - M\Delta) \neq 0,\ \forall\Delta \in \mathbf{B\Delta} \Longleftrightarrow \mu(M) < 1$
- if $\mathbf{\Delta} = \{\delta I_n :\ \delta \in \mathcal{C}\}$ $(s = 1, f = 0;\ r_1 = n) \Longrightarrow \mu(M) = \rho(M)$ (3.72)
- if $\mathbf{\Delta} = \mathcal{C}^{n\times n}$ $(s = 0, f = 1;\ m_1 = n) \Longrightarrow \mu(M) = \bar{\sigma}(M)$ (3.73)

where I_n denotes the identity matrix with dimension $n \times n$. (3.72) and (3.73) together imply the following theorem [Doy82].

Theorem 3.8-1: $\rho(M) \leq \mu(M) \leq \bar{\sigma}(M)$ □

These bounds are not practical for our purposes because the gap between $\rho(M)$ and $\bar{\sigma}(M)$ can be arbitrarily large. However, they can be refined by considering transformations on M that do not affect $\mu(M)$, but do affect $\rho(M)$ and $\bar{\sigma}(M)$. Let

$$\mathbf{U} := \{U : U = \text{diag}\,[U_1, \cdots, U_n],\ U_i^* U_i = I,\ U \in \mathbf{\Delta}\}$$

and

$$\mathbf{D} := \left\{D : D = \text{diag}\,[D_1, \cdots, D_s, d_1 I_{m_1}, \cdots, d_f I_{m_f}],\ D_i \in C^{r_i \times r_i},\ D_i = D_i^* > 0,\ d_i > 0\right\}$$

where the matrix sets $\mathbf{U}$ and $\mathbf{D}$ match the structure of $\mathbf{\Delta}$. Obviously $\mathbf{U}$ is a diagonal structure of unitary matrices and D commutes with Δ, for all $D \in \mathbf{D}$ and $\Delta \in \mathbf{\Delta}$. It is easy to check that all three structures shown in Figures 3.26, 3.27 and 3.28 are equivalent. Furthermore, it is useful to note that $\mathbf{U}$ and $\mathbf{D}$ leave $\mathbf{\Delta}$ invariant in the sense that

- $U \in \mathbf{U}$ and $\Delta \in \mathbf{\Delta} \Longrightarrow U^* \in \mathbf{U}$ and $U^*\Delta \in \mathbf{\Delta}$, with $\bar{\sigma}(U^*\Delta) = \bar{\sigma}(\Delta)$
- $D \in \mathbf{D}$ and $\Delta \in \mathbf{\Delta} \Longrightarrow D\Delta D^{-1} = \Delta \Longrightarrow D\Delta D^{-1} \in \mathbf{\Delta}$, with $\bar{\sigma}(D\Delta D^{-1}) = \bar{\sigma}(\Delta)$

Theorem 3.8-1 and the above facts imply that

$$\rho(MU) \leq \mu(MU) = \mu(M) = \mu(DMD^{-1}) \leq \bar{\sigma}(DMD^{-1}) \qquad (3.74)$$

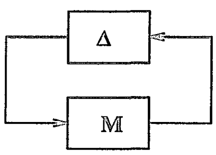

Figure 3.26: $M - \Delta$ structure.

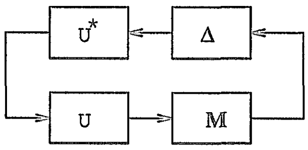

Figure 3.27: $M - \Delta$ structure with $U \in \mathbf{U}$.

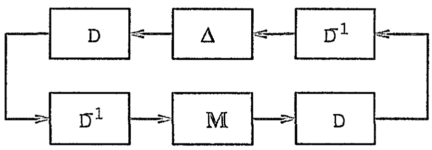

Figure 3.28: $M - \Delta$ structure with $D \in \mathbf{D}$.

The equality $\mu(M) = \mu(DMD^{-1})$ means that the structured singular value of M with respect to $\mathbf{\Delta}$ is invariant under diagonal scaling. The consequence of (3.74) leads to the following theorem [Doy82].

Theorem 3.8-2: $\max_{U\in\mathbf{U}} \rho(MU) \leq \mu(M) \leq \inf_{D\in\mathbf{D}} \bar{\sigma}(DMD^{-1})$ ◻

This theorem provides the tighter upper and lower bounds on $\mu(M)$. Mathematically $\inf_{D\in\mathbf{D}} \bar{\sigma}(DMD^{-1})$ denotes the least upper bound of $\bar{\sigma}(DMD^{-1})$ for $\forall D \in \mathbf{D}$. In [Doy82] Doyle proved that the lower bound is actually an equality:

$$\max_{U\in\mathbf{U}} \rho(MU) = \mu(M)$$

Unfortunately, this optimization problem is not convex. $\rho(MU)$ can have multiple local maxima which are not global and so direct computation of $\max_{U\in\mathbf{U}} \rho(MU)$ by gradient search might not find the actual maximum.

Example 3.8-3: Consider $\Delta = \text{diag}\,\{\Delta_1, \Delta_2, \Delta_3\}$, and

$$M = \begin{bmatrix} 0 & 0 & \omega_0 \\ \omega_p & \omega_p & -\omega_p \\ c_n & c_n & 0 \end{bmatrix}$$

taken from [SkM88].

Let $U = \text{diag}\left\{e^{j\theta_1}, e^{j\theta_2}, e^{j\theta_3}\right\} \in \mathbf{U}$. The algebraic manipulation gives the characteristic equation of MU as

$$\lambda\left\{\lambda^2 - \omega_p e^{j\theta_2}\lambda + \left[c_n\omega_p e^{j(\theta_2+\theta_3)} - c_n\omega_0 e^{j(\theta_1+\theta_3)}\right]\right\} = 0$$

The roots of the above equation are $\lambda = 0$ and

$$\lambda = \frac{1}{2}\left[\omega_p e^{j\theta_2} \pm \sqrt{\omega_p^2 e^{j2\theta_2} - 4c_n\omega_p e^{j(\theta_2+\theta_3)} + 4c_n\omega_0 e^{j(\theta_1+\theta_3)}}\right] \tag{3.75}$$

Now

$$\mu(M) = \max_{U\in\mathbf{U}} \rho(MU) = \max_{\theta_i} \left|\bar{\lambda}(MU)\right| \tag{3.76}$$

which suggests we take the positive sign in (1.75) and set

$$\omega_p e^{j\theta_2} = |\omega_p| \implies \angle\omega_p + \theta_2 = 0 \tag{3.77}$$

$$\omega_p^2 e^{j2\theta_2} = |\omega_p^2| \implies 2\angle\omega_p + 2\theta_2 = 0 \tag{3.78}$$

$$-4c_n\omega_p e^{j(\theta_2+\theta_3)} = 4|c_n\omega_p| \implies \angle c_n + \angle\omega_p + (\theta_2+\theta_3) = \pi \tag{3.79}$$

$$4c_n\omega_0 e^{j(\theta_1+\theta_3)} = 4|c_n\omega_0| \implies \angle c_n + \angle\omega_0 + (\theta_1+\theta_3) = 0 \tag{3.80}$$

It is easy to check that the solution $\theta_2 = -\angle\omega_p$, $\theta_3 = \pi - \angle c_n$ and $\theta_1 = -(\angle\omega_0 + \pi)$ satisfies the simultaneous equations (1.77)-(1.80). Therefore (1.76) gives

$$\mu(M) = \frac{1}{2}\left[|\omega_p| + \sqrt{|\omega_p|^2 + 4|c_n|\left(|\omega_p| + |\omega_0|\right)}\right]$$

On the other hand, the upper bound of $\mu(M)$ is more easily found since $\bar{\sigma}(DMD^{-1})$ is convex in $\ln D$ [Doy87] [SeO90]. Unfortunately, the upper bound is not always equal to $\mu(M)$. It can be shown that

$$\mu(M) = \inf_{D\in\mathbf{D}} \bar{\sigma}(DMD^{-1}), \quad \text{if} \quad 2s + f \leq 3 \tag{3.81}$$

The problem of $\mu(M)$ is hence reduced to an optimal diagonal scaling problem. Most algorithms for computing the structured singular value actually compute this upper bound, which Doyle has conjectured, is always within 15% of the true value of $\mu(M)$. The lower bound can then be used to check the closeness of $\bar{\sigma}(DMD^{-1})$ to $\mu(M)$.

Remark: The definition of $\mathbf{D}$ shows that $D_i > 0$ and $d_i > 0$. The reason can be explained briefly as follows. It is well known that any complex matrix D can be represented in the polar form [LaT85]

$$D = UH$$

where $H \geq 0$, is a positive semidefinite Hermitian matrix, and U is a unitary matrix. Since the maximum singular value is invariant under unitary transformation, this implies

$$\bar{\sigma}(DMD^{-1}) = \bar{\sigma}(UHMH^{-1}U^{*}) = \bar{\sigma}(HMH^{-1}), \quad H > 0 \tag{3.82}$$

assuming D is invertible, and so only positive Hermitian matrices are needed to define the matrix set $\mathbf{D}$.

Example 3.8-4: For the *MIMO* case, consider

$$M = \begin{bmatrix} 0 & M_{12} \\ M_{21} & 0 \end{bmatrix} \quad \text{and} \quad \Delta = \begin{bmatrix} \Delta_1 & 0 \\ 0 & \Delta_2 \end{bmatrix}$$

Both M_{12} and M_{21} are matrices. Since Δ has just two non-repeated uncertainty blocks, (3.81) holds. Let $D = \text{diag}\{I, dI\}$, $d > 0$, then

$$DMD^{-1} = \begin{bmatrix} 0 & d^{-1}M_{12} \\ dM_{21} & 0 \end{bmatrix}$$

Choose a permutation matrix

$$P = \begin{bmatrix} 0 & I \\ I & 0 \end{bmatrix}$$

which is also a unitary matrix. This leads to

$$\begin{aligned} \bar{\sigma}(DMD^{-1}) &= \bar{\sigma}(PDMD^{-1}) = \bar{\sigma}\left(\begin{bmatrix} dM_{21} & 0 \\ 0 & d^{-1}M_{12} \end{bmatrix}\right) \\ &= \max\left\{d\bar{\sigma}(M_{21})\ ,\ d^{-1}\bar{\sigma}(M_{12})\right\} \end{aligned}$$

Thus

$$\begin{aligned} \mu(M) &= \inf_{D \in \mathbf{D}} \bar{\sigma}(DMD^{-1}) \\ &= \inf_{d>0}\ \max\left\{d\bar{\sigma}(M_{21})\ ,\ d^{-1}\bar{\sigma}(M_{12})\right\} && (3.83) \\ &= \sqrt{\bar{\sigma}(M_{12})\bar{\sigma}(M_{21})} && (3.84) \end{aligned}$$

The solution d for the min-max optimization problem in (3.83) can be obtained by setting $d\bar{\sigma}(M_{21}) = d^{-1}\bar{\sigma}(M_{12})$.

Example 3.8-5: Let

$$M = \begin{bmatrix} m_{11} & m_{12} \\ m_{21} & m_{22} \end{bmatrix} \in \mathcal{C}^{2\times 2}, \quad \text{and} \quad \Delta = \begin{bmatrix} \Delta_1 & 0 \\ 0 & \Delta_2 \end{bmatrix}$$

Choose $D = \operatorname{diag}\{1, \tilde{d}\}$, $\tilde{d} > 0$. Let $N := (DMD^{-1})^*(DMD^{-1})$, then the characteristic equation of N is

$$\lambda^2 - (\operatorname{tr} N)\lambda + \det N = 0 \tag{3.85}$$

where $\operatorname{tr} N$ denotes the trace of N. It follows that

$$\bar{\lambda} + \underline{\lambda} = \operatorname{tr} N \tag{3.86}$$

$$\bar{\lambda} \cdot \underline{\lambda} = \det N \tag{3.87}$$

where $\bar{\lambda}$ and $\underline{\lambda}$ denote, respectively, the maximum and minimum roots of equation (1.85). Differentiating both sides in (1.86) and (1.87) with respect to $\tilde{d}$, and noting that $\det N = |\det(DMD^{-1})|^2 = |\det M|^2$ is independent of $\tilde{d}$ yields

$$\frac{\mathrm{d}\bar{\lambda}}{\mathrm{d}\tilde{d}} + \frac{\mathrm{d}\underline{\lambda}}{\mathrm{d}\tilde{d}} = \frac{\mathrm{d}(\operatorname{tr} N)}{\mathrm{d}\tilde{d}}$$
$$\frac{\mathrm{d}\bar{\lambda}}{\mathrm{d}\tilde{d}} \cdot \underline{\lambda} + \bar{\lambda} \cdot \frac{\mathrm{d}\underline{\lambda}}{\mathrm{d}\tilde{d}} = 0$$

It follows that

$$\frac{\mathrm{d}\bar{\lambda}}{\mathrm{d}\tilde{d}} = 0 \Longleftrightarrow \frac{\mathrm{d}(\operatorname{tr} N)}{\mathrm{d}\tilde{d}} = 0, \quad \bar{\lambda} \neq \underline{\lambda} \tag{3.88}$$

Since $\operatorname{tr} N = \operatorname{tr}\,[(DMD^{-1})^*(DMD^{-1})] = \|DMD^{-1}\|_F^2$, with $\|\bullet\|_F$ denoting the Frobenius norm, we have

$$\frac{\mathrm{d}(\operatorname{tr} N)}{\mathrm{d}\tilde{d}} = 0 \Longrightarrow \tilde{d} = \sqrt{\frac{|m_{12}|}{|m_{21}|}} \tag{3.89}$$

Manipulation then leads to

$$\mu(M) = \inf_{\tilde{d}>0} \bar{\sigma}(DMD^{-1}) = \bar{\sigma}\left\{\begin{bmatrix} m_{11} & \sqrt{\frac{|m_{21}|}{|m_{12}|}} \cdot m_{12} \\ \sqrt{\frac{|m_{12}|}{|m_{21}|}} \cdot m_{21} & m_{22} \end{bmatrix}\right\} \tag{3.90}$$

$$= \left\{\frac{k + \sqrt{k^2 - 4|m_{11}m_{22} - m_{12}m_{21}|^2}}{2}\right\}^{1/2} \tag{3.91}$$

with

$$k := |m_{11}|^2 + |m_{22}|^2 + 2|m_{12}m_{21}| \tag{3.92}$$

It is interesting to note that:

∘ (1) the anti-diagonal elements of (DMD^{-1}) in (3.90) have the same modulus.

∘ (2) if $m_{12} = 0$ or $m_{21} = 0$, then

$$\mu(M) = \max\{|m_{11}|, |m_{22}|\}$$

∘ (3) if $m_{11} = 0$ and $m_{22} = 0$, then

$$\mu(M) = \sqrt{|m_{12}| \cdot |m_{21}|}$$

∘ (4) if $\det M = 0$, i.e. $m_{11}m_{22} = m_{12}m_{21}$, then

$$\mu(M) = |m_{11}| + |m_{22}| \tag{3.93}$$

which coincides with $\mu(M)$ in Example 3.8-2.

μ-Computation : (Osborne's Method) Gradient search techniques can be used to minimize $\bar{\sigma}(DMD^{-1})$. However it becomes complicated by the fact that $\bar{\sigma}(DMD^{-1})$ is not always differentiable at a "cusp" of repeated maximum singular values. The alternative diagonal scaling approach of Osborne is fast and efficient. In 1960, Osborne developed an iterative scheme to minimize $\|DMD^{-1}\|_F$, [Osb60]. Based on the fact that $\|\bullet\|_F$ and $\bar{\sigma}(\circ)$ are equivalent norms [MoZ89]:

$$\frac{1}{\sqrt{n}}\left\|DMD^{-1}\right\|_F \leq \bar{\sigma}(DMD^{-1}) \leq \left\|DMD^{-1}\right\|_F \tag{3.94}$$

where n is the dimension of (DMD^{-1}). The minimization of $\|DMD^{-1}\|_F$ usually yields very good approximations for the optimal D which minimizes $\bar{\sigma}(DMD^{-1})$. Mathematically the Frobenius norm is defined as

$$\|A\|_F^2 := \sum_{i=1}^{n}\sum_{j=1}^{n}|a_{ij}|^2 = \mathrm{tr}\,(A^*A) \tag{3.95}$$

and inequality (3.94) follows directly from the fact that A^*A is positive semidefinite (i.e. $\lambda_i(A^*A) \geq 0$); and

$$\begin{aligned}\bar{\sigma}(A)^2 &= \bar{\lambda}(A^*A) \leq \sum_{i=1}^{n}\lambda_i(A^*A) = \mathrm{tr}\,(A^*A) \\ &= \|A\|_F^2 = \sum_{i=1}^{n}\lambda_i(A^*A) \leq n\bar{\lambda}(A^*A) = n\bar{\sigma}(A)^2\end{aligned} \tag{3.96}$$

That is,

$$\bar{\sigma}(A)^2 \le \|A\|_F^2 \le n\bar{\sigma}(A)^2 \tag{3.97}$$

which is equivalent to (3.94).

For simplicity, suppose $M \in \mathcal{C}^{3\times 3}$ and $D = \mathrm{diag}\{1, d_1, d_2\},\ d_1 > 0,\ d_2 > 0,$ then

$$DMD^{-1} = \begin{bmatrix} m_{11} & m_{12}d_1^{-1} & m_{13}d_2^{-1} \\ m_{21}d_1 & m_{22} & m_{23}d_1d_2^{-1} \\ m_{31}d_2 & m_{32}d_2d_1^{-1} & m_{33} \end{bmatrix} \tag{3.98}$$

and

$$\begin{aligned} \left\|DMD^{-1}\right\|_F^2 &= \left(|m_{21}|^2 + |m_{23}d_2^{-1}|^2\right) d_1^2 + \left(|m_{12}|^2 + |m_{32}d_2|^2\right) d_1^{-2} + \\ &\quad \left(|m_{11}|^2 + |m_{22}|^2 + |m_{33}|^2 + |m_{31}d_2|^2 + |m_{13}d_2^{-1}|^2\right) \\ &=: \beta_1 d_1^2 + \gamma_1 d_1^{-2} + \alpha_1 \end{aligned} \tag{3.99}$$

or

$$\begin{aligned} \left\|DMD^{-1}\right\|_F^2 &= \left(|m_{31}|^2 + |m_{32}d_1^{-1}|^2\right) d_2^2 + \left(|m_{13}|^2 + |m_{23}d_1|^2\right) d_2^{-2} + \\ &\quad \left(|m_{11}|^2 + |m_{22}|^2 + |m_{33}|^2 + |m_{21}d_1|^2 + |m_{12}d_1^{-1}|^2\right) \\ &=: \beta_2 d_2^2 + \gamma_2 d_2^{-2} + \alpha_2 \end{aligned} \tag{3.100}$$

where $\beta_i,\ \gamma_i,\ \alpha_i$ are independent of d_i, for $i = 1, 2$. Then taking $\frac{\partial}{\partial d_1}\|DMD^{-1}\|_F^2$ in (3.99) and $\frac{\partial}{\partial d_2}\|DMD^{-1}\|_F^2$ in (3.100) to minimize the $\|DMD^{-1}\|_F^2$ with respect to d_1 and d_2, respectively, yields

$$\begin{aligned} \frac{\partial}{\partial d_i}\left\|DMD^{-1}\right\|_F^2 &= 2\beta_i d_i - 2\gamma_i d_i^{-3} = 0 \\ \Longrightarrow d_i &= \left(\frac{\gamma_i}{\beta_i}\right)^{1/4}, \qquad i = 1, 2 \end{aligned} \tag{3.101}$$

The optimal D is determined iteratively to find:

$$\min_{d_i > 0} \left\|DMD^{-1}\right\|_F^2 \tag{3.102}$$

Osborne's algorithm can be summarized as follows:

Step 1: Start with some initial guesses for d_i, e.g. $D = I$, for $k = 0$.

Step 2: Find β_i and γ_i from $\|DMD^{-1}\|_F^2$, $i = 1, 2$.

Step 3: Let $d_i = \left(\frac{\gamma_i}{\beta_i}\right)^{1/4}, \quad i = 1, 2.$

Step 4: Increase $k := k + 1$.

Step 5: Go to Step 2 and repeat until convergence is obtained.

More information about numerical algorithms to compute μ is given in the papers [FaT88] [Hel88] [PFD88] [PaD88]. It should be appreciated that if some uncertainties are real parameter variations or if phase information is available, then complex-μ analysis might give excessively conservative results. In such situations real-μ or mixed-μ computations are necessary for robustness analysis [Dai90] [DeS88] [FTD91].

3.9 Robust Stability (RS) and Robust Performance (RP)

In this section, two basic theorems are given relating μ, and robust performance and robust stability for structured uncertainty [DWS82]. In control engineering we want to design a control system which remains stable and maintains minimum performance levels despite the presence of model uncertainties and disturbance signals. The minimum requirement is usually robust stability.

Consider a system interconnection represented by an $M-\Delta$ structure as shown in Figure 3.29. Let

$$\mathbf{B}\mathcal{RH}^{\infty} := \{\Delta(s) : \Delta \in \mathcal{RH}^{\infty},\ \Delta(s_0) \in \mathbf{B}\boldsymbol{\Delta},\ \ \forall s_0 \ni \Re e(s_0) \geq 0\} \qquad (3.103)$$

be a set of structured, stable, real rational transfer function matrices. The maximum modulus theorem shows that if $\Delta \in \mathbf{B}\mathcal{RH}^{\infty}$, then $\|\Delta\|_{\infty} \leq 1$, (i.e. $\bar{\sigma}[\Delta(j\omega)] \leq 1,\ \forall\omega \in \mathcal{R}$). Assume that the interconnection matrix $M(s)$ is a stable nominal system (with $\Delta = 0$); and $\Delta(s)$ is a normalized, block diagonal, stable real rational transfer function uncertainty matrix. Then the following theorem is established [Doy85]:

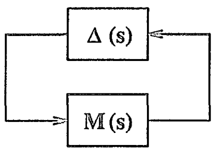

Figure 3.29: $M - \Delta$ structure without input: for RS analysis.

Theorem 3.9-1 (Robust Stability for Structured Uncertainty):
Assume that
(1) the nominal matrix $M(s)$ is stable, and
(2) $\Delta(s) \in \mathbf{B}\boldsymbol{\Delta}$ and stable (i.e. $\Delta(s) \in \mathbf{B}\mathcal{RH}^{\infty}$).
Then the perturbed closed-loop system in Figure 3.29 is stable *iff*

$$\|M\|_{\mu} < 1$$

where $\|M\|_{\mu} := \sup_{\omega} \mu[M(j\omega)]$. □

Note that the convenient notation $\|M\|_{\mu}$ is not actually a norm; it depends not only on M but also the assumed structure of Δ. A general extension of the small-μ test for the robust stability is given in [FoP88], in which assumption (2) in Theorem 3.9-1 can be removed if the plant is assumed to belong to an arcwise connected set of strictly proper rational transfer function matrices in the graph topology. Anyway Theorem 3.9-1 guarantees that if the frequency plot of $\mu[M(j\omega)]$ is less than 1 for all frequency, then the closed-loop system is stable for all structured uncertainties $\Delta(s) \in \mathbf{B}\mathcal{RH}^{\infty}$. Otherwise, if $\mu[M(j\omega)] \geq 1$ at ω_0, then there exists a structured uncertainty $\Delta(s) \in \mathbf{B}\mathcal{RH}^{\infty}$ which destabilizes the system [ChD82]. The peak value on the μ-curve indicates the worst case of stability. Hence Theorem 3.9-1 may be interpreted as a generalized small gain theorem or small-μ theorem [DWS82].

In addition to the robust stability the performance of the closed-loop system must be robust to perturbations such as exogenous disturbances acting on the system. Typically these disturbances are caused by environmental effects: load variations, sensor noise, wind gusts, road surface variations, wave surges, temperature changes, and so on. Disturbances result in regulation and tracking error, and the performance will degrade to the point of unacceptability. Therefore the issue of robust performance is to design a feedback system to maintain at least minimum performance levels under external disturbances.

Let us now consider a general framework for this problem as illustrated in Figure 3.30. In this figure, d and e are vector-valued signals: d is the exogenous input with components typically consisting of command signals, disturbances and sensor noise; e is the output with components typically being regulator output, tracking errors, filtered actuator signals and error outputs due to disturbances and/or noise, and so on. Δ is a normalized model uncertainty, unstructured or structured, which is uncertain but norm-bounded. $M(s)$ is the interconnection matrix with element $M_{22}(s)$ representing nominal performance (NP) with $\Delta = 0$. Robust performance analysis is to determine whether the error e remains in a desired set for the sets of inputs d and uncertainties Δ. What is required is a yardstick to indicate the worst case level of performance degradation associated with a given level of uncertainties.

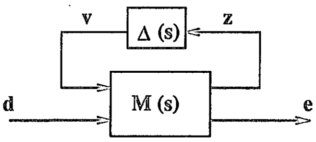

Figure 3.30: $M - \Delta$ structure with input: for RP analysis.

Obviously, the transfer function matrix from d to e can be expressed as the linear fractional transformation.

$$\begin{aligned} e &= F_u(M, \Delta)d \\ &= \left[M_{22} + M_{21}\Delta(I - M_{11}\Delta)^{-1}M_{12}\right] d \end{aligned} \tag{3.104}$$

and the maximum gain of the system is

$$\begin{aligned} \sup_{d \neq 0} \frac{\|e\|_2}{\|d\|_2} &= \sup_{\|d\|_2 \leq 1} \|e\|_2 \\ &= \|F_u(M, \Delta)\|_{i2} \\ &= \|F_u(M, \Delta)\|_{\infty} \end{aligned} \tag{3.105}$$

Hence the worst case of system gain in the presence of the uncertainties $\Delta \in \mathbf{B}\boldsymbol{\Delta}$ is given by

$$\sup_{\Delta \in \mathbf{B}\boldsymbol{\Delta}} \sup_{d \neq 0} \frac{\|e\|_2}{\|d\|_2} = \sup_{\Delta \in \mathbf{B}\boldsymbol{\Delta}} \|F_u(M, \Delta)\|_\infty \tag{3.106}$$

This leads to the following definition of robust performance.

Definition 3.9-1 (Robust Performance): The performance of the stable system in Figure 3.30 is said to be robust if

$$\|F_u(M, \Delta)\|_\infty < 1 \tag{3.107}$$

for all $\Delta \in \mathbf{B}\boldsymbol{\Delta}$. Equivalently, if $\|d\|_2 \leq 1$, then $\|e\|_2 < 1$, $\forall \Delta \in \mathbf{B}\boldsymbol{\Delta}$. □

Example 3.9-1 (SISO system): Consider a $SISO$ system illustrated in Figure 3.31. $G_0(s)$ and $K(s)$ denote the nominal plant and controller, respectively. Δ represents the normalized multiplicative input uncertainty, with $\|\Delta\|_\infty \leq 1$. $W_2(s)$ describes a modelling error function and $W_1(s)$ denotes a performance weighting function. The transfer function "seen" by Δ is given by

$$\frac{z}{v} = \frac{-KG_0W_2}{1 + KG_0} =: -W_2T_0$$

where $T_0 := \frac{KG_0}{1+KG_0}$ denotes the nominal complementary sensitivity function. It follows directly from the robust stability theorem 3.5-1 that

$$RS \Longleftrightarrow \|W_2T_0\|_\infty < 1$$

Furthermore, the perturbed weighted sensitivity function S from d to e is given by

$$\begin{aligned} W_1S &:= \frac{e}{d} = \frac{W_1}{1 + K(1 + W_2\Delta)G_0} \\ &= \frac{\frac{W_1}{1+KG_0}}{1 + \frac{KG_0W_2}{1+KG_0}\Delta} =: \frac{W_1S_0}{1 + W_2T_0\Delta} \end{aligned} \tag{3.108}$$

where $S_0 := \frac{1}{1+KG_0}$ is the nominal sensitivity function. This gives the worst case of $|W_1S|$ as

$$\sup_{\|\Delta\|_\infty \leq 1} \sup_{\omega \in \mathcal{R}} \left| \frac{W_1S_0}{1 + W_2T_0\Delta} \right| \leq \sup_{\omega \in \mathcal{R}} \sup_{\|\Delta\|_\infty \leq 1} \frac{|W_1S_0|}{1 - |W_2T_0| \cdot |\Delta|} \leq \sup_{\omega \in \mathcal{R}} \frac{|W_1S_0|}{1 - |W_2T_0|}$$

The above inequalities follow from $\|W_2T_0\|_\infty < 1$ and $\|\Delta\|_\infty \leq 1$. Furthermore if we choose $\Delta = -e^{-j\angle(W_2T_0)}$, $|\Delta| = 1$, then the worst case of $|W_1S|$ is equal to

$$\sup_{\omega\in\mathcal{R}} \frac{|W_1S_0|}{1-|W_2T_0|}$$

which should be less than 1, for the requirement of robust performance. That is

$$\frac{|W_1S_0|}{1-|W_2T_0|} < 1, \quad \forall\omega\in\mathcal{R} \iff |W_1S_0| + |W_2T_0| < 1, \quad \forall\omega\in\mathcal{R}$$
$$\iff \left\| |W_1S_0| + |W_2T_0| \right\|_\infty < 1$$

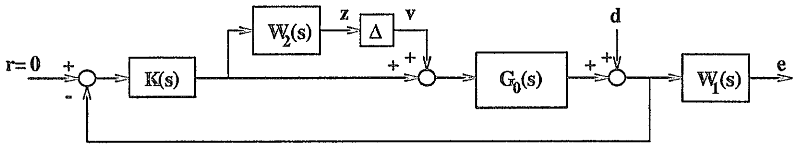

Figure 3.31: A *SISO* system with multiplicative input uncertainty.

Now let us close the loop from e to d in Figure 3.30 by an artificial stable transfer function matrix Δ_p, $\|\Delta_p\|_\infty \leq 1$, which is illustrated in Figure 3.32. The Δ_p is referred to as a fictitious performance uncertainty matrix and is a full matrix of appropriate dimensions. Figure 3.32 is an $\tilde{M} - \Delta_p$ structure without input. The transfer function matrix "seen" by Δ_p is given by

$$\tilde{M} = F_u(M, \Delta) \tag{3.109}$$

Recall from the robust stability theorem 3.5-1 that if $\tilde{M}(s)$ is stable, then system in Figure 3.32 is robustly stable *iff*

$$\left\|\tilde{M}\right\|_\infty < 1 \tag{3.110}$$

Thus (3.109) and (3.110) show the equivalence between robust stability in Figure 3.32 and robust performance in Figure 3.30. In summary, we have robust performance for the system in Figure 3.30 *iff* we have robust stability for the system in Figure 3.32 with respect to the augmented block diagonal structure

$$\tilde{\Delta} = \begin{bmatrix} \Delta & 0 \\ 0 & \Delta_p \end{bmatrix}, \quad \left\|\tilde{\Delta}\right\|_\infty \leq 1 \tag{3.111}$$

The stability test for Figure 3.32 can be expressed in terms of the structured singular value μ of M with respect to $\tilde{\Delta}$.

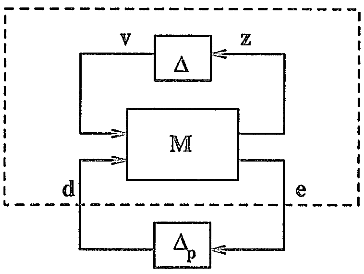

Figure 3.32: $\tilde{M} - \Delta_p$ structure without input.

Theorem 3.9-2 (Robust Performance) [Doy85]: Assume that
(1) $F_u(M, \Delta)$ is robustly stable for $\forall \Delta \in \mathbf{B}\mathcal{RH}^\infty$, and
(2) $\|\Delta_p\|_\infty \leq 1$.
Then the performance of the perturbed system in Figure 1.30 is robust *iff*

$$\|M\|_\mu < 1 \tag{3.112}$$

where μ is taken with respect to the structure

$$\tilde{\mathbf{\Delta}} = \left\{\tilde{\Delta} : \ \tilde{\Delta} = \operatorname{diag}\{\Delta, \Delta_p\}, \ \Delta \in \mathbf{B\Delta}, \ \|\Delta_p\|_\infty \leq 1\right\}$$

□

Mathematically the conditions (1.111) and (1.112) show that

$$\begin{aligned}
&\|M\|_\mu < 1 && (3.113)\\
&\iff \mu\left[M(j\omega)\right] < 1, \ \ \forall\omega \in \mathcal{R}\\
&\iff \det\left(I - M\tilde{\Delta}\right) \neq 0, \ \ \forall\omega \in \mathcal{R}, \ \forall\tilde{\Delta} \in \mathbf{B\Delta}\\
&\iff \det\begin{bmatrix} I - M_{11}\Delta & -M_{12}\Delta_p \\ -M_{21}\Delta & I - M_{22}\Delta_p \end{bmatrix} \neq 0, \ \ \forall\omega \in \mathcal{R}, \ \forall\Delta \in \mathbf{B\Delta}, \ \forall\Delta_p \in \mathbf{B\Delta}\\
&\iff \det(I - M_{11}\Delta)\cdot\det\left\{(I - M_{22}\Delta_p) - M_{21}\Delta(I - M_{11}\Delta)^{-1}M_{12}\Delta_p\right\} \neq 0 && (3.114)\\
&\iff \det(I - M_{11}\Delta)\cdot\det\left\{I - \left[M_{22} + M_{21}\Delta(I - M_{11}\Delta)^{-1}M_{12}\right]\Delta_p\right\} \neq 0\\
&\iff \det(I - M_{11}\Delta)\cdot\det\left\{I - F_u(M,\Delta)\Delta_p\right\} \neq 0, \ \ \forall\omega \in \mathcal{R}, \ \forall\Delta, \forall\Delta_p \in \mathbf{B\Delta}\\
&\iff \det(I - M_{11}\Delta) \neq 0 \ \text{ and } \ \det\left[I - F_u(M,\Delta)\Delta_p\right] \neq 0, \ \forall\omega \in \mathcal{R}, \ \forall\Delta, \forall\Delta_p \in \mathbf{B\Delta}\\
&\iff \|M_{11}\|_\mu < 1 \ \text{ and } \ \|F_u(M,\Delta)\|_\infty < 1, \ \ \forall\Delta_p \in \mathbf{B\Delta}\\
&\iff RS \text{ and } RP \text{ for Figure 1.30} && (3.115)
\end{aligned}$$

(1.114) follows directly from Schur's formula.

For the general case, consider a block diagonal structure. Let

$$\mathbb{\Delta} = \{\Delta : \Delta = \operatorname{diag}\{\Delta_1, \Delta_2\};\ \Delta_1 \in \mathbb{\Delta}_1,\ \Delta_2 \in \mathbb{\Delta}_2\} \tag{3.116}$$

Both $\mathbb{\Delta}_1$ and $\mathbb{\Delta}_2$ are structured. Let $\mu_1(\circ)$ denote the SSV with respect to $\mathbb{\Delta}_1$, and $\mu_2(\circ)$ with respect to $\mathbb{\Delta}_2$. Derivations similar to the above lead to the following theorem [BDGPS91].

Theorem 3.9-3 (Main Loop Theorem):

$$\mu_{\mathbb{\Delta}}(M) < 1 \iff \begin{cases} \mu_1(M_{11}) < 1, & \text{and} \\ \mu_2\left[F_u(M, \Delta_1)\right] < 1, & \forall \Delta_1 \in \mathbf{B}\mathbb{\Delta}_1 \end{cases}$$

$$\iff \begin{cases} \mu_2(M_{22}) < 1, & \text{and} \\ \mu_1\left[F_l(M, \Delta_2)\right] < 1, & \forall \Delta_2 \in \mathbf{B}\mathbb{\Delta}_2 \end{cases}$$

Therefore it is interesting to note that stability and performance robustness are achieved simultaneously if and only if the perturbed system in Figure 1.32 is stable for all perturbations with a particular block diagonal structure, $\operatorname{diag}[\Delta, \Delta_p]$. Note also that Theorem 3.9-2 is of great importance in the analysis of perturbed feedback system and opens the way to systematic methods of synthesis.

Furthermore, let $\tilde{\Delta}_1 := \operatorname{diag}\{\Delta, 0\}$ and $\tilde{\Delta}_2 := \operatorname{diag}\{0, \Delta_p\}$. Obviously, both $\tilde{\Delta}_1$ and $\tilde{\Delta}_2$ are special structures of $\tilde{\Delta} := \operatorname{diag}\{\Delta, \Delta_p\}$, so that

$$\mu_{\tilde{\Delta}}(M) \geq \max\left\{\mu_{\tilde{\Delta}_1}(M), \mu_{\tilde{\Delta}_2}(M)\right\} = \max\left\{\mu_{\Delta}(M_{11}), \mu_{\Delta_p}(M_{22})\right\} \tag{3.117}$$

The above inequality implies that a necessary condition for robust performance (RP), $[\mu_{\tilde{\Delta}}(M) < 1]$, is robust stability ($RS$), $[\mu_{\Delta}(M_{11}) < 1]$, and nominal performance (NP), $\left[\mu_{\Delta_p}(M_{22}) = \bar{\sigma}(M_{22}) < 1\right]$.

To recap, we list the following consequences:

For an interconnected system in Figure 1.30, assume that $M(s)$ is nominally stable and $\Delta(s) \in \mathbf{B}\mathcal{RH}^{\infty}$, then

- $NS \Longleftrightarrow M$ is internally stable.
- $NP \Longleftrightarrow \|M_{22}\|_{\infty} < 1$
- $RS \Longleftrightarrow \|M_{11}\|_{\infty} < 1$, for unstructured uncertainty.
- $RS \Longleftrightarrow \|M_{11}\|_{\mu} < 1$, for structured uncertainty.
- $RP \Longleftrightarrow \|M\|_{\mu} < 1$.

Example 3.9-2 (A SISO system): Consider the *SISO* system in Figure 3.31. To minimize the weighted perturbed sensitivity function from d to e, the interconnection matrix M derived directly from the block diagram is given by

$$M = \begin{bmatrix} -W_2T_0 & -W_2KS_0 \\ W_1G_0S_0 & W_1S_0 \end{bmatrix}$$

Since $\det M = 0$, it follows directly from (3.93) that

$$\mu(M) = |W_2T_0| + |W_1S_0|$$

and Theorem 3.9-2 guarantees that

$$RP \Longleftrightarrow |W_2T_0| + |W_1S_0| < 1, \quad \forall \omega \in \mathcal{R}$$

This coincides with the findings in Example 3.9-1.

3.10 μ-Synthesis

The objective of feedback control system design is to achieve certain desired levels of performance and to be tolerant of uncertainties. Performance levels concern such things as command following, disturbance rejection, noise attenuation, sensitivity reduction, etc. Yet this generic design problem is still largely unsolved. The *RSRP* problem is to design an optimal stabilizing controller $K(s)$ for robust stability (RS) and robust performance (RP). From the mathematical point of view, the design objective is

$$\inf_{K(s)} \sup_{\omega \in \mathcal{R}} \mu\left[M(P,K)\right] \tag{3.118}$$

where $P(s)$ is the nominal generalized plant compatible with structured error model $\Delta(s)$, shown in Figures 1.33 and 1.34, and

$$\begin{aligned} M(P,K) &= F_l(P,K) \\ &= \begin{bmatrix} P_{11} & P_{12} \\ P_{21} & P_{22} \end{bmatrix} + \begin{bmatrix} P_{13} \\ P_{23} \end{bmatrix} K(I - P_{33}K)^{-1} \begin{bmatrix} P_{31} & P_{32} \end{bmatrix} \end{aligned} \quad (3.119)$$

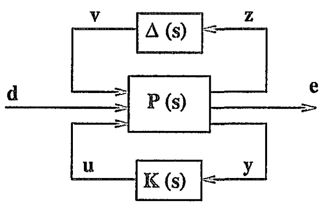

Figure 3.33: General framework.

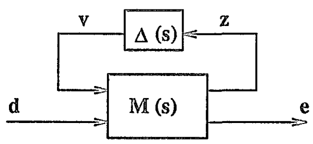

Figure 3.34: $M - \Delta$ structure with input.

In [Doy85] Doyle suggested that the μ-synthesis in problem (1.118) could be solved by an iterative scheme, called $D - K$ iteration. This is based on finding a stabilizing controller K and diagonal scaling matrix D so that

$$\inf_{K(s)} \sup_{\omega \in \mathcal{R}} \inf_{D \in \mathbf{D}} \bar{\sigma} \left[D F_l(P,K) D^{-1} \right] \quad (3.120)$$

has a solution; see Figure 1.35.

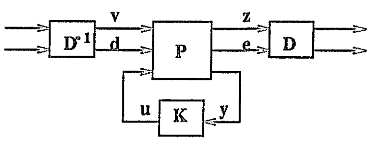

Figure 3.35: A scaled generalized feedback system.

One approximate method to do this is to alternately minimize the above expression for either K or D while keeping the other constant. For fixed D the expression

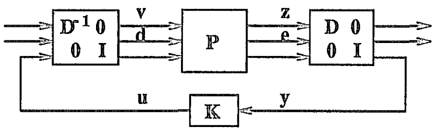

Figure 3.36: An equivalent system.

(3.120) is just an $\mathcal{H}^\infty$ control problem and can be solved by an $\mathcal{H}^\infty$-optimization method. For fixed K, the expression (3.120) can be minimized at each frequency as a convex optimization problem in D (actually $\ln D$). The resulting diagonal scaling matrix D can be approximated by a stable, rational transfer function with stable inverse (the phase of D does not affect the norm). More precisely, it is easy to see that both Figures 3.35 and 3.36 are equivalent to each other and hence we can write

$$DM(P,K)D^{-1} = DF_l(P,K)D^{-1} = F_l(\tilde{D}P\tilde{D}^{-1},K) = F_l(\tilde{P},K) \tag{3.121}$$

with

$$\tilde{D} := \begin{bmatrix} D & 0 \\ 0 & I \end{bmatrix} \quad \text{and } \tilde{P} := \tilde{D}P\tilde{D}^{-1} \tag{3.122}$$

So for fixed D, (3.121) implies that (3.120) becomes

$$\inf_{K(s)} \left\| F_l(\tilde{P},K) \right\|_\infty \tag{3.123}$$

Recall that $\|\circ\|_\infty := \sup_\omega \bar{\sigma}(\circ)$.

This is a standard form of $\mathcal{H}^\infty$-optimization problem and (3.123) plays a key role in μ-synthesis. In real-μ or mixed-μ analysis, which arises when the elements of Δ are purely real or a mixture of real and complex values, it might not be possible to approximate the structured singular value $\mu(M)$ by $\inf_{D\in\mathbf{D}} \bar{\sigma}(DMD^{-1})$, and then $D-K$ iteration fails. This is why μ-synthesis by $D-K$ iteration is only applicable to feedback systems with complex uncertainties. If the technique is applied to design a μ-optimal controller of a system with real parametric uncertainties, then the degree of conservatism may be arbitrarily large!

Let us consider a simple example in Figure 3.29. Assume M is stable and Δ is a real scalar uncertainty with $-1 \le \Delta \le 1$. Theorem 3.9-1 guarantees that the perturbed system is robustly stable *iff* $\|M\|_\mu = \sup_{\omega\in\mathcal{R}} \mu\left[M(j\omega)\right] = \sup_{\omega\in\mathcal{R}} |M(j\omega)| < 1$ under the assumption that Δ is a complex number with modulus less than or equal to 1. This means that the Nyquist plot of $M(j\omega)$ should be inside a unit circle centred at the origin. However the system is robustly stable against the real uncertainty $-1 \leq \Delta \leq 1$ if the Nyquist plot of $M(j\omega)$ is any curve which does not intersect the real axis at a distance greater than or equal to one from the origin. This shows that the complex-μ analysis gives conservative results when the uncertainty is real. In Chapter 5, we present a new method for synthesis, called $\mu - K$ iteration, which is applicable for complex-μ, real-μ and mixed-μ cases. At this point we will outline the $D - K$ iteration algorithm [BDGPS91]:

Step 1: Start with an initial guess for D, normally $D = I$.
Step 2: Fix D, and solve for K by $\mathcal{H}^\infty$-optimization. That is

$$K = \arg \inf_K \left\| F_l(\tilde{P}, K) \right\|_\infty$$

where $\tilde{P}$ is given in (1.122).
Step 3: Fix K, and solve for D at each frequency by convex optimization. That is

$$D = \arg \inf_{D\in\mathbf{D}} \bar{\sigma}\left[D F_l(P, K) D^{-1}\right]$$

Step 4: Curve fit $D(j\omega)$ to get $D(s)$, then go to Step 2 and repeat until a specified convergence tolerance is achieved.

This approximate solution has been implemented by Doyle [Doy85] who reports good results. However he has also discovered a simple counterexample for which such an iterative scheme will fail to find the $K(s)$ and $D(s)$. The reason can be explained as follows:

It is well known that the Youla parametrization of all stabilizing controllers can be described by

$$K = F_l(J, Q) \tag{3.124}$$

where the "parameter" Q ranges over all proper, stable transfer functions, (i.e. $Q \in \mathcal{RH}^\infty$) [YJB76]. Substitution of (3.124) into (3.119) yields [Fra87]

$$F_l(P,K) = F_l[P, F_l(J,Q)] = T_1 + T_2 Q T_3 \tag{3.125}$$

Furthermore, let $f(Q) := \bar{\sigma}(T_1 + T_2 Q T_3)$ and

$$Q := \lambda Q_1 + (1-\lambda) Q_2, \quad 0 \le \lambda \le 1, \quad Q_1, Q_2 \in \mathcal{RH}^\infty \tag{3.126}$$

Obviously $Q \in \mathcal{RH}^\infty$ and

$$\begin{aligned} f(Q) &= \bar{\sigma}\big\{T_1 + T_2[\lambda Q_1 + (1-\lambda)Q_2]T_3\big\} \\ &= \bar{\sigma}\big[\lambda(T_1 + T_2 Q_1 T_3) + (1-\lambda)(T_1 + T_2 Q_2 T_3)\big] \\ &\le \lambda \cdot \bar{\sigma}(T_1 + T_2 Q_1 T_3) + (1-\lambda) \cdot \bar{\sigma}(T_1 + T_2 Q_2 T_3) \\ &= \lambda f(Q_1) + (1-\lambda) f(Q_2) \end{aligned} \tag{3.127}$$

Therefore $\bar{\sigma}(T_1 + T_2 Q T_3)$ is convex in Q and the optimization problem

$$\inf_K \sup_{\omega \in \mathcal{R}} \inf_{D \in \mathbf{D}} \bar{\sigma}\left[D F_l(P,K) D^{-1}\right] = \inf_Q \sup_{\omega \in \mathcal{R}} \inf_{D \in \mathbf{D}} \bar{\sigma}\left[D(T_1 + T_2 Q T_3) D^{-1}\right] \tag{3.128}$$

is convex in either D (actually $\ln D$) or Q individually when the other is fixed. Unfortunately, this does not guarantee however that (3.128) is jointly convex.

Furthermore, the compensator so obtained is not guaranteed to be globally optimal. It depends on the initial guess of the diagonal matrix D. For the ill-conditioned high purity distillation column [SkM86] considered in Chapter 6, an initial guess of D as the identity matrix yields a very bad result. $D-K$ iteration might even fail to converge. In addition, the compensator obtained by $D-K$ iteration always has a relatively high order, which often needs to be reduced via model reduction techniques. Several applications of μ-synthesis can be found in [BCD89] [STBS90] [Enn87] [DLP87] [MoZ89] [BaD89].

3.11 Simultaneous Uncertainties

In this section, we first consider a simple configuration of a two-degrees-of-freedom controller as shown in Figure 3.37. G_0 denotes the nominal plant with stable multiplicative output uncertainty $\Delta = \operatorname{diag}\{\Delta_1, \Delta_2\}$, $\Delta_1, \Delta_2 \in \mathcal{C}$ and $K = \operatorname{diag}\{K_1, K_2\}$ is the controller. G_0 is a model of a spinning satellite which is considered to be a symmetric spinning body with torque input along two orthogonal transverse axes. The transfer function matrix from input torque to output angular velocity is given by [Cam90]

$$G_0(s) = \frac{1}{s^2 + a^2} \begin{bmatrix} s - a^2 & a(s+1) \\ -a(s+1) & s - a^2 \end{bmatrix}, \quad a = 10 \tag{3.129}$$

Let

$$K_1(s) = \frac{1}{1 + a^2} \begin{bmatrix} 1 & -a \\ a & 1 \end{bmatrix}, \quad K_2(s) = \begin{bmatrix} 1 & 0 \\ 0 & 1 \end{bmatrix} \tag{3.130}$$

It is easy to see that the interconnection matrix M "seen" from Δ is given by

$$M(s) = -G_0(s)K_2(s)[I + G_0(s)K_2(s)]^{-1} = \frac{-1}{s+1} \begin{bmatrix} 1 & a \\ -a & 1 \end{bmatrix} \tag{3.131}$$

which is illustrated in Figure 3.38 and obviously $M(s)$ is stable. It is interesting to note that the conditions for robust stability with respect to individual uncertainties are:

$$\text{if } \Delta_1 = 0, \text{ then} \quad RS \Longleftrightarrow \|\Delta_2\|_\infty < \frac{1}{\|M_{22}\|_\infty} = 1 \tag{3.132}$$

and

$$\text{if } \Delta_2 = 0, \text{ then} \quad RS \Longleftrightarrow \|\Delta_1\|_\infty < \frac{1}{\|M_{11}\|_\infty} = 1 \tag{3.133}$$

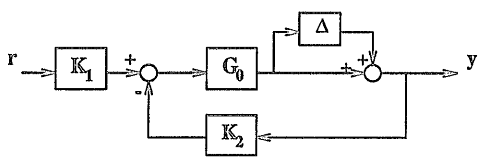

Figure 3.37: System with two-degree-of-freedom control.

Note that these conditions are independent of the parameter a, and M_{12} and M_{21} have no effect on robust stability. Now let us consider robust stability of the system with simultaneous uncertainties. With simple calculations, formula (3.91) yields

$$\mu[M(j\omega)] = \frac{\sqrt{1 + a^2}}{\sqrt{1 + \omega^2}} \tag{3.134}$$

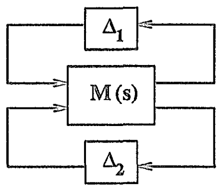

Figure 3.38: $M - \Delta$ structure.

Thus $\|M\|_\mu = \sqrt{1+a^2}$, and for robust performance Theorem 3.9-2 gives

$$\|\Delta\|_\infty = \max\{\|\Delta_1\|_\infty, \|\Delta_2\|_\infty\} < \frac{1}{\|M\|_\mu} = \frac{1}{\sqrt{1+a^2}} \tag{3.135}$$

This means that both $\|\Delta_1\|_\infty$ and $\|\Delta_2\|_\infty$ should be less than $\frac{1}{\sqrt{1+a^2}}$. If a is large, then the stability margin is small. These consequences show that small simultaneous modelling errors can interact to cause instability in a system that is robustly stable against much larger individual modelling errors. To gain insight, it is instructive to consider the transfer function "seen" from Δ_2 in Figure 3.38, which is given by

$$F_u(M, \Delta_1) = m_{22} + m_{21}\Delta_1(1 - m_{11}\Delta_1)^{-1}m_{12} \tag{3.136}$$

where m_{ij} denotes the (i,j) element of M. The characteristic equation of the closed-loop system is equivalent to $\det[I - F_u(M, \Delta_1)\Delta_2] = 0$, namely

$$\left[m_{22} + m_{21}\Delta_1(1 - m_{11}\Delta_1)^{-1}m_{12}\right]\Delta_2 = 1 \tag{3.137}$$

Suppose Δ_1 is very small, then (3.137) can be rewritten as

$$[m_{22} + m_{21}\Delta_1 m_{12}]\Delta_2 \approx 1 \tag{3.138}$$

It follows directly from (3.131) that

$$|m_{ij}| \gg |m_{22}|, \quad i \neq j \tag{3.139}$$

if $a \gg 1$, and by (3.139) we have

$$m_{21}\Delta_1 m_{12}\Delta_2 \approx 1 \tag{3.140}$$

The minimum size of uncertainties Δ_1 and Δ_2 which satisfy (3.140) is

$$|\Delta_1| = |\Delta_2| \approx \frac{1}{\sqrt{|m_{12}m_{21}|}} = \frac{\sqrt{1+\omega^2}}{a} \tag{3.141}$$

This result almost satisfies (3.137) when $a \gg 1$; and gives

$$\mu[M(j\omega)] \approx \frac{a}{\sqrt{1+\omega^2}} \tag{3.142}$$

which is approximately the same as (3.134) when $a \gg 1$.

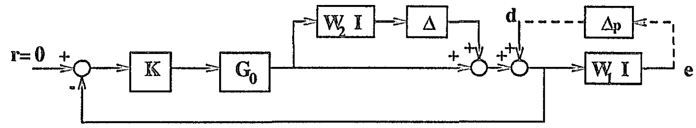

Figure 3.39: System with multiplicative output uncertainty.

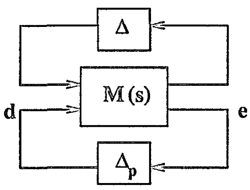

Figure 3.40: $M - \Delta$ structure.

Next we study the robust performance problem for the $MIMO$ system shown in Figure 3.39 where G_0 is a nominal plant with normalized multiplicative output uncertainty Δ. The scaling functions W_2 and W_1 denote the error bounding function and performance weighting function, respectively. The control objective is to minimize the effect of the load disturbance, d. The interconnection matrix M, shown in Figure 3.40, derived from the block diagram in Figure 3.39, is given by

$$M = \begin{bmatrix} -W_2T_0 & -W_2T_0 \\ W_1S_0 & W_1S_0 \end{bmatrix} \tag{3.143}$$

where $T_0 := G_0K(I+G_0K)^{-1}$ and $S_0 := (I+G_0K)^{-1}$ denote the nominal output complementary sensitivity function and nominal output sensitivity function, respectively. Robust performance is guaranteed by Theorem 3.9-2 if and only if $\mu(M) < 1$ where μ is evaluated with respect to the uncertainty structure $\tilde{\Delta} = \text{diag}\,\{\Delta, \Delta_p\}$. We have

$$
\begin{aligned}
& \det(I - M\tilde{\Delta}) = 0 && (3.144) \\
\Longleftrightarrow \quad & \det\left\{ I - \begin{bmatrix} -W_2T_0 \\ W_1S_0 \end{bmatrix} [I \quad I] \begin{bmatrix} \Delta & 0 \\ 0 & \Delta_p \end{bmatrix} \right\} = 0 \\
\Longleftrightarrow \quad & \det\left\{ I - \begin{bmatrix} -W_2T_0 \\ W_1S_0 \end{bmatrix} [\Delta \quad \Delta_p] \right\} = 0 \\
\Longleftrightarrow \quad & \det\left\{ I - [\Delta \quad \Delta_p] \begin{bmatrix} -W_2T_0 \\ W_1S_0 \end{bmatrix} \right\} = 0 \\
\Longleftrightarrow \quad & \det\left(I + \Delta W_2T_0 - \Delta_p W_1S_0\right) = 0 \\
\Longleftrightarrow \quad & 0 = \underline{\sigma}\left[I + \Delta W_2T_0 - \Delta_p W_1S_0\right] \\
\Longrightarrow \quad & 0 \geq 1 - \bar{\sigma}\left[\Delta W_2T_0 - \Delta_p W_1S_0\right], \quad \text{by (2.71)} \\
\Longrightarrow \quad & 0 \geq 1 - \bar{\sigma}(\Delta)\bar{\sigma}(W_2T_0) - \bar{\sigma}(\Delta_p)\bar{\sigma}(W_1S_0), \quad \text{by (2.68) (2.67)} \\
\Longleftrightarrow \quad & \bar{\sigma}(\Delta)\bar{\sigma}(W_2T_0) + \bar{\sigma}(\Delta_p)\bar{\sigma}(W_1S_0) \geq 1 && (3.145) \\
\Longrightarrow \quad & \max\{\bar{\sigma}(\Delta), \bar{\sigma}(\Delta_p)\} \cdot [\bar{\sigma}(W_2T_0) + \bar{\sigma}(W_1S_0)] \geq 1 \\
\Longleftrightarrow \quad & \max\{\bar{\sigma}(\Delta), \bar{\sigma}(\Delta_p)\} \geq [\bar{\sigma}(W_2T_0) + \bar{\sigma}(W_1S_0)]^{-1}, \quad \forall\Delta, \forall\Delta_p \\
\Longleftrightarrow \quad & \min_{\Delta,\Delta_p} \max\{\bar{\sigma}(\Delta), \bar{\sigma}(\Delta_p)\} \geq [\bar{\sigma}(W_2T_0) + \bar{\sigma}(W_1S_0)]^{-1} \\
\Longleftrightarrow \quad & \mu^{-1}(M) \geq [\bar{\sigma}(W_2T_0) + \bar{\sigma}(W_1S_0)]^{-1} \\
\Longleftrightarrow \quad & \mu(M) \leq \bar{\sigma}(W_2T_0) + \bar{\sigma}(W_1S_0) && (3.146)
\end{aligned}
$$

It follows directly from (3.143) that (3.146) is an equality for $SISO$ systems. The inequality (3.146) reveals that the sufficient condition for robust performance is

$$RP \Longleftarrow \bar{\sigma}(W_2T_0) + \bar{\sigma}(W_1S_0) < 1, \quad \forall\omega \in \mathcal{R} \tag{3.147}$$

and this condition is somewhat conservative for $MIMO$ systems. Moreover, inspection of the matrix M in (3.143) leads to

$$NP \quad \Longleftrightarrow \quad \bar{\sigma}(W_1S_0) < 1, \quad \forall\omega \in \mathcal{R}$$

and

$$RS \quad \Longleftrightarrow \quad \bar{\sigma}(W_2T_0) < 1, \quad \forall\omega \in \mathcal{R}$$

A comparison with (3.146) reveals that both nominal performance (NP) and robust stability (RS) cannot guarantee the robust performance (RP) of the system, but they can give an approximate check for RP.

Similarly, for the $MIMO$ system shown in Figure 3.41, we have

$$M = \begin{bmatrix} -W_2 T_0 & -W_2 S_0 \\ W_1 T_0 & W_1 S_0 \end{bmatrix} = \begin{bmatrix} -W_2 I \\ W_1 I \end{bmatrix} [T_0 \quad S_0] \tag{3.148}$$

and calculations then lead to the same result in (3.146).

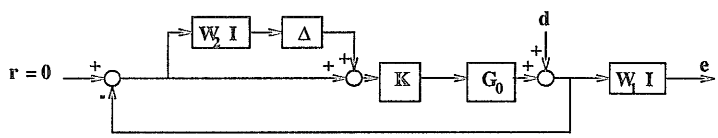

Figure 3.41: A perturbed system.

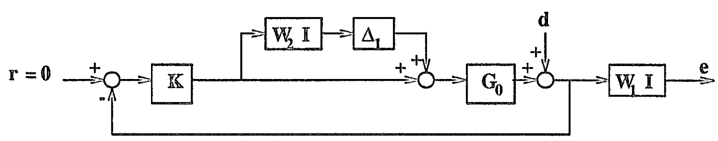

Figure 3.42: System with multiplicative input uncertainty.

Figures 3.39 and 3.41 show that both uncertainties Δ and Δ_p occur at the same position. However for a system with multiplicative input uncertainty, shown in Figure 3.42, the modelling uncertainty Δ_1 and the fictitious performance uncertainty Δ_p are separated by the nominal plant G_0. From a control point of view, Figures 3.42, 3.43 and 3.44 are all equivalent. Therefore comparing Figure 3.44 with Figure 3.39 gives

$$G_0 \Delta_1 W_2 I G_0^{-1} = \Delta W_2 I \tag{3.149}$$

with

$$\Delta = G_0 \Delta_1 G_0^{-1} \tag{3.150}$$

and

$$\bar{\sigma}(\Delta) \leq \bar{\sigma}(G_0)\bar{\sigma}(\Delta_1)\bar{\sigma}\left(G_0^{-1}\right) = \text{cond}\,(G_0) \cdot \bar{\sigma}(\Delta_1) \tag{3.151}$$

where $\text{cond}\,(G_0) := \bar{\sigma}(G_0)\bar{\sigma}\left(G_0^{-1}\right) = \frac{\bar{\sigma}(G_0)}{\underline{\sigma}(G_0)}$ denotes the condition number of G_0. Substituting the inequality (3.151) into (3.145), we can derive

$$\mu(M) \leq \text{cond}\,(G_0) \cdot \bar{\sigma}(W_2 T_0) + \bar{\sigma}(W_1 S_0) \tag{3.152}$$

This implies

$$RP \Longleftarrow \text{cond}\,(G_0) \cdot \bar{\sigma}(W_2 T_0) + \bar{\sigma}(W_1 S_0) < 1, \quad \forall \omega \in \mathcal{R} \tag{3.153}$$

Figure 3.43: An equivalent system.

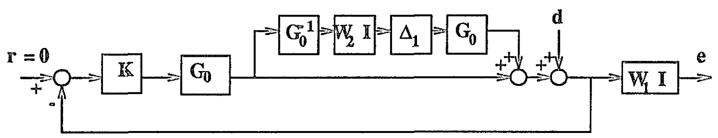

Figure 3.44: An equivalent system.

Similarly, shifting the blocks $W_2 I$ and Δ_1 backwards to pass over the controller K, we also have the equivalent system, shown in Figure 3.45. A comparison with Figure 3.41 leads to $\Delta = K^{-1}\Delta_1 K$ and $\bar{\sigma}(\Delta) \leq \text{cond}\,(K) \cdot \bar{\sigma}(\Delta_1)$, then we obtain

$$\mu(M) \leq \text{cond}\,(K) \cdot \bar{\sigma}(W_2 T_0) + \bar{\sigma}(W_1 S_0) \tag{3.154}$$

This gives

$$RP \Longleftarrow \text{cond}\,(K) \cdot \bar{\sigma}(W_2 T_0) + \bar{\sigma}(W_1 S_0) < 1, \quad \forall \omega \in \mathcal{R} \tag{3.155}$$

The consequences of (3.152) and (3.155) are that if $\text{cond}\,(G_0)$ or if $\text{cond}\,(K)$ is small (i.e. near to 1), then the sufficient condition is almost the same as that derived for the multiplicative output uncertainty. However if either plant or controller is ill-conditioned (i.e. with high condition number), then the value of $\mu(M)$

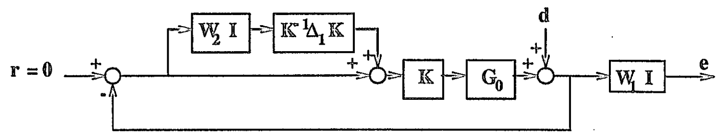

Figure 3.45: An equivalent system.

might be quite large and the sufficient condition for robust performance may be violated, even if the system is NP ($\|W_1 S_0\|_\infty < 1$) and RS ($\|W_2 T_I\|_\infty < 1$), where $T_I := KG_0(I + KG_0)^{-1}$. This is the reason why the loop shaping method proposed by Stein [Ste85] can be used to successfully design a robust controller for a $MIMO$ system with multiplicative output uncertainty, which then fails with multiplicative input uncertainty.

Chapter 4

A LOOP SHAPING APPROACH TO ROBUST PERFORMANCE FOR SISO SYSTEMS

4.1 Introduction

The performance specifications of a control system are said to be robust if they are satisfied despite the presence of disturbance signals and model uncertainties. A general framework for analyzing robust performance using the structured singular value "μ" was introduced by Doyle [Doy82] who also developed a controller synthesis procedure called μ-synthesis or D-K iteration [Doy85]. The procedure, which aims to minimize μ, is computationally demanding and the resulting controller may not be globally optimal. Nevertheless it represents a practical, systematic approach for addressing this important problem of robust performance; an alternative is given in Chapter 5.

In 1988, Milich et al. presented a Causality Recovery Methodology (CRM) to modify D-K iteration to obtain a globally optimal controller [MAVS88]. However, the CRM is computationally inefficient and the huge number of computations required makes this method impractical.

In this chapter we will examine a particular robust performance problem for $SISO$ systems and show how the corresponding structured singular value can be effectively minimized using a loop shaping approach. The approach is not computationally demanding and has the advantage of being an extension of a design procedure already familiar to practising control engineers.

In Section 4.2 we formulate $\mu_{\hat{\Delta}}(M)$ for $SISO$ perturbed systems with additive uncertainty, multiplicative input uncertainty or multiplicative output uncertainty. The relationship between a mixed sensitivity $\mathcal{H}^\infty$-optimization problem and classical loop shaping is then investigated in the Section 4.3. It is shown how classical loop shaping can be used to minimize the $\mathcal{H}^\infty$ cost function. This then provides, in Section 4.4, insight into a further development of loop shaping to minimize the structured singular value for robust performance. In Section 4.5, the approach is demonstrated by its application to the control of a robot arm whose moment of inertia varies considerably with angle. Finally a brief summary will be given in the last section.

4.2 Motivation

Consider the scalar feedback configuration of Figure 4.1, where G_0 is a nominal plant model, Δ is a perturbation representing uncertainty, d is an energy-bounded disturbance signal and K is a controller to be designed. The weights W_1 and W_2 describe the frequency-domain characteristics of the performance specifications and model uncertainty, and can also be used for normalization purposes.

The robust performance (disturbance rejection) problem is to find a stabilizing controller K such that the energy gain from d to e is less than 1 for all stable perturbations Δ, where $|\Delta| \leq 1$.

The feedback configuration of Figure 4.1 can be redrawn as in Figure 4.2 where the interconnection matrix is

$$M(s) = \begin{bmatrix} \frac{-KW_2}{1+G_0K} & \frac{-KW_1W_2}{1+G_0K} \\ \frac{1}{1+G_0K} & \frac{W_1}{1+G_0K} \end{bmatrix} \tag{4.1}$$

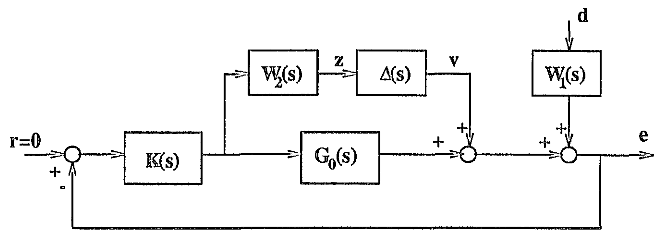

Figure 4.1: System with additive uncertainty.

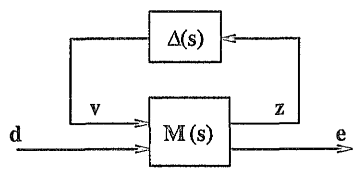

Figure 4.2: Equivalent $M - \Delta$ structure.

If we now introduce a fictitious performance perturbation Δ_p, as shown in Figure 4.3, where $|\Delta_p| \leq 1$, then robust performance is achieved if

$$\mu_{\tilde{\Delta}}[M(j\omega)] < 1 \ , \quad \forall \omega \in \mathcal{R} \tag{4.2}$$

where $\mu_{\tilde{\Delta}}[\circ]$ denotes Doyle's structured singular value (Doyle, 1982) with respect to $\tilde{\Delta}$.

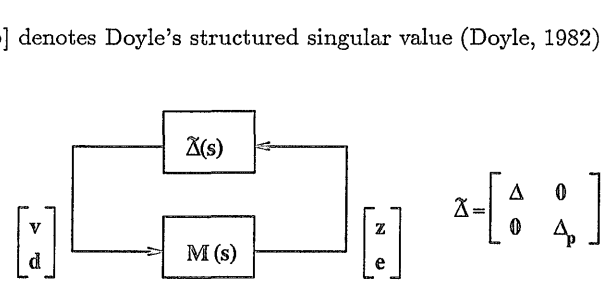

Figure 4.3: General $M - \tilde{\Delta}$ structure.

Furthermore, it follows directly from (3.93) that

$$\begin{aligned} \mu_{\tilde{\Delta}}(M) &= \left|\frac{KW_2}{1+G_0K}\right| + \left|\frac{W_1}{1+G_0K}\right| \\ &= \left|\frac{W_2 t}{G_0}\right| + |W_1 s| \end{aligned} \tag{4.3}$$

where

$$s(s) := \frac{1}{1+G_0(s)K(s)} = \frac{1}{1+l(s)} \tag{4.4}$$

is the nominal sensitivity function,

$$t(s) := \frac{G_0(s)K(s)}{1+G_0(s)K(s)} = \frac{l(s)}{1+l(s)} \tag{4.5}$$

is the nominal complementary sensitivity function, and

$$l(s) := G_0(s)K(s) \tag{4.6}$$

denotes the nominal open-loop transfer function.

Similarly, if the model uncertainty is represented by a multiplicative input perturbation as shown in Figure 4.4, we have

$$M(s) = \begin{bmatrix} \frac{-G_0KW_2}{1+G_0K} & \frac{-KW_1W_2}{1+G_0K} \\ \frac{G_0}{1+G_0K} & \frac{W_1}{1+G_0K} \end{bmatrix} \tag{4.7}$$

$$\begin{aligned} \mu_{\tilde{\Delta}}(M) &= \left|\frac{G_0KW_2}{1+G_0K}\right| + \left|\frac{W_1}{1+G_0K}\right| \\ &= |W_2t| + |W_1s| \end{aligned} \tag{4.8}$$

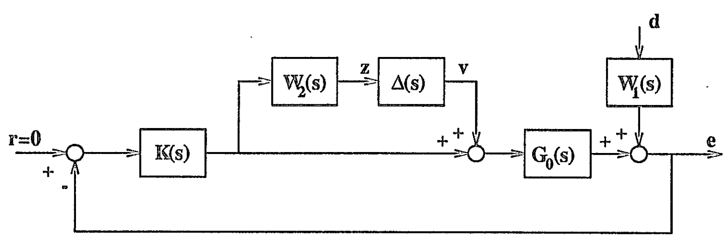

Figure 4.4: System with multiplicative input uncertainty.

For a multiplicative output perturbation as in Figure 4.5, we have

$$M(s) = \begin{bmatrix} \frac{-G_0KW_2}{1+G_0K} & \frac{-G_0KW_1W_2}{1+G_0K} \\ \frac{1}{1+G_0K} & \frac{W_1}{1+G_0K} \end{bmatrix} \tag{4.9}$$

$$\begin{aligned} \mu_{\tilde{\Delta}}(M) &= \left|\frac{G_0KW_2}{1+G_0K}\right| + \left|\frac{W_1}{1+G_0K}\right| \\ &= |W_2t| + |W_1s| \end{aligned} \tag{4.10}$$

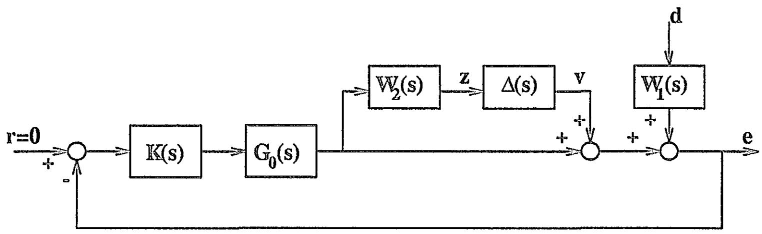

Figure 4.5: System with multiplicative output uncertainty.

It is interesting to note that $\mu_{\tilde{\Delta}}(M)$ in expressions (4.3), (4.8) and (4.10) can be expressed in a general form

$$\mu_{\tilde{\Delta}}(M) = |r_1s| + |r_2t| \tag{4.11}$$

where the generalized weighting functions r_1 and r_2 are

$$r_1(s) := W_1(s) \tag{4.12}$$

$$r_2(s) := \begin{cases} W_2(s) & \text{for multiplicative uncertainty} \\ \frac{W_2(s)}{G_0(s)} & \text{for additive uncertainty} \end{cases} \tag{4.13}$$

Therefore, given one of the above uncertainty models the robust performance design problem is to find a stabilizing controller $K(s)$ which satisfies

$$\inf_{K(s)} \sup_{\omega\in\mathcal{R}} \mu_{\tilde{\Delta}}[M(j\omega)] = \inf_{K(s)} \sup_{\omega\in\mathcal{R}} \left\{|r_1(j\omega)s(j\omega)| + |r_2(j\omega)t(j\omega)|\right\} \tag{4.14}$$

This is a nontrivial optimization problem. In the next section we will examine a closely related $\mathcal{H}^\infty$-optimization problem and establish a relationship with classical loop shaping.

4.3 Mixed Sensitivity $\mathcal{H}^\infty$-Optimization and Classical Loop Shaping

An $\mathcal{H}^\infty$-optimization problem which has received considerable attention in the literature is the so-called mixed sensitivity problem described by

$$\begin{aligned}\inf_{K(s)} \left\| \begin{bmatrix} r_1 s \\ r_2 t \end{bmatrix} \right\|_\infty &= \inf_{K(s)} \sup_{\omega \in \mathcal{R}} \sqrt{|r_1(j\omega)s(j\omega)|^2 + |r_2(j\omega)t(j\omega)|^2} \\ &=: \inf_{K(s)} \sup_{\omega \in \mathcal{R}} J(\omega) \qquad (4.15)\end{aligned}$$

where

$$J(\omega) := \sqrt{|r_1(j\omega)s(j\omega)|^2 + |r_2(j\omega)t(j\omega)|^2} \qquad (4.16)$$

Let ω_c denote the crossover frequency of loop gain $|l(j\omega)|$, that is

$$|l(j\omega_c)| = 1 \qquad (4.17)$$

and without loss of generality, let us assume that

$$|l(j\omega)| \gg 1, \quad \text{for } \omega \ll \omega_c \qquad (4.18)$$

$$|l(j\omega)| \ll 1, \quad \text{for } \omega \gg \omega_c \qquad (4.19)$$

Assumption (4.18) is essential for load disturbance rejection, and is therefore a requirement for good performance. On the other hand, assumption (4.19) is necessary for noise attenuation and robust stability. Moreover the assumptions imply that

$$J(\omega) = \sqrt{|r_1 s|^2 + |r_2 t|^2} \approx \begin{cases} \sqrt{|r_1 \frac{1}{l}|^2 + |r_2|^2} & \text{for } \omega \ll \omega_c \\ \sqrt{|r_1|^2 + |r_2 l|^2} & \text{for } \omega \gg \omega_c \end{cases} \qquad (4.20)$$

where we have neglected the angular frequency ω for brevity. Clearly, $J(\omega)$ is expressed as a function of the open-loop transfer function $l(j\omega)$ and the generalized weighting functions in the low and high frequency ranges. In classical loop shaping $|l(j\omega)|$ is required to be large at low frequencies and small at high frequencies. From (4.20) we see that these loop shaping objectives appear to be compatible with the

$\mathcal{H}^\infty$-optimization problem in (4.15) since they each have the effect of decreasing $J(\omega)$ for a given pair of weights.

It is now interesting to investigate the shape of $J(\omega)$ in the intermediate frequency range around $\omega = \omega_c$. It follows from (4.17) that

$$\begin{aligned} |s(j\omega_c)| &= |t(j\omega_c)| \\ &= \frac{1}{|1 + l(j\omega_c)|} \\ &= \frac{1}{2\cos[\frac{\angle l(j\omega_c)}{2}]} \end{aligned} \tag{4.21}$$

where $\angle l(j\omega_c)$ denotes the phase angle of $l(j\omega)$ at $\omega = \omega_c$. This implies

$$J(\omega_c) = \sqrt{|r_1(j\omega_c)|^2 + |r_2(j\omega_c)|^2} \cdot \frac{1}{2\cos[\frac{\angle l(j\omega_c)}{2}]} \tag{4.22}$$

For an open-loop stable and minimum-phase system it is well known that phase lag is approximately proportional to the roll-off rate of the Bode-plot of $|l(j\omega)|$. Therefore in classical loop shaping, stability margins are improved by "flattening" $|l(j\omega)|$ in the intermediate frequency range. This again is compatible with the $\mathcal{H}^\infty$-optimization problem under consideration since in (4.22) we see that $J(\omega_c)$ decreases as the roll-off rate of $|l(j\omega_c)|$ (and hence $-\angle l(j\omega_c)$) is decreased. However, if $|l(j\omega)|$ is too large at low frequencies and/or too small at high frequencies, then there may be little scope for flattening $|l(j\omega)|$ in the intermediate range.

Loosely speaking, $J(\omega)$ will have a peak near ω_c if $|l(j\omega)|$ is too large at low frequencies and/or too small at high frequencies.

To summarize, equations (4.20) and (4.22) yield

$$J(\omega) \approx \begin{cases} |r_1 \frac{1}{l}| & \text{for } \omega \ll \omega_c, \quad \text{if } |r_1 \frac{1}{l}|^2 \gg |r_2|^2 \\ |r_2 l| & \text{for } \omega \gg \omega_c, \quad \text{if } |r_1|^2 \ll |r_2 l|^2 \\ \frac{\sqrt{|r_1|^2 + |r_2|^2}}{2\cos[\frac{\angle l(j\omega_c)}{2}]} & \text{for } \omega \approx \omega_c \end{cases} \tag{4.23}$$

Now it is well known that the optimal $\mathcal{H}^\infty$ cost function $J(\omega)$ is a constant independent of frequency. Therefore, the above expressions for $J(\omega)$ indicate that if classical loop shaping was being used to minimize the $\mathcal{H}^\infty$ cost function, then $|l(j\omega)|$ should be made parallel to $|r_1(j\omega)|$ in the low frequency range, parallel to

$|r_2(j\omega)|^{-1}$ in the high frequency range, and be shaped as flat as possible in the intermediate frequency range.

Finally let us consider more carefully the effect of the numerator of $J(\omega_c)$. Define the crossover-gap

$$\Delta\omega = \omega_2 - \omega_1 \tag{4.24}$$

where ω_1 and ω_2 are respectively the first and second crossover frequencies for $\sqrt{|r_1(j\omega)|^2 + |r_2(j\omega)|^2}$ as shown in Figure 4.6. If the crossover-gap is wide enough, then $|l(j\omega)|$ can be shaped easily near ω_c to decrease the cost function $J(\omega)$. Therefore the $\mathcal{H}^\infty$-optimal cost function can be decreased by further separating the curves of generalized weighting functions $|r_1(j\omega)|$ and $|r_2(j\omega)|$. In a given design problem, however, the freedom for changing the weights may be limited by other constraints. Thus the design difficulty is inversely proportional to the width $\Delta\omega$ of the crossover gap.

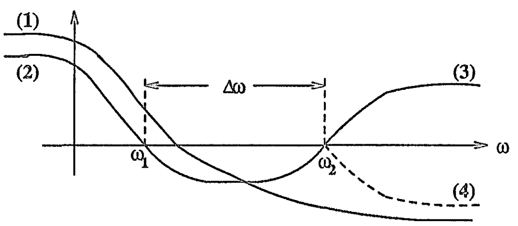

Figure 4.6: Crossover-gap $\Delta\omega$ and $|l(j\omega)|$:
(1) $|l(j\omega)|$; (2) $\sqrt{|r_1(j\omega)|^2 + |r_2(j\omega)|^2} \approx |r_1(j\omega)|$;
(3) $\sqrt{|r_1(j\omega)|^2 + |r_2(j\omega)|^2} \approx |r_2(j\omega)|$ and
(4) $\left(\sqrt{|r_1(j\omega)|^2 + |r_2(j\omega)|^2}\right)^{-1} \approx |r_2(j\omega)|^{-1}$.

4.4 Robust Performance by Loop Shaping

Consider the robust performance problem of finding a stabilizing controller $K(s)$ which satisfies (4.14), i.e.

$$\begin{aligned}\inf_{K(s)}\sup_{\omega\in\mathcal{R}} \mu_{\tilde{\Delta}}(M) &= \inf_{K(s)}\sup_{\omega\in\mathcal{R}} \left\{|r_1(j\omega)s(j\omega)| + |r_2(j\omega)t(j\omega)|\right\} \\ &=: \inf_{K(s)}\sup_{\omega\in\mathcal{R}} \mu(\omega) \end{aligned} \tag{4.25}$$

where

$$\mu(\omega) := |r_1(j\omega)s(j\omega)| + |r_2(j\omega)t(j\omega)| \tag{4.26}$$

Since

$$\mu(\omega) \geq J(\omega) \tag{4.27}$$

the crossover-gap of $\mu(\omega)$ is narrower than that of $J(\omega)$ which implies that loop shaping for robust performance will be more difficult than for the $\mathcal{H}^\infty$ mixed sensitivity problem of Section 3.

The following two facts are useful in understanding the relationship between $J(\omega)$ and $\mu(\omega)$.

Fact 1: $J(\omega) \leq \mu(\omega) \leq \sqrt{2}J(\omega), \quad \forall\omega \in \mathcal{R}$

Fact 2: If there exits ω_0, such that

$$|l(j\omega_0)| = \left|\frac{r_1(j\omega_0)}{r_2(j\omega_0)}\right| \tag{4.28}$$

then for the $\mathcal{H}^\infty$-optimal controller $K_\infty(s)$ satisfying (4.15) we have

$$\max_{\omega\in\mathcal{R}} \mu(\omega) = \sqrt{2}\gamma_0 \tag{4.29}$$

where γ_0 denotes the $\mathcal{H}^\infty$-optimal cost. An illustration of this fact is shown in Figure 4.7.

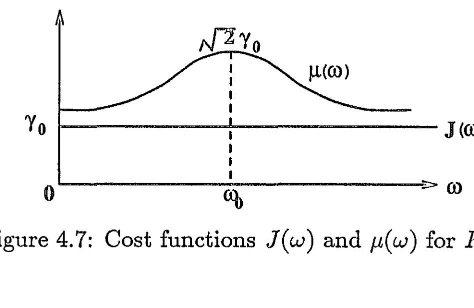

Figure 4.7: Cost functions $J(\omega)$ and $\mu(\omega)$ for $K_\infty(s)$.

In [Hel85] a general theorem is given which can be applied to the optimization problem in (4.25) to infer that the optimal robust performance cost function $\mu(\omega)$ is a constant independent of frequency for some cases. This result together with Fact 2 suggests the following loop shaping method for finding an approximate solution to the robust performance problem:

Step 1: Obtain an $\mathcal{H}^\infty$-controller $K_\infty(s)$, either approximately by loop shaping as in Section 3, or exactly by $\mathcal{H}^\infty$-optimization. This gives

$$l_\infty(s) = K_\infty(s)G_0(s) \tag{4.30}$$

and the corresponding $\mu(\omega)$ will be similar in shape to that shown in Figure 4.7.
Step 2: Introduce a cascade compensator to decrease the maximum value of $\mu(\omega)$ by loop shaping, that is, decrease the loop gain at low frequencies and increase it at high frequencies.

Step 2 has the effect of flattening the loop transfer function in the intermediate frequency range thereby decreasing the peak value of $\mu(\omega)$. Note that as $\mu(\omega)$ is decreased to improve robust performance the $\mathcal{H}^\infty$ cost $J(\omega)$ will increase causing a deterioration in nominal performance. This inherent trade-off between nominal performance and robust performance should be no surprise.

4.5 A Robot Arm Example

In the section, the loop shaping approach to robust performance will be applied to the design of a controller for an industrial robot arm [ÅNG86]. The transfer function of the robot arm, from the motor current to the motor angular velocity is

$$G(s) = \frac{k_m(J_a s^2 + ds + k)}{(s+p)[J_a J_m s^2 + d(J_a + J_m)s + k(J_a + J_m)]} \tag{4.31}$$

where

$$\begin{aligned} J_m &= 0.002, \quad k = 100, \quad k_m = 0.5, \quad d = 0.0001, \quad p = 0.01 \text{ and} \\ J_a &\in [0.0002, 0.002] \end{aligned}$$

The moment of inertia of the arm varies considerably with arm angle. The small constant p is added to avoid the so-called Model Matching Transformation zero [OPG89] caused by a plant pole at the origin.

Let us examine the numerator of (4.31). The ratio of the coefficient of s^2 to the constant term is very small, about 10^{-5}, and so (4.31) is numerically ill-conditioned. After some manipulation, (4.31) can be changed to

$$G(\hat{s}) = \frac{\hat{k}_m(\hat{J}_a\hat{s}^2 + \hat{d}\hat{s} + \hat{k})}{(\hat{s}+\hat{p})[\hat{J}_a\hat{J}_m\hat{s}^2 + \hat{d}(\hat{J}_a + \hat{J}_m)\hat{s} + \hat{k}(\hat{J}_a + \hat{J}_m)]} \tag{4.32}$$

where

$$\begin{aligned} \hat{s} &= \frac{s}{100}, \\ \hat{p} &= 0.0001, \quad \hat{J}_m = 2, \quad \hat{k} = 10, \quad \hat{k}_m = 5, \quad \hat{d} = 0.001 \text{ and} \\ \hat{J}_a &\in [0.2, 2] \end{aligned}$$

which is numerically easier to work with.

We will describe the uncertain moment of inertia by an additive perturbation as shown in Figure 4.1. The perturbed plant is therefore

$$G(s) = G_0(s) + \Delta(s) \tag{4.33}$$

In Figure 4.8 Bode plots of the perturbed plant are shown for a range of values of J_a. The nominal plant $G_0(s)$ corresponds to $J_a = 0.0011$, the middle value of the variation. By a curve fitting method, the maximum additive-error can be tightly bounded by a rational function $W_2(s)$ which is stable and minimum phase; see Figure 4.9. If the error is not bounded tightly, the design will be more conservative. However the order of $W_2(s)$ increases as the error bound is tightened. The weighting function $W_2(s)$ is selected as

$$W_2(s) = 1.2731 \times 10^3 \frac{(s+20.1 \pm j238)(s+59.7 \pm j226)(s+49.8 \pm j99.2)(s+99.5 \pm j31.5)}{(s+194 \pm j521)(s+44.9 \pm j396)(s+4.42 \pm j332)(s+0.01)(s+1500)}$$

Note that it is not allowed to roll off at high frequencies since this would encourage high gains in the $\mathcal{H}^\infty$-controller.

On the other hand, the performance bounding function $W_1(s)^{-1}$ is chosen as

$$W_1(s) = 316\frac{(\frac{s}{115}+1)^2}{(\frac{s}{1.2}+1)^2}$$

which is compatible with the sensitivity functions achieved in [OHÅP88].

Step 1.

Using the command hinf in the robust-control toolbox of MATLAB, $K_\infty(s)$ is found to be

$$K_\infty(s) = 0.04\frac{(s+4.42\pm j332)(s+194\pm j521)(s+44.8\pm j396)(s+0.01)(s+17.1)(s+1500)}{(s+7312)(s+176)(s+22.9\pm j231)(s+46.5\pm j226)(s+84.8\pm j151)(s+1.21)^2}$$

with

$$\gamma_0 = 0.7$$

The order of the controller is high because of the high order of $W_2(s)$. The results for the $\mathcal{H}^\infty$-controller are shown in Figures 4.10 and 4.11. It is interesting to note that $|l(j\omega)|$ is parallel with $W_1(s)$ at low frequencies and parallel with $|\frac{W_2(j\omega)}{G_0(j\omega)}|^{-1}$ at high frequencies.

Step 2.

The loop shaping method is now used to reduce the maximum value of $\mu(\omega)$. The μ-controller $K_\mu(s)$ is chosen as

$$K_\mu(s) = \frac{(s+41.8)}{(s+38)} \times \frac{(\frac{s}{200}+1)}{(\frac{s}{264}+1)} \times K_\infty(s) \tag{4.34}$$

by introducing compensation to shape the loop transfer function at low frequencies and at high frequencies. The results for the μ controller are shown in Figures 4.12 and 4.13. At high frequencies both $\mu(\omega)$ and $J(\omega)$ go to zero because a suboptimal nonequalizing $\mathcal{H}^\infty$-controller is obtained from hinf.

Figure 4.14 shows the Bode plots of the output sensitivity function, the transfer function from the disturbance d to the output e for 3 different values of J_a. The bandwidth is about $\omega = 30 \sim 50$ rad/sec. Figure 4.15 illustrates the output step-responses to a unit disturbance for a variety of values of J_a. The response is oscillatory for small J_a, i.e. $J_a = 0.0002$, but is otherwise satisfactory.

4.6 Summary

A loop shaping method has been presented for solving a scalar robust performance problem. Useful insight was given into the relationship between classical loop shaping and an $\mathcal{H}^\infty$ mixed sensitivity problem. The approach was demonstrated by its application to the control of a robot arm whose moment of inertia varies considerably with angle. This was modelled as a perturbed plant with additive uncertainty. To tightly bound the uncertainty thereby reducing conservatism a high order weight was required which resulted in a high order controller.

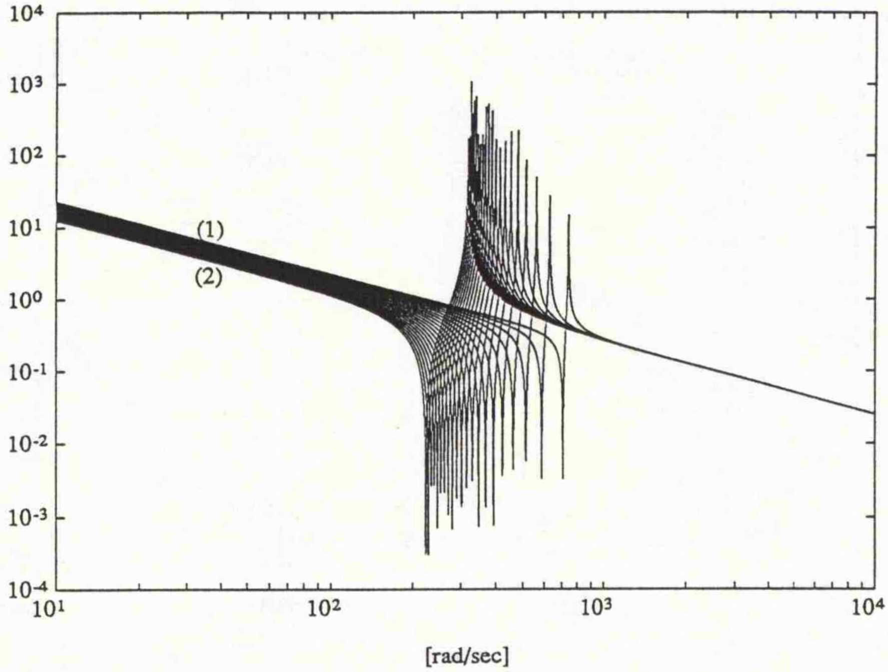

Figure 4.8: Bode plots of the perturbed plant for different values of J_a: (1) $Ja = 0.0002$ and (2) $Ja = 0.002$.

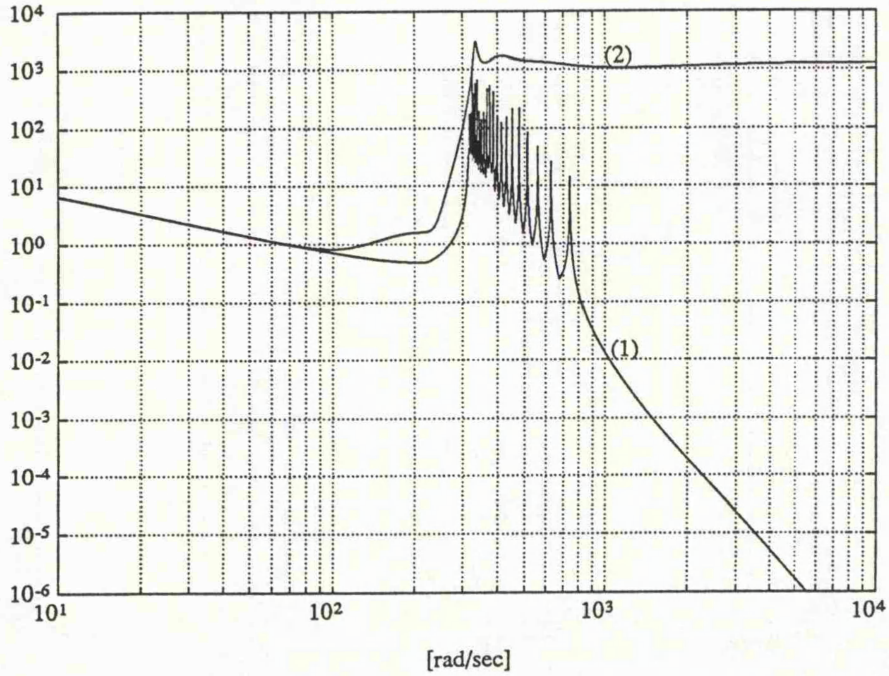

Figure 4.9: Bode plots of the additive-error and the error-bounding function: (1) additive-error and (2) error-bounding function $W_2(s)$.

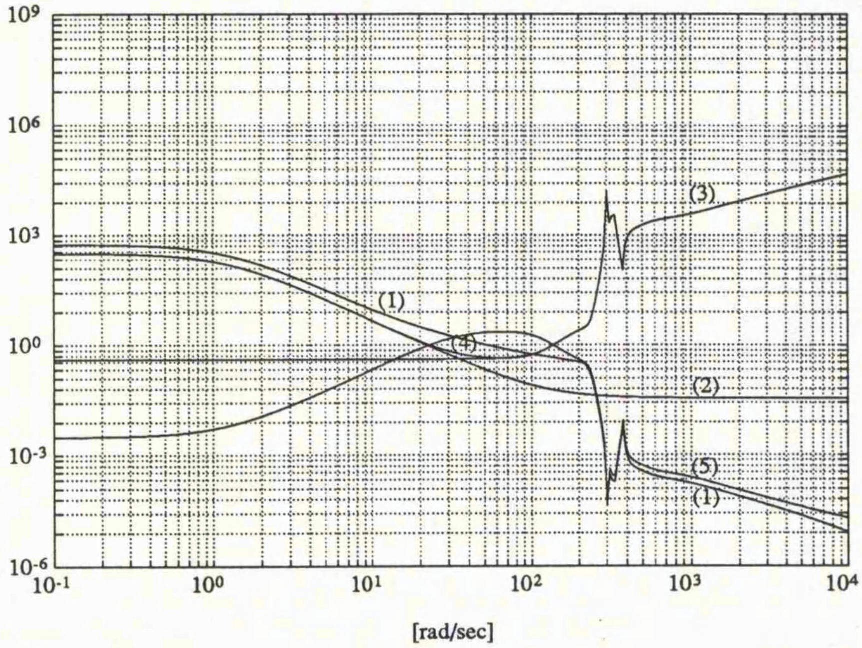

Figure 4.10: $\mathcal{H}^\infty$-optimal controller characteristics:
(1) $|l(j\omega)|$; (2) $|W_1(j\omega)|$; (3) $|W_2(j\omega)/G_0(j\omega)|$;
(4) $\sqrt{|W_1|^2 + |W_2(j\omega)/G_0(j\omega)|^2}$ and (5) $\left(\sqrt{|W_1|^2 + |W_2(j\omega)/G_0(j\omega)|^2}\right)^{-1}$.

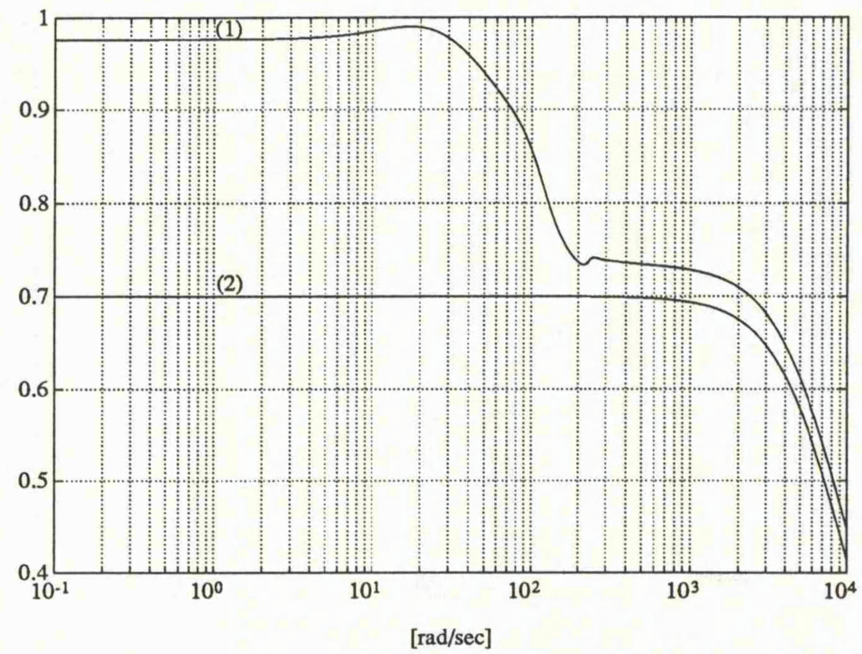

Figure 4.11: For $\mathcal{H}^\infty$-controller: (1) $\mu(\omega)$ and (2) $J(\omega)$.

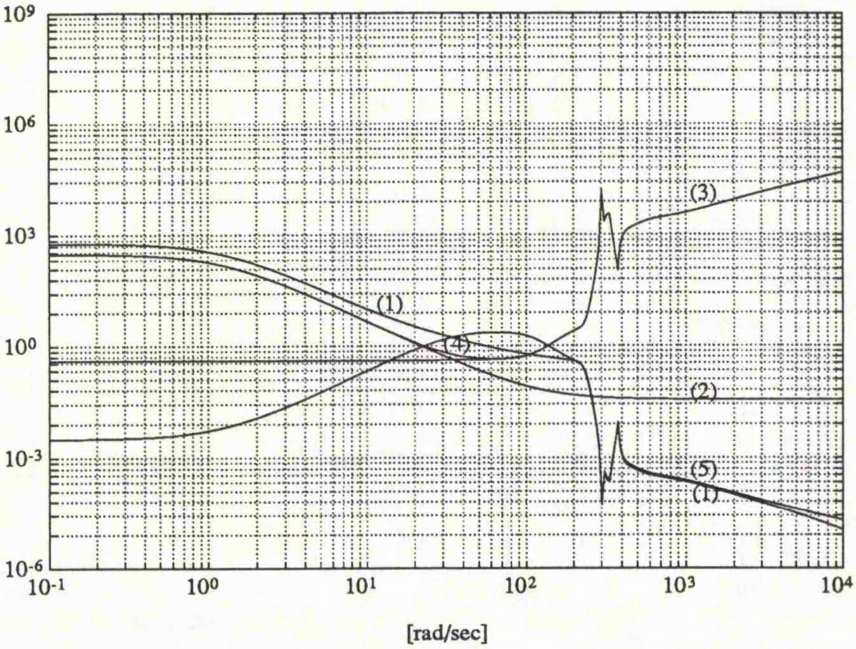

Figure 4.12: μ-optimal controller characteristics:

(1) $|l(j\omega)|$; (2) $|W_1(j\omega)|$; (3) $|W_2(j\omega)/G_0(j\omega)|$;

(4) $\sqrt{|W_1|^2 + |W_2(j\omega)/G_0(j\omega)|^2}$ and (5) $\left(\sqrt{|W_1|^2 + |W_2(j\omega)/G_0(j\omega)|^2}\right)^{-1}$.

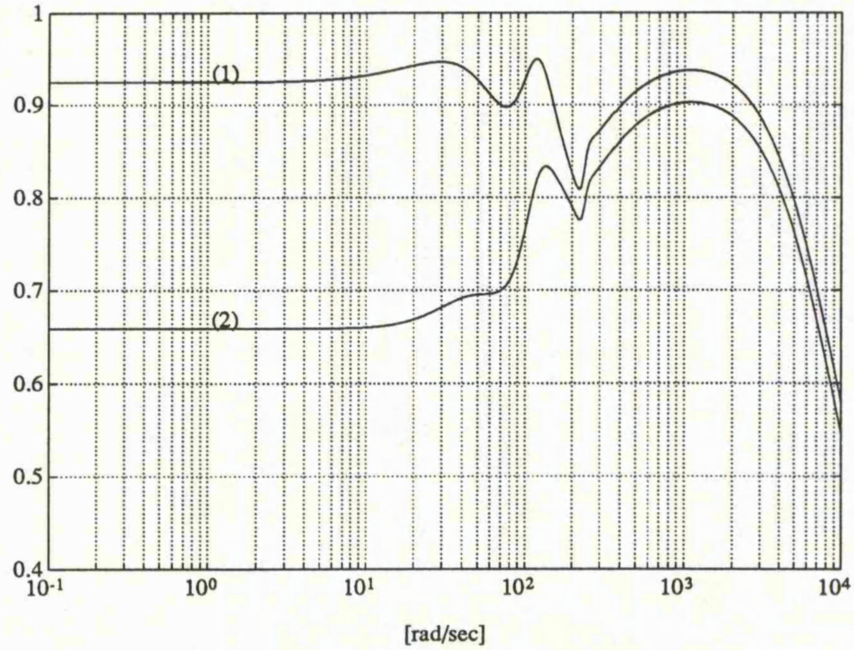

Figure 4.13: For μ-controller: (1) $\mu(\omega)$ and (2) $J(\omega)$.

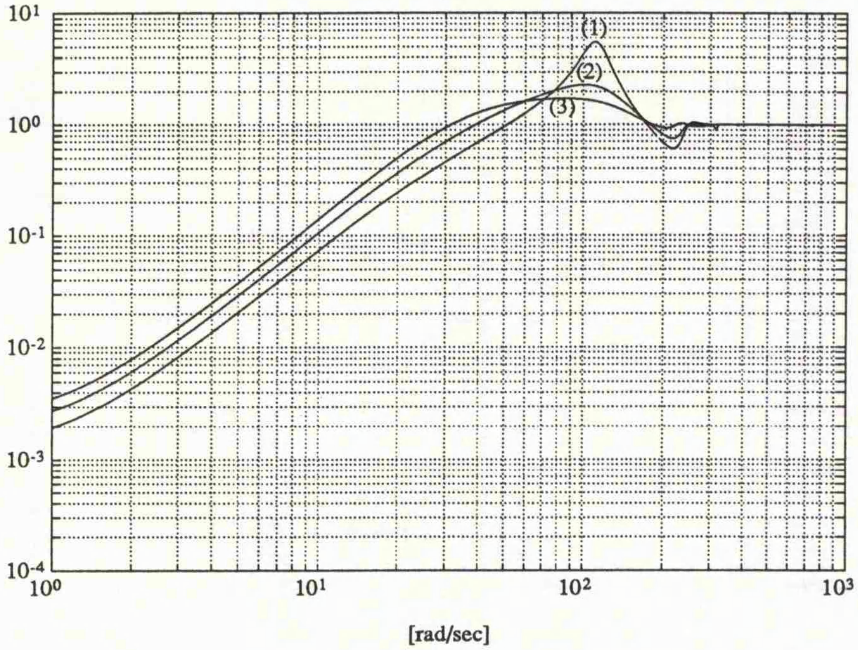

Figure 4.14: Bode plots of sensitivity function for different values of J_a: (1) $J_a = 0.0002$; (2) $J_a = 0.0011$ and (3) $J_a = 0.002$.

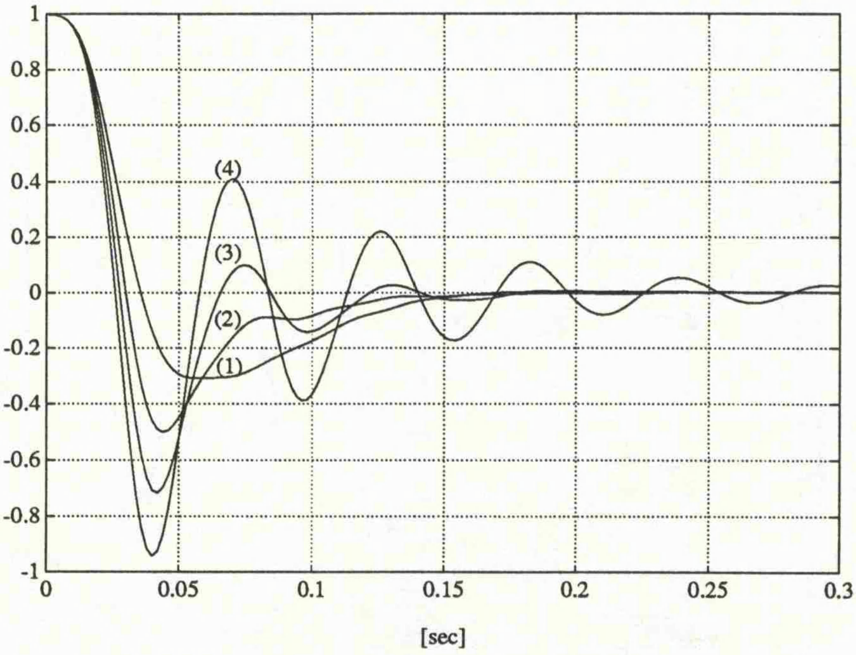

Figure 4.15: Step responses of the disturbance for different values of J_a: (1) $J_a = 0.002$; (2) $J_a = 0.0011$; (3) $J_a = 0.0006$ and (4) $J_a = 0.0002$.

Chapter 5

μ-K ITERATION: A NEW ALGORITHM FOR μ-SYNTHESIS

5.1 Introduction

Robust performance is said to be achieved if the design specifications of a controlled system are satisfied in the presence of disturbance signals and model uncertainties. A general framework for analyzing robust performance using the structured singular value μ as a measure of performance was introduced by Doyle [Doy82], who later proposed a controller synthesis procedure, called μ-synthesis [Doy85]. In this procedure a controller is sought which minimizes μ, or which achieves level of performance arbitrarily close to the optimum μ. This minimization problem has not yet been solved, but in [Doy85] an approximate solution is given involving a sequence of minimizations, called $D - K$ iteration.

Recall that in Section 3.10, the robust performance design problem can be stated as

$$\inf_{K \text{ stabilizing}} \sup_{\omega \in \mathcal{R}} \mu_{\tilde{\Delta}}(M) \tag{5.1}$$

This problem has proved difficult to solve and a solution is still not available. However, an approximate solution has been given by Doyle [Doy85] based on the following bound

$$\mu_{\tilde{\Delta}}(M) \leq \inf_{D \in \mathbf{D}} \bar{\sigma}\left(DMD^{-1}\right) \tag{5.2}$$

The idea is to look for a solution to

$$\inf_{K \ \mathit{stabilizing}} \sup_{\omega \in \mathcal{R}} \inf_{D \in \mathbf{D}} \bar{\sigma}\left(DMD^{-1}\right) \tag{5.3}$$

even though the upper bound is not always equal to μ. For fixed D, (1.3) is equivalent to

$$\inf_{K(s)} \left\| F_l(\tilde{P}, K) \right\|_\infty \tag{5.4}$$

as shown in (3.123), where $\tilde{P} := \tilde{D}P\tilde{D}^{-1}$ and $\tilde{D} := \operatorname{diag}\{D, I\}$. This is a standard form of $\mathcal{H}^\infty$-optimization problem. Therefore the approximation of $\inf_{D \in \mathbf{D}} \bar{\sigma}(DMD^{-1})$ to $\mu_{\tilde{\Delta}}(M)$ plays a key role in μ-synthesis. In real-μ or mixed-μ analysis, the structured singular value $\mu_{\tilde{\Delta}}(M)$ with respect to real parametric uncertainties or mixed real/complex uncertainties might not be approximated by $\inf_{D \in \mathbf{D}} \bar{\sigma}(DMD^{-1})$, in which case $D - K$ iteration fails. This is the reason why μ-synthesis is only applicable to a feedback system with complex uncertainties. In those cases Doyle has conjectured that this upper bound is within 15% for the true value of $\mu_{\tilde{\Delta}}(M)$. If μ-synthesis is used to design a μ-optimal controller of a system with real parametric uncertainties, the degree of conservatism is arbitrarily large! However, $\mu - K$ iteration as proposed in this chapter can overcome these problems and is applicable for controller design for complex-μ, real-μ or mixed-μ cases.

The new procedure, $\mu - K$ iteration, which will be presented here is motivated by the following:

- In Helton [Hel85], it is stated that many optimization problems have the property that an optimum solution must make the objective function constant in ω almost everywhere.

- In many examples, using $D - K$ iteration it can be observed that the "μ-optimal" controller appears to flatten $\mu_{\tilde{\Delta}}(M)$ at least over the bandwidth of the system. A peak in the μ-curve implies that a small perturbation exists for which the desired levels of robust stability and robust performance will not be achieved.

The idea then in the new algorithm is to determine a sequence of controllers which yield a flat structured singular value. This after all is what happens in $\mathcal{H}^\infty$ optimization where the $\mathcal{H}^\infty$-optimal controller results in a cost function with a flat maximum singular value.

To get some insight into how this might be done we will consider a specific robust performance problem for a single-input single-output plant. This is covered in Section 5.2. Then in Section 5.3 the $\mu-K$ iteration algorithm is presented for the general robust performance problem. Convergence of the algorithm is considered in Section 5.4, and two illustrative examples are described in Section 5.5. A brief summary is given in the last section.

5.2 A SISO Robust Performance Problem

To gain insight into the new algorithm, $\mu - K$ iteration, let us consider a *SISO* control system configuration of Figure 5.1, with the following nomenclature:

G_0 : nominal plant, with multiplicative input uncertainty

Δ : normalized model error, $\|\Delta\|_\infty \leq 1$

W_2 : (model) error bounding function

W_1 : performance weighting function

Δ_p : normalized fictitious uncertainty to characterize performance, $\|\Delta_p\|_\infty \leq 1$

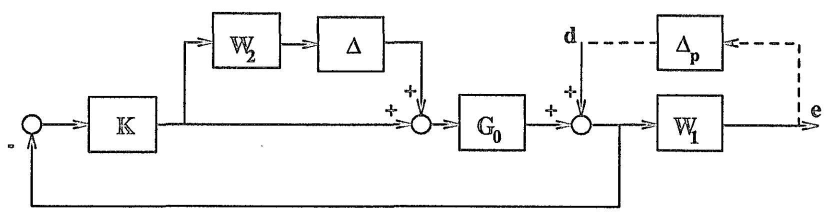

Figure 5.1: A *SISO* robust performance problem.

The configuration can be rearranged into the standard $M - \tilde{\Delta}$ structure of by setting

$$\tilde{\Delta} = \text{diag}(\Delta, \Delta_p) \tag{5.5}$$

In which case, the interconnection matrix M is given by

$$M = \begin{bmatrix} -W_2T_0 & -W_2T_0G_0^{-1} \\ W_1S_0G_0 & W_1S_0 \end{bmatrix} \tag{5.6}$$

where

$$T_0 := KG_0(I + KG_0)^{-1} \tag{5.7}$$

is the nominal complementary sensitivity function, and

$$S_0 := (I + G_0K)^{-1} \tag{5.8}$$

is the nominal sensitivity function.

The robust performance problem is to find a stabilizing controller K such that the $\mathcal{H}^\infty$ norm of the transfer function from d to e is less than 1 for all perturbations Δ, $\|\Delta\|_\infty \leq 1$. This is equivalent to finding a stabilizing controller K such that $\mu_{\tilde{\Delta}}(M) < 1$, and therefore it makes sense to try to solve (5.1).

For this relatively simple interconnection matrix M the following facts can be shown:

Fact 1:

$$\mu_{\tilde{\Delta}}(M) \leq \bar{\sigma}(M), \quad \forall \omega \in \mathcal{R} \tag{5.9}$$

Fact 2:

$$\bar{\sigma}(M) = \|M\|_F\,, \quad \text{the Frobenius norm of } M \tag{5.10}$$

Fact 3:

$$\mu_{\tilde{\Delta}}(M) = |W_1S_0| + |W_2T_0|\ , \quad \text{where } |\cdot| \text{ denotes modulus} \tag{5.11}$$

Fact 4:

If at some frequency ω_0

$$|W_1S_0G_0| = |W_2T_0G_0^{-1}| \tag{5.12}$$

then

$$\mu_{\tilde{\Delta}}(M) = \bar{\sigma}(M) \tag{5.13}$$

at the same frequency ω_0.

Suppose now that an $\mathcal{H}^\infty$-optimal controller K_0 is found for M, i.e. we solve

$$\inf_{K \text{ stabilizing}} \|M\|_\infty \tag{5.14}$$

It is well known that $\bar{\sigma}[M(K_0)]$ is flat over frequency, and from the above facts (and our observations) $\mu_{\tilde{\Delta}}[M(K_0)]$ will often have a bandpass-like characteristic as illustrated in Figure 1.2. A little thought suggests that a controller which forces $\mu_{\tilde{\Delta}}(M)$ to be flat will result in a convex $\bar{\sigma}(M)$. Suppose then that we multiply M by a bandpass-like rational function $r(s)$ similar to the shape of $\mu_{\tilde{\Delta}}[M(K_0)]$ and calculate the $\mathcal{H}^\infty$-optimal controller K_1 for the product rM. One might then expect $\bar{\sigma}[M(K_1)]$ to be convex with $\mu_{\tilde{\Delta}}[M(K_1)]$ flatter than $\mu_{\tilde{\Delta}}[M(K_0)]$. This leads us into the $\mu - K$ iteration algorithm presented for a general multivariable problem in the next section.

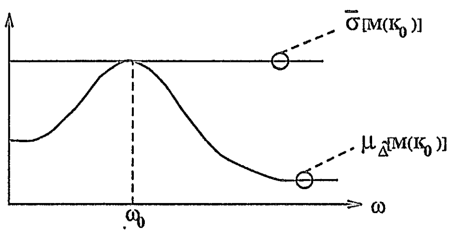

Figure 5.2: The maximum and structured singular values of $M(K_0)$.

5.3 $\mu - K$ Iteration

The above discussion motivates the algorithm now proposed for finding an approximate solution to the general robust performance problem

$$\inf_{K \text{ stabilizing}} \sup_{\omega \in \mathcal{R}} \mu_{\tilde{\Delta}}\left[F_l(P,K)\right] \tag{5.15}$$

The basic strategy is to "flatten" the μ-curve.

Step 1:

Find the stabilizing $\mathcal{H}^\infty$-optimal controller (a variety of methods exist)

$$K_0 := \arg \inf_K \|F_l(P,K)\|_\infty \tag{5.16}$$

The optimization is over stabilizing K, but for notational convenience in (1.16) and much of what follows the word "stabilizing" has been omitted.

Step 2:

Find the μ-curve corresponding to K_0 (the Matlab toolbox, μ-Tools [BDGPS91], could be used for this)

$$\mu_0(j\omega) := \mu_{\tilde{\Delta}}\left[F_l(P, K_0)\right] \tag{5.17}$$

over a suitable range of frequencies.

Step 3:

Normalize $\mu_0(j\omega)$ by its maximum value. Let $\tilde{\mu}_0(j\omega)$ denote the normalized $\mu_0(j\omega)$.

Step 4:

Find a scalar stable minimum phase real rational function $\tilde{\mu}_0(s)$ by fitting to the $\tilde{\mu}_0(j\omega)$-curve obtained in Step 3.

Step 5:

Multiply the interconnection matrix $F_l(P, K)$ by $\tilde{\mu}_0(s)$. In the specific example of Section 2 this would correspond to multiplying each of the weights W_1 and W_2 by $\tilde{\mu}_0(s)$.

Step 6:

Find the $\mathcal{H}^\infty$-optimal controller

$$K_1(s) := \arg \inf_K \left\|\tilde{\mu}_0(s) F_l(P, K)\right\|_\infty \tag{5.18}$$

Step 7:

Find the μ-curve corresponding to K_1

$$\mu_1(j\omega) := \mu_{\tilde{\Delta}}\left[F_l(P, K_1)\right] \tag{5.19}$$

over the frequency range of interest.

Step 8:

Normalize $\mu_1(j\omega)$ and denote it by $\tilde{\mu}_1(j\omega)$.

Step 9:

Curve fit $\tilde{\mu}_1(j\omega)$ to get $\tilde{\mu}_1(s)$.

Step 10:

Find the $\mathcal{H}^\infty$-optimal controller

$$K_2(s) := \arg \inf_K \|\tilde{\mu}_1(s)\tilde{\mu}_0(s)F_l(P,K)\|_\infty \tag{5.20}$$

Step 11:

Find the μ-curve corresponding to K_2

$$\mu_2(j\omega) = \mu_{\tilde{\Delta}}\left[F_l(P,K_2)\right] \tag{5.21}$$

Subsequent steps of the algorithm should now be clear, and in practice would be continued until the μ-curve was sufficiently flat over the frequency range of interest or until the desired level of performance (as measured by the peak value of μ) had been reached.

5.4 Convergence

In this section we consider the convergence properties of the proposed $\mu - K$ algorithm.

The algorithm generates the following sequences:

$$\begin{array}{rclll} K_0 & = & \arg \inf_K \|F_l(P,K)\|_\infty & & \mu_0 = \mu_{\tilde{\Delta}}\left[F_l(P,K_0)\right] \\ K_1 & = & \arg \inf_K \|\tilde{\mu}_0 F_l(P,K)\|_\infty & & \mu_1 = \mu_{\tilde{\Delta}}\left[F_l(P,K_1)\right] \\ K_2 & = & \arg \inf_K \|\tilde{\mu}_1\tilde{\mu}_0 F_l(P,K)\|_\infty & & \mu_2 = \mu_{\tilde{\Delta}}\left[F_l(P,K_2)\right] \\ & & \vdots & & \vdots \end{array} \tag{5.22}$$

Suppose that we normalize each of the μ-functions by dividing each curve by its maximum value:

$$\tilde{\mu}_n := \frac{\mu_n}{\|\mu_n\|_\infty}, \quad n = 0,1,2,\cdots \tag{5.23}$$

Then, it is easy to see that

$$0 \leq \tilde{\mu}_n(j\omega) \leq 1 \;\; \forall\omega \in \mathcal{R} \quad \text{and} \quad \|\tilde{\mu}_n\|_\infty = 1, \quad n = 0,1,2,\cdots \tag{5.24}$$

Consider the infinite sequence $\{c_n\}_{n=0}^{\infty}$ defined by

$$\begin{aligned} c_0 &:= \left\|F_l(P, K_0)\right\|_\infty = \inf_K \left\|F_l(P, K)\right\|_\infty \\ c_1 &:= \left\|\tilde{\mu}_0 F_l(P, K_1)\right\|_\infty = \inf_K \left\|\tilde{\mu}_0 F_l(P, K)\right\|_\infty \\ c_2 &:= \left\|\tilde{\mu}_1 \tilde{\mu}_0 F_l(P, K_2)\right\|_\infty = \inf_K \left\|\tilde{\mu}_1 \tilde{\mu}_0 F_l(P, K)\right\|_\infty \\ &\vdots \end{aligned} \tag{5.25}$$

Now because $\bar{\sigma}[\tilde{\mu}_{n-1} \cdots \tilde{\mu}_0 F_l(P, K_n)]$ is constant in ω, it follows from (5.24) that

$$\left\|\tilde{\mu}_{n-1} \cdots \tilde{\mu}_0 F_l(P, K_n)\right\|_\infty = \left\|\tilde{\mu}_n \tilde{\mu}_{n-1} \cdots \tilde{\mu}_0 F_l(P, K_n)\right\|_\infty \tag{5.26}$$

and hence

$$\begin{aligned} c_n &= \left\|\tilde{\mu}_{n-1} \cdots \tilde{\mu}_0 F_l(P, K_n)\right\|_\infty \\ &= \left\|\tilde{\mu}_n \tilde{\mu}_{n-1} \cdots \tilde{\mu}_0 F_l(P, K_n)\right\|_\infty \\ &\geq \inf_K \left\|\tilde{\mu}_n \tilde{\mu}_{n-1} \cdots \tilde{\mu}_0 F_l(P, K)\right\|_\infty \\ &= c_{n+1} \end{aligned} \tag{5.27}$$

That is

$$c_n \geq c_{n+1} \geq 0 \tag{5.28}$$

The sequence $\{c_n\}_{n=0}^{\infty}$ is therefore monotonically decreasing and bounded, and by the Bolzano-Weierstrass theorem [Bar66] it has a limit point. That is

$$c_n \longrightarrow \text{limit point}, \qquad \text{as} \quad n \longrightarrow \infty \tag{5.29}$$

We now present a reasoned argument for believing that the sequence $\{\tilde{\mu}_n\}$ will converge to a frequency independent function equal to 1.

First, a Lemma which follows from [Hel85]:

Lemma 5.4-1 Let $J(\cdot)$ be a "well-posed" cost function i.e. it satisfies Helton's assumptions (1985, Theorem 4.1). Then if for a given controller K_i, $\bar{\sigma}[J(K_i)]$ is frequency dependent, then there exists another controller K_j such that $\bar{\sigma}[J(K_j)]$ is frequency independent and $\left\|J(K_j)\right\|_\infty < \left\|J(K_i)\right\|_\infty$. ▫

Next, let

$$J_n(K) = \tilde{\mu}_{n-1} \cdots \tilde{\mu}_0 F_l(P, K) \tag{5.30}$$

and assume that Helton's assumptions are satisfied. Then with this notation we have from (5.27) that

$$c_n = \|J_n(K_n)\|_\infty \geq \|\tilde{\mu}_n J_n(K_n)\|_\infty \tag{5.31}$$

Therefore if $\tilde{\mu}_n$ is frequency dependent we have by the Lemma that

$$\inf_K \|\tilde{\mu}_n J_n(K)\|_\infty < \|\tilde{\mu}_n J_n(K_n)\|_\infty \tag{5.32}$$

or equivalently

$$c_{n+1} < c_n \tag{5.33}$$

But we have already shown that the sequence $\{c_n\}$ converges and therefore the sequence $\{\tilde{\mu}_n\}$ must also converge to a frequency independent function (which must be 1 by normalization), otherwise $\{c_n\}$ may well decrease below the positive limit.

The above argument is clearly lacking in rigour, but it does offer support to the observed effectiveness of the algorithm.

5.5 Examples

Two examples are given to illustrate the application of the $\mu - K$ iteration algorithm. Example 5.5-1 is $SISO$ and example 5.5-2 is $MIMO$.

Example 5.5-1: In this example we solve the following robust performance problem:

$$\inf_{K \text{ stabilizing}} \sup_{\omega \in \mathcal{R}} \mu_{\tilde{\Delta}}(M)$$

where

$$M = \begin{bmatrix} -W_2 T_0 G_0^{-1} & -W_1 W_2 T_0 G_0^{-1} \\ S_0 & W_1 S_0 \end{bmatrix}, \quad \mu_\Delta(M) = |W_1 S_0| + \left|W_2 T_0 G_0^{-1}\right|$$

and

$$\begin{aligned} G_0(s) &= \frac{0.5(1-s)}{(s+2)(s+0.5)} \\ W_1(s) &= 50\frac{1+\frac{s}{1.245}}{1+\frac{s}{0.007}} \\ W_2(s) &= 0.1256\frac{1+\frac{s}{0.502}}{1+\frac{s}{2}} \end{aligned}$$

The design problem corresponds to meeting disturbance rejection requirements in the presence of plant uncertainty modelled by an additive perturbation; see Figure 5.3.

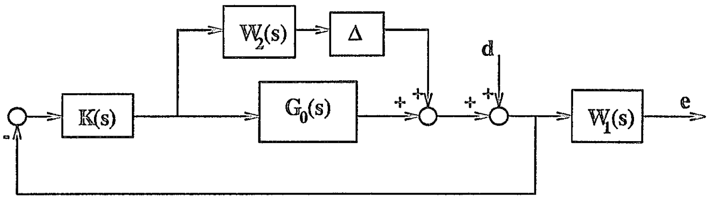

Figure 5.3: System with additive uncertainty.

Bode magnitude diagrams of the weighting functions and the open-loop gain are shown in Figure 5.4. The μ-curve is approximately flat after just 3 $\mu - K$ iterations as shown in Figure 5.5. The Bode magnitude diagram of the μ-optimal controller is given in Figure 5.6.

Example 5.5-2: This *MIMO* example is taken from the MATLAB toolbox manual, μ-TOOLS [BDGPS91] where it is used to demonstrate μ-synthesis. The problem is to meet disturbance rejection requirements in the presence of plant uncertainty modelled as a multiplicative perturbation at the plant input. The plant model is known as HIMAT and represents a scaled version of a remotely piloted aircraft. The nominal state-space model is

$$A = \begin{bmatrix} -0.0226 & -36.6 & -18.9 & -32.1 \\ 0 & -1.9 & 0.983 & 0 \\ 0.0123 & -11.7 & -2.63 & 0 \\ 0 & 0 & 1 & 0 \end{bmatrix} \qquad B = \begin{bmatrix} 0 & 0 \\ -0.414 & 0 \\ -77.8 & 22.4 \\ 0 & 0 \end{bmatrix}$$

$$C = \begin{bmatrix} 0 & 57.3 & 0 & 0 \\ 0 & 0 & 0 & 57.3 \end{bmatrix} \qquad D = \begin{bmatrix} 0 & 0 \\ 0 & 0 \end{bmatrix}$$

and the weighting functions for the multivariable version of the interconnection matrix M as shown in (5.6) are

$$\begin{aligned} W_1(s) &= \frac{0.5(s+3)}{s+0.03} I_2 \\ W_2(s) &= \frac{50(s+100)}{s+10000} I_2 \end{aligned}$$

where I_2 is the 2×2 identity matrix.

Bode magnitude diagrams of the weighting functions and the singular values of the open-loop gain are shown in Figure 5.7. The μ-curves for several $\mu - K$ iterations are shown in Figure 5.8. The Bode diagrams of the singular values of the μ-optimal controller are shown in Figure 5.9.

5.6 Summary

A new algorithm, $\mu - K$ iteration, has been presented for μ-synthesis. The accuracy of the algorithm depends on the curve fitting of the $\tilde{\mu}(j\omega)$ curves. In the examples tested so far the algorithm compares well with $D - K$ iteration and only requires a single scalar function to be fitted over frequency at each iteration. Each iteration does, however, require the calculation of μ over a range of frequencies, and this computation is known to be difficult in general. As with $D - K$ iteration, there is no *a priori* guarantee that the $\mu - K$ iteration algorithm will converge to a global minimum. When applied to ill-conditioned plants it has been observed (although not shown here) that the $\mu - K$ iteration is more stable (computationally) than $D - K$ iteration; this will be the topic of further research in the next chapter. Furthermore, as will be shown in Chapter 7, the algorithm can be also used to design a μ-optimal controller for robust performance if the perturbed systems have parametric (real) modelling uncertainties.

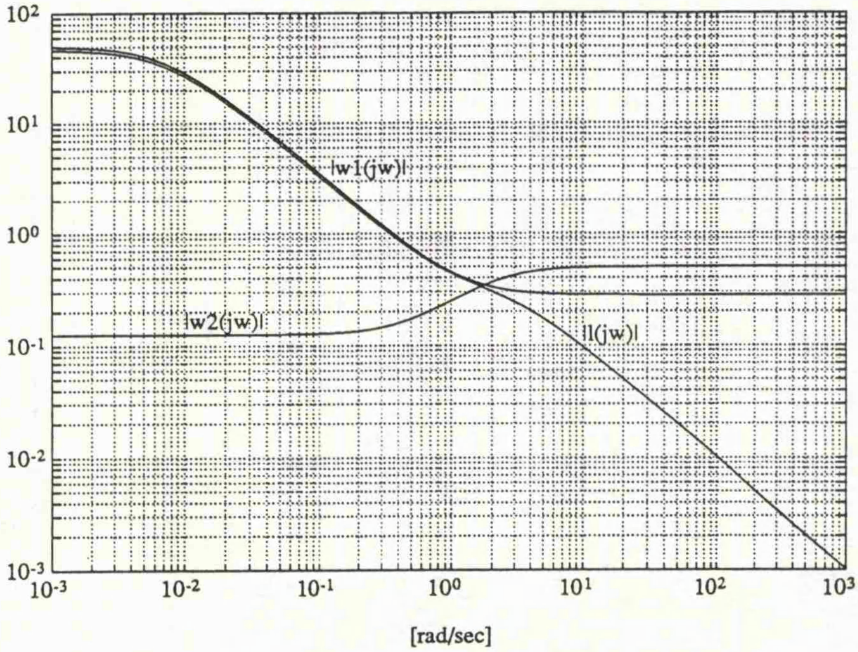

Figure 5.4: Bode magnitude diagrams of the weighting functions and the open-loop gain (Example 1).

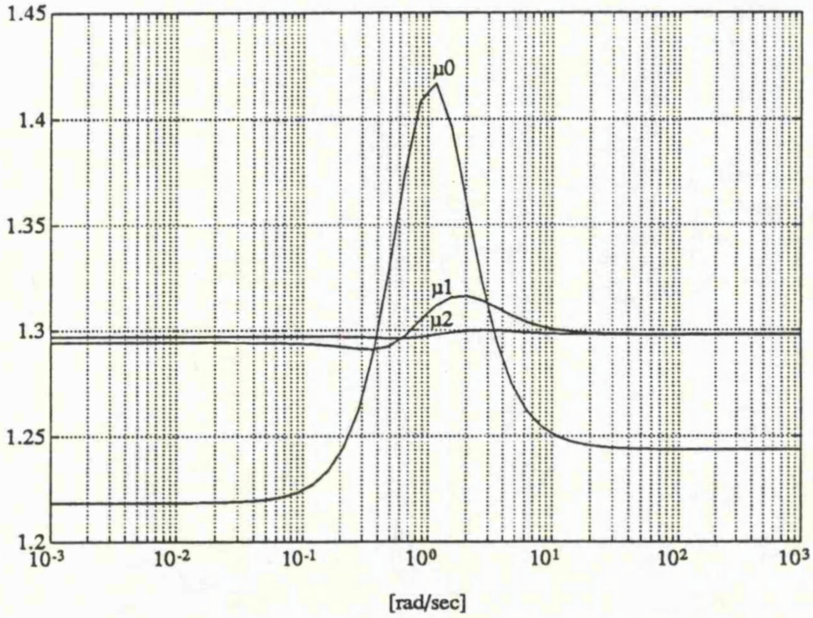

Figure 5.5: Bode magnitude diagrams of the μ curves of the 3 $\mu - K$ iterations (Example 1).

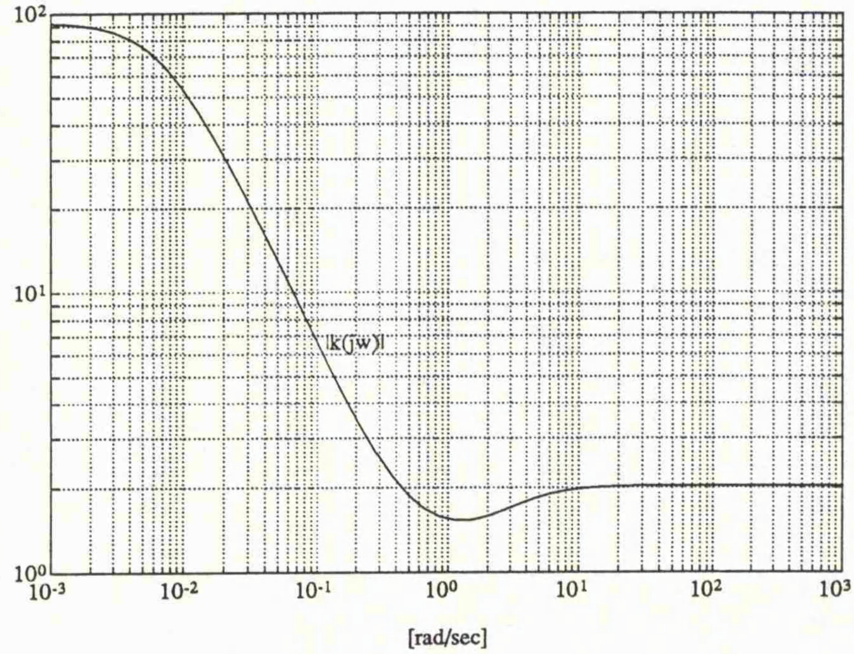

Figure 5.6: Bode magnitude diagram of the μ-optimal controller (Example 1).

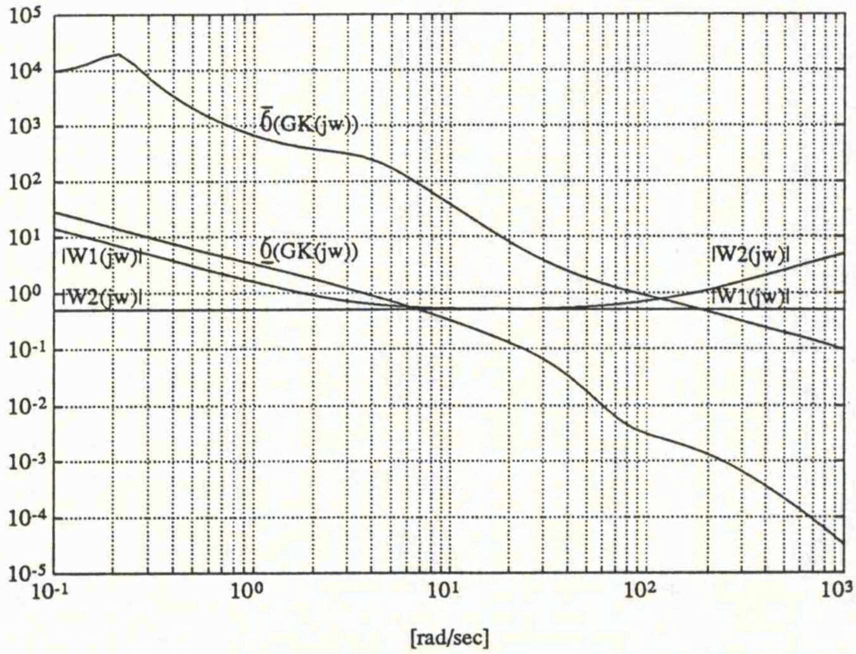

Figure 5.7: Bode magnitude diagrams of the weighting functions and the singular values of the open-loop gain (Example 2).

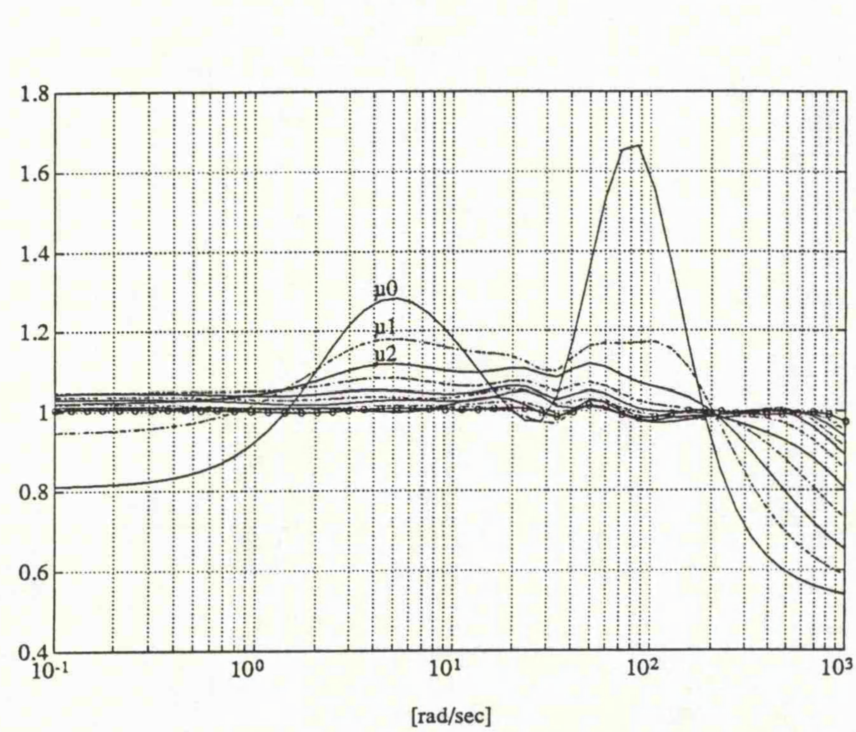

Figure 5.8: The μ-curves for several $\mu - K$ iterations (Example 2).

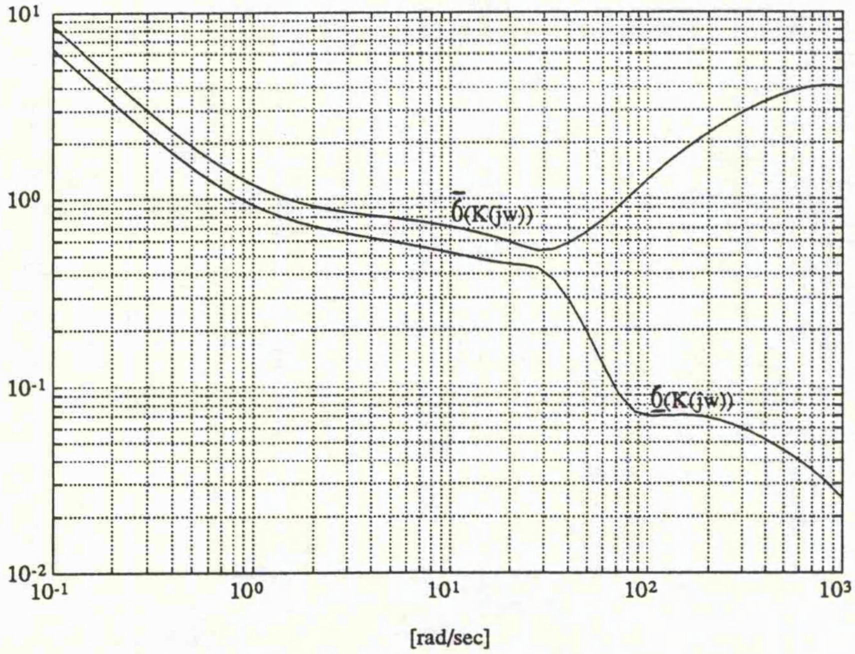

Figure 5.9: Bode diagrams of the singular values of the μ-optimal controller (Example 2).

Chapter 6

ROBUST CONTROL OF A DISTILLATION COLUMN

6.1 Introduction

The purpose of this chapter is to give insight into the problems associated with the control of ill-conditioned plants, and to illustrate the usefulness of μ-synthesis by $\mu - K$ iteration. As in [SMD88] we focus on the control of a high purity distillation column, and use the same linear plant model.

The paper of Skogestad, Morari and Doyle [SMD88] generated interest in controller design for ill-conditioned distillation column systems and was followed up by a design case study attempted by several authors at the 30th IEEE Conference on Decision and Control held in Brighton, 1991, [HHL91] [PLG91b] [ZhK91] and [YaH91]. Skogestad, Morari and Doyle [SMD88] also applied $D-K$ iteration to design a μ-optimal controller. It is therefore of interest in this thesis to use this same example to design a μ-optimal controller using $\mu - K$ iteration.

A full description of the distillation column is given in [SMD88]. A brief description of the model is given below. The distillation column configuration to be studied is given in Figure 6.19. The purpose of the distillation column is to separate the output feed into its light (concentrated in the distillate) and heavy components (concentrated in the bottom product). The manipulated variables are the boilup, the reflux and the distillate flow. The measurements are the controlled variables, namely the top and bottom compositions. We will only consider using two manipulated variables: reflux and boilup, which is so-called

LV configuration. We will use the same linear model as in [SMD88].

Before determining the μ-optimal controller we will consider some general problems associated with ill-conditioned plants. By analyzing a particular controller structure and design strategy, the potentially damaging effects of an ill-conditioned plant on robust stability and robust performance are revealed. The structured singular value μ, used to measure robustness, is shown to be determined at high frequencies by the high plant gain (largest singular value) and at low frequencies by the low plant gain (smallest singular value). This is as one might expect since small loop gain is typically required at high frequencies for robust stability, while large loop gain is usually required at low frequencies for robust performance. In the intermediate frequency range both the low and high plant gains are significant in determining μ.

A design is carried out for the distillation column using the $\mu - K$ iteration algorithm proposed in Chapter 5. This design example addresses the μ-optimal control problem also considered by Skogestad et al. [SMD88] using $D-K$ iteration, and by Freudenberg [Fre89b] using a loop shaping method. It is observed that the $\mu - K$ iteration method is able to reduce the size of μ below that reported in (Skogestad et al., 1988) and (Freudenberg, 1989) after 5 iterations. The design objective are the same as in [SMD88], and consequently the same weights are chosen. However, the design example is not very practical because no amplitude and bandwidth constraints are placed on the controller.

The chapter is organized as follows. In Section 6.2, a particular controller structure is presented for a 2-input 2-output system (corresponding to the distillation column). Analysis in Section 6.3 then shows how an ill-conditioned plant can be easily destabilized. In Section 6.4, it is shown how the optimal robustness measure μ is determined at high frequencies by the high plant gain and at low frequencies by the low plant gain. The robustness measure μ is analyzed in Section 6.5 for a plant inverting controller, thereby establishing the unsuitability of such a controller. From the analysis of Sections 6.3-6.5 a design strategy for shaping the loop gains is established in Section 6.6. The strategy is not easy to implement, but fortunately $\mu - K$ iteration can be used as shown in Section 6.7 where it is applied to the distillation column example. The chapter concludes in Section 6.8 with a summary and discussion of some of the important features of μ.

6.2 A Particular Controller Structure

Consider a $FDLTI$ perturbed plant with multiplicative uncertainty. The control requirement is to design a control system which remains stable and maintains a minimum performance level despite the presence of a disturbance signal d and model uncertainty Δ. The control configuration is shown in Figure 6.1, where G_0 is a nominal plant model with multiplicative input uncertainty. The uncertainty is represented by a normalized perturbation Δ ($\|\Delta\|_\infty \leq 1$), and an error bounding (weighting) function W_2. δ is a normalized fictitious performance perturbation ($\|\delta\|_\infty \leq 1$), with an associated weighting function W_1. For round directionality [Fre89b], the weights W_1 and W_2 are each assumed to be an identity matrix multiplied by a scalar stable and minimum-phase rational function (i.e. $W_1 = w_1 I$, $W_2 = w_2 I$). We will also assume that G_0 is nonsingular in the field of real rational matrix functions of s.

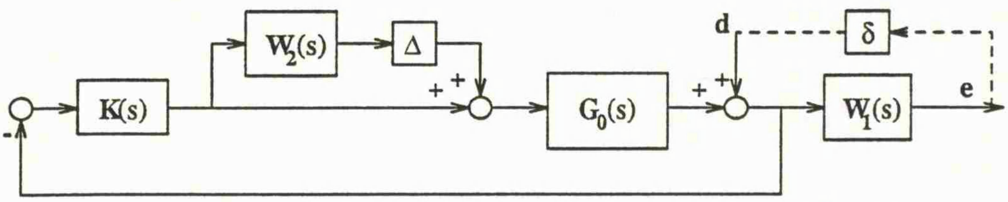

Figure 6.1: System with multiplicative input uncertainty.

Figure 6.1 can be rearranged into the $M - \tilde{\Delta}$ structure of Figure 6.2, where $\tilde{\Delta} :=$ diag $\{\Delta, \delta\}$, absorbing into M the weighting functions used to model the uncertainty and performance. The interconnection matrix is

$$M = \begin{bmatrix} -w_2 T_I & -w_2 T_I G_0^{-1} \\ w_1 S_O G_0 & w_1 S_O \end{bmatrix} \tag{6.1}$$

where the input complementary sensitivity function matrix is

$$T_I := KG_0(I + KG_0)^{-1} \tag{6.2}$$

and the output sensitivity function matrix is

$$S_O := (I + G_0 K)^{-1} \tag{6.3}$$

Recall that the ratio of the largest to the smallest singular value of a matrix is defined to be its condition number, and therefore

$$\text{cond } [G_0(j\omega)] = \frac{\bar{\sigma}\,[G_0(j\omega)]}{\underline{\sigma}\,[G_0(j\omega)]} \tag{6.4}$$

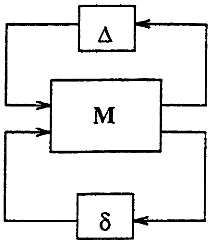

Figure 6.2: $M - \tilde{\Delta}$ structure of Figure 6.1.

If at some frequency the condition number equals one, then the level of gain is uniform in all directions at that frequency. A large value of the condition number implies that the gain of the system has a strong directional dependence and we say that it is ill-conditioned at that frequency.

Now suppose the singular value decomposition of G_0 is given by

$$G_0 = U\Sigma_0 V^* \tag{6.5}$$

It is then interesting, as in [Fre89b], to let the left and right singular subspaces of the controller $K(s)$ be dictated by the right and left singular subspaces of the plant. That is we will assume that the controller can be written as

$$K = V\Gamma U^* \tag{6.6}$$

By mathematical manipulation, this yields

$$T_I = KG_0(I+KG_0)^{-1} = V\Gamma\Sigma_0(I+\Gamma\Sigma_0)^{-1}V^* = V\tilde{T}_I V^* \tag{6.7}$$

$$T_I G_0^{-1} = V\tilde{T}_I V^* \cdot V\Sigma_0^{-1}U^* = V\tilde{T}_I\Sigma_0^{-1}U^* \tag{6.8}$$

$$S_O = (I+G_0K)^{-1} = U(I+\Sigma_0\Gamma)^{-1}U^* = U\tilde{S}_O U^* \tag{6.9}$$

$$S_O G_0 = U\tilde{S}_O U^* \cdot U\Sigma_0 V^* = U\tilde{S}_O\Sigma_0 V^* \tag{6.10}$$

where $\tilde{T}_I := \Gamma\Sigma_0(I+\Gamma\Sigma_0)^{-1}$ and $\tilde{S}_O := (I+\Sigma_0\Gamma)^{-1}$.

On substituting (6.7)-(6.10) into (6.1), the interconnection matrix M becomes

$$\begin{aligned} M &= \begin{bmatrix} -w_2 V\tilde{T}_I V^* & -w_2 V\tilde{T}_I \Sigma_0^{-1} U^* \\ w_1 U\tilde{S}_O \Sigma_0 V^* & w_1 U\tilde{S}_O U^* \end{bmatrix} \\ &= \begin{bmatrix} V & 0 \\ 0 & U \end{bmatrix} \begin{bmatrix} -w_2\tilde{T}_I & -w_2\tilde{T}_I\Sigma_0^{-1} \\ w_1\tilde{S}_O\Sigma_0 & w_1\tilde{S}_O \end{bmatrix} \begin{bmatrix} V & 0 \\ 0 & U \end{bmatrix}^* \\ &=: \begin{bmatrix} V & 0 \\ 0 & U \end{bmatrix} M_{svd} \begin{bmatrix} V & 0 \\ 0 & U \end{bmatrix}^* \end{aligned} \tag{6.11}$$

where

$$M_{svd} := \begin{bmatrix} -w_2\tilde{T}_I & -w_2\tilde{T}_I\Sigma_0^{-1} \\ w_1\tilde{S}_O\Sigma_0 & w_1\tilde{S}_O \end{bmatrix} \tag{6.12}$$

Since

$$\begin{bmatrix} V & 0 \\ 0 & U \end{bmatrix}$$

is a block diagonal unitary matrix which conforms with the block diagonal matrix

$$\tilde{\Delta} := \begin{bmatrix} \Delta & 0 \\ 0 & \delta \end{bmatrix}$$

it follows that

$$\bar{\sigma}(M) = \bar{\sigma}(M_{svd}) \tag{6.13}$$

and

$$\mu_{\tilde{\Delta}}(M) = \mu_{\tilde{\Delta}}(M_{svd}) \tag{6.14}$$

As far as the determination of μ is concerned, therefore, Figure 6.1 can be simplified to Figure 6.3 below.

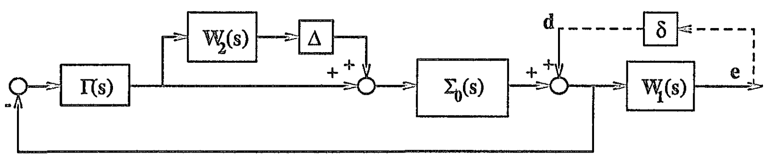

Figure 6.3: An simplified system of Figure 6.1.

In Figure 6.3 the plant Σ_0 and controller Γ are both diagonal and the corresponding interconnection matrix is M_{svd}. Therefore, for ease of notation we will in the following discussions assume that the nominal plant G_0 and controller K are diagonal. Also since we will principally be concerned with 2-input 2-output ill-conditioned plants we will assume that the nominal plant is given by

$$G_0(s) = \text{diag}\ \{g_1(s), g_2(s)\} \tag{6.15}$$

where

$$|g_1(j\omega)| \gg |g_2(j\omega)|\,, \quad \forall\omega \in \mathcal{R} \tag{6.16}$$

In the next section we show how such an ill-conditioned system is potentially very sensitive to small simultaneous perturbations.

6.3 Ill-Conditioned Plants and Robustness

The term "directionality" refers to the fact that multivariable systems possess properties that vary spatially, or with direction, as well as with frequency. For example, a multivariable plant may possess much higher levels of gain when acting on signals in certain loops than when acting on signals in others.

It is well known that when the plant is ill-conditioned with high condition number

$$\text{cond}\ [G_0(j\omega)] := \frac{|g_1(j\omega)|}{|g_2(j\omega)|} \gg 1, \quad \forall\omega \in \mathcal{R} \tag{6.17}$$

and when uncertainty and disturbances are present simultaneously at different points in the feedback loops, a singular value analysis may fail to yield a useful assessment of robustness [StD85]. From a system viewpoint ill-conditioning at a certain frequency means that the gain of the plant exhibits a strong directional dependence.

An ill-conditioned plant can be destabilized by small simultaneous perturbations as is now illustrated. Consider the system described in Figure 6.4 which is equivalent to Figure 6.3.

When the perturbations are chosen as

$$\Delta = \begin{bmatrix} \Delta_{11} & \Delta_{12} \\ \Delta_{21} & \Delta_{22} \end{bmatrix} = \begin{bmatrix} 0 & \Delta_{12} \\ 0 & 0 \end{bmatrix}, \quad \delta = \begin{bmatrix} \delta_{11} & \delta_{12} \\ \delta_{21} & \delta_{22} \end{bmatrix} = \begin{bmatrix} 0 & 0 \\ \delta_{21} & 0 \end{bmatrix} \tag{6.18}$$

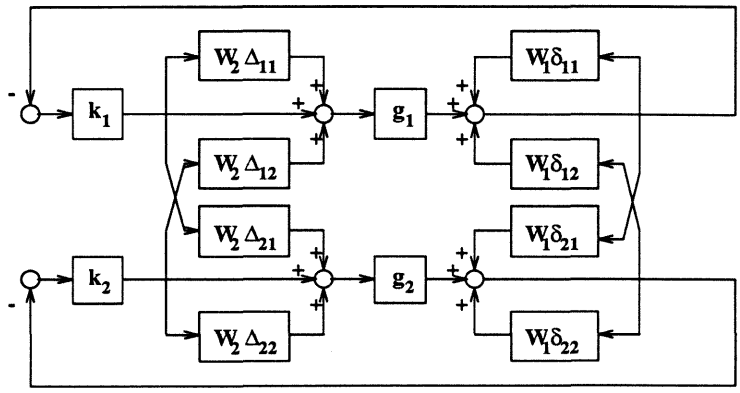

Figure 6.4: An equivalent system.

the characteristic equation, $\det(I - M\tilde{\Delta}) = 0$, of the closed-loop system is

$$(1 + k_1 g_1)(1 + k_2 g_2) + k_2 w_2 \Delta_{12} g_1 w_1 \delta_{21} = 0 \tag{6.19}$$

This implies

$$1 + \frac{w_1}{1 + k_1 g_1} \cdot \frac{w_2 k_2 g_2}{1 + k_2 g_2} \cdot \frac{g_1}{g_2} \Delta_{12} \delta_{21} = 0 \tag{6.20}$$

that is

$$1 + w_1 s_1 \cdot w_2 t_2 \cdot \frac{g_1}{g_2} \Delta_{12} \delta_{21} = 0 \tag{6.21}$$

where s_1 and t_2 denote the nominal sensitivity and nominal complementary sensitivity functions, respectively.

Choose

$$\Delta_{12} = \frac{1}{\sqrt{|w_1 s_1| \cdot |w_2 t_2| \cdot \left|\frac{g_1}{g_2}\right|}} \, e^{j\theta_1} \tag{6.22}$$

and

$$\delta_{21} = \frac{1}{\sqrt{|w_1 s_1| \cdot |w_2 t_2| \cdot \left|\frac{g_1}{g_2}\right|}} \, e^{j\theta_2} \tag{6.23}$$

where

$$\theta_1 + \theta_2 = \pi - \angle\left(w_1 s_1 \cdot w_2 t_2 \cdot \frac{g_1}{g_2} \right) \tag{6.24}$$

It is clear that Δ_{12} in (6.22) and δ_{21} in (6.23) satisfy equation (6.21) and

$$|\Delta_{12}| = |\delta_{21}| = \frac{1}{\sqrt{|w_1 s_1| \cdot |w_2 t_2| \cdot \left|\frac{g_1}{g_2}\right|}} \tag{6.25}$$

Therefore the structured singular value $\mu_{\tilde{\Delta}}(M)$ with respect to the structure $\tilde{\Delta} =$ diag $\{\Delta, \delta\}$ is

$$\begin{aligned}\mu_{\tilde{\Delta}}^{-1}(M) &= \min_{\tilde{\Delta}\in\tilde{\mathbf{\Delta}}} \left\{\bar{\sigma}\left(\tilde{\Delta}\right) : \det(I - M\tilde{\Delta}) = 0\right\} = \min_{\tilde{\Delta}\in\tilde{\mathbf{\Delta}}} \max\left\{\bar{\sigma}(\Delta), \bar{\sigma}(\delta)\right\} \\ &\leq \max\left\{|\Delta_{12}|, |\delta_{21}|\right\} = \frac{1}{\sqrt{|w_1 s_1| \cdot |w_2 t_2| \cdot \left|\frac{g_1}{g_2}\right|}}\end{aligned} \tag{6.26}$$

This implies

$$\mu_{\tilde{\Delta}}(M) \geq \sqrt{|w_1 s_1| \cdot |w_2 t_2| \cdot \left|\frac{g_1}{g_2}\right|} \tag{6.27}$$

The term $|g_1/g_2|$ in the right hand side of the above inequality is just the condition number of the plant. Hence a feedback system whose plant is ill-conditioned, ($|g_1(j\omega)/g_2(j\omega)| \gg 1,\ \forall\omega \in \mathcal{R}$), is potentially very sensitive to small sizes of "simultaneous" perturbations shown in (6.25) even though relatively much larger "individual" perturbations cannot cause instability. For individual perturbations, the system is robustly stable *iff*

$$|w_2 t_i| < 1, \quad \forall\omega \in \mathcal{R},\ i = 1, 2 \tag{6.28}$$

and

$$|w_1 s_i| < 1, \quad \forall\omega \in \mathcal{R},\ i = 1, 2 \tag{6.29}$$

Furthermore, the design strategy (of keeping μ small) requires that the terms $|w_1 s_1|$ and $|w_2 t_2|$ in (6.27) be kept small. This results from the interaction between the upper and lower loops.

It is very instructive for us to study further the inequality (6.27). Define

$$J(\omega) := \sqrt{|w_1(j\omega)s_1(j\omega)| \cdot |w_2(j\omega)t_2(j\omega)| \cdot \left|\frac{g_1(j\omega)}{g_2(j\omega)}\right|} \tag{6.30}$$

We will consider the value of $J(\omega)$ for 3 situations characterized by the nominal open-loop transfer functions

$$\begin{aligned}l_1(s) &:= k_1(s)g_1(s), \quad \text{and} \\ l_2(s) &:= k_2(s)g_2(s)\end{aligned}$$

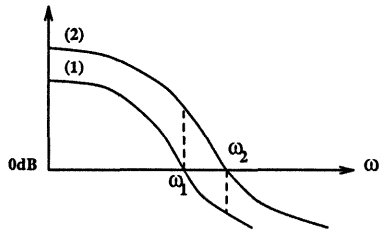

Figure 6.5: System with $|l_1(j\omega)| < |l_2(j\omega)|$. $(1): \; |l_1(j\omega)|$ and $(2): \; |l_2(j\omega)|$.

• **case (1):** $|l_1(j\omega)| < |l_2(j\omega)|, \; \forall \omega \in \mathcal{R}$; see Figure 6.5.

(a) at $\omega = \omega_1$:

$$\begin{aligned} |l_1(j\omega_1)| = 1 \;\Longrightarrow\; |s_1(j\omega_1)| &= \tfrac{1}{|1+l_1(j\omega_1)|} = \tfrac{1}{\left|2\cos\frac{\angle l_1(j\omega_1)}{2}\right|} \\ &= 1.3 \quad \text{if } \angle l_1(j\omega_1) = -135^o \\ \text{i.e. } & \text{ the phase margin } PM = 45^o \\ |l_2(j\omega_1)| \gg 1 \;\Longrightarrow\; |t_2(j\omega_1)| &= \left|\tfrac{l_2(j\omega_1)}{1+l_2(j\omega_1)}\right| \approx 1 \end{aligned}$$

Thus

$$J(\omega_1) \approx \sqrt{1.3\,|w_1(j\omega_1)| \cdot |w_2(j\omega_1)| \cdot \left|\frac{g_1(j\omega_1)}{g_2(j\omega_1)}\right|}$$

(b) at $\omega = \omega_2$:

$$\begin{aligned} |l_1(j\omega_2)| \ll 1 \;\Longrightarrow\; |s_1(j\omega_2)| &= \tfrac{1}{|1+l_1(j\omega_2)|} \approx 1 \\ |l_2(j\omega_2)| = 1 \;\Longrightarrow\; |t_2(j\omega_2)| &= \tfrac{|l_2(j\omega_2)|}{|1+l_2(j\omega_2)|} = 1.3 \quad \text{if } PM = 45^o \end{aligned}$$

Thus

$$J(\omega_2) \approx \sqrt{1.3\,|w_1(j\omega_2)| \cdot |w_2(j\omega_2)| \cdot \left|\frac{g_1(j\omega_2)}{g_2(j\omega_2)}\right|}$$

It is obvious that in this case both $J(\omega_1)$ and $J(\omega_2)$ will be large for an ill-conditioned plant. Note that the weights w_1 and w_2 will typically be near 1 in the crossover region.

• **case (2):** $|l_1(j\omega)| = |l_2(j\omega)|, \; \forall \omega \in \mathcal{R}$; see Figure 6.6.

This is the case for a plant-inverting controller. Let

$$|l_1(j\omega)| = |l_2(j\omega)| =: |l(j\omega)|$$

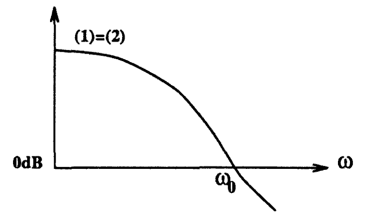

Figure 6.6: System with $|l_1(j\omega)| = |l_2(j\omega)|$. $(1):\ |l_1(j\omega)|$ and $(2):\ |l_2(j\omega)|$.

At unity-gain crossover frequency ω_0, $|l(j\omega_0)| = 1$, and we have

$$\begin{aligned} |s(j\omega_0)| &= \frac{1}{|1 + l(j\omega_0)|} = 1.3 \quad \text{if } PM = 45^o \\ |t(j\omega_0)| &= \frac{|l(j\omega_0)|}{|1 + l(j\omega_0)|} = 1.3 \quad \text{if } PM = 45^o \end{aligned}$$

Thus

$$J(\omega_0) = 1.3\sqrt{|w_1(j\omega_0)| \cdot |w_2(j\omega_0)| \cdot \left|\frac{g_1(j\omega_0)}{g_2(j\omega_0)}\right|}$$

which is large for an ill-conditioned plant.

- **case (3):** $|l_1(j\omega)| > |l_2(j\omega)|$, $\forall \omega \in \mathcal{R}$; see Figure 6.7.

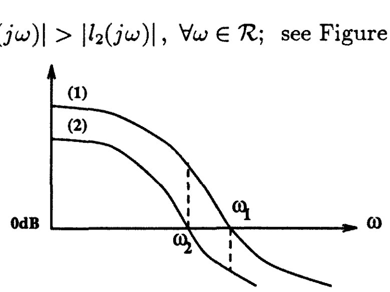

Figure 6.7: System with $|l_1(j\omega)| > |l_2(j\omega)|$. $(1):\ |l_1(j\omega)|$ and $(2):\ |l_2(j\omega)|$.

(a) at $\omega = \omega_2$:

$$\begin{aligned} |l_1(j\omega_2)| \gg 1 \implies |s_1(j\omega_2)| &= \tfrac{1}{|1+l_1(j\omega_2)|} \ll 1 \\ |l_2(j\omega_2)| = 1 \implies |t_2(j\omega_2)| &= \tfrac{|l_2(j\omega_2)|}{|1+l_2(j\omega_2)|} = 1.3 \quad \text{if } PM = 45^o \end{aligned}$$

Thus $J(\omega_2)$ will not be too large even if the plant is ill-conditioned.

(b) at $\omega = \omega_1$:

$$\begin{aligned} |l_1(j\omega_1)| = 1 \implies |s_1(j\omega_1)| &= \tfrac{1}{|1+l_1(j\omega_1)|} = 1.3 \quad \text{if } PM = 45^o \\ |l_2(j\omega_1)| \ll 1 \implies |t_2(j\omega_1)| &= \tfrac{|l_2(j\omega_1)|}{|1+l_2(j\omega_1)|} \approx |l_2(j\omega_1)| \ll 1 \end{aligned}$$

Thus $J(\omega_1)$ will not be too large even if the plant is ill-conditioned.

The above discussions reveal that case (3), in which

$$|l_1(j\omega)| > |l_2(j\omega)|, \quad \forall\omega \in \mathcal{R} \tag{6.31}$$

is the best way of keeping the value of $\mu_{\tilde{\Delta}}(M)$ small for all frequencies of interest.

6.4 Analysis for μ-Optimal Design

From the analysis of Section 6.2 it is clear that for the particular choice of controller we can, without loss of generality, assume that both G_0 and K are diagonal. Therefore (6.1) gives

$$M = \left[\begin{array}{cc|cc} -w_2 t_1 & 0 & -w_2 t_1 g_1^{-1} & 0 \\ 0 & -w_2 t_2 & 0 & -w_2 t_2 g_2^{-1} \\ \hline w_1 s_1 g_1 & 0 & w_1 s_1 & 0 \\ 0 & w_1 s_2 g_2 & 0 & w_1 s_2 \end{array}\right] \tag{6.32}$$

It follows from [Doy82] that if the number of nonrepeated uncertainty blocks in $\tilde{\Delta}$ is equal to or less than 3 in complex perturbation case, then

$$\mu_{\tilde{\Delta}}(M) = \inf_{D\in\mathbf{D}} \bar{\sigma}\left(DMD^{-1}\right) \tag{6.33}$$

where the scaling matrix $D = \operatorname{diag}\{I_2, dI_2\}$, with $d > 0$. Consider, therefore,

$$DMD^{-1} = \left[\begin{array}{cc|cc} -w_2 t_1 & 0 & -w_2 t_1 g_1^{-1} d^{-1} & 0 \\ 0 & -w_2 t_2 & 0 & -w_2 t_2 g_2^{-1} d^{-1} \\ \hline w_1 s_1 g_1 d & 0 & w_1 s_1 & 0 \\ 0 & w_1 s_2 g_2 d & 0 & w_1 s_2 \end{array}\right] \tag{6.34}$$

The rows and columns of the matrix DMD^{-1} can be interchanged by a permutation matrix P, $P = P^{-1} = P^T$. Choose

$$P = \begin{bmatrix} 1 & 0 & 0 & 0 \\ 0 & 0 & 1 & 0 \\ 0 & 1 & 0 & 0 \\ 0 & 0 & 0 & 1 \end{bmatrix} \tag{6.35}$$

Then direct manipulation gives

$$
\begin{aligned}
P\left(DMD^{-1}\right)P^{-1} &= \left[\begin{array}{cc|cc} -w_2t_1 & -w_2t_1g_1^{-1}d^{-1} & 0 & 0 \\ w_1s_1g_1d & w_1s_1 & 0 & 0 \\ \hline 0 & 0 & -w_2t_2 & -w_2t_2g_2^{-1}d^{-1} \\ 0 & 0 & w_1s_2g_2d & w_1s_2 \end{array}\right] \\
&=: \begin{bmatrix} \tilde{M}_{11}(d) & 0 \\ 0 & \tilde{M}_{22}(d) \end{bmatrix} =: \tilde{M}(d) \qquad (6.36)
\end{aligned}
$$

Thus

$$
\begin{aligned}
\mu_{\tilde{\Delta}}(M) &= \inf_{D\in\mathbf{D}} \bar{\sigma}\left(DMD^{-1}\right) = \inf_{D\in\mathbf{D}} \bar{\sigma}\left(PDMD^{-1}P^{-1}\right) \\
&= \inf_{d>0} \max\left\{\bar{\sigma}\left[\tilde{M}_{11}(d)\right], \bar{\sigma}\left[\tilde{M}_{22}(d)\right]\right\} \qquad (6.37)
\end{aligned}
$$

Mathematical manipulation then gives

- $\bar{\sigma}\left[\tilde{M}_{11}(d)\right] = \left\|\tilde{M}_{11}(d)\right\|_F, \quad \bar{\sigma}\left[\tilde{M}_{22}(d)\right] = \left\|\tilde{M}_{22}(d)\right\|_F$
- both $\bar{\sigma}\left[\tilde{M}_{11}(d)\right]$ and $\bar{\sigma}\left[\tilde{M}_{22}(d)\right]$ are convex functions of d.
- $\min_{d>0} \bar{\sigma}\left[\tilde{M}_{ii}(d)\right] = |w_2t_i| + |w_1s_i|, \quad i = 1,2, \quad$ when

$$
d = \sqrt{\left|\frac{w_2t_ig_i^{-1}}{w_1s_ig_i}\right|} =: d_i
$$

- $\mu_{\tilde{\Delta}}(M) \geq \max\{|w_2t_1| + |w_1s_1|, |w_2t_2| + |w_1s_2|\}$

The curves $\bar{\sigma}\left[\tilde{M}_{11}(d)\right]$ and $\bar{\sigma}\left[\tilde{M}_{22}(d)\right]$ are crucial in determining $\mu_{\tilde{\Delta}}(M)$ and therefore their study is clearly worthwhile. Three cases are shown in Figure 6.8.

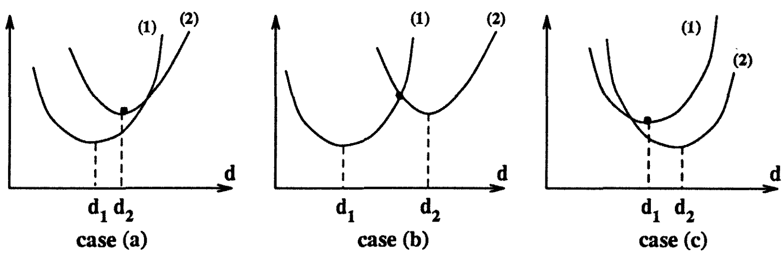

Figure 6.8: Curves of (1) : $\bar{\sigma}\left[\tilde{M}_{11}(d)\right]$ and (2) : $\bar{\sigma}\left[\tilde{M}_{22}(d)\right]$.

Furthermore, recall from Section 6.3 that for optimal μ the open-loop transfer functions should satisfy $|l_1(j\omega)| > |l_2(j\omega)|, \quad \forall\omega \in \mathcal{R}$. This directly implies the following results:

∘ <u>at low frequencies:</u> $|l_i(j\omega)| \gg 1, \quad i = 1, 2$

$$\begin{aligned} |t_2(j\omega)| &\approx |t_1(j\omega)| \approx 1 \\ |s_2(j\omega)| &\approx |l_2(j\omega)|^{-1}, \quad |s_1(j\omega)| \approx |l_1(j\omega)|^{-1} \end{aligned}$$

Thus

$$\begin{aligned} (6.31) &\implies |s_2(j\omega)| > |s_1(j\omega)| \\ &\implies |w_2 t_2| + |w_1 s_2| > |w_2 t_1| + |w_1 s_1| \\ &\implies \inf_{d>0} \bar{\sigma}\left[\tilde{M}_{22}(d)\right] > \inf_{d>0} \bar{\sigma}\left[\tilde{M}_{11}(d)\right] \end{aligned}$$

This corresponds to case (a) in Figure 6.8 and $\mu_{\tilde{\Delta}}(M) = \inf_{d>0} \bar{\sigma}\left[\tilde{M}_{22}(d)\right]$.

∘ <u>at high frequencies:</u> $|l_i(j\omega)| \ll 1, \quad i = 1, 2$

$$\begin{aligned} |s_2(j\omega)| &\approx |s_1(j\omega)| \approx 1 \\ |t_2(j\omega)| &\approx |l_2(j\omega)|, \quad |t_1(j\omega)| \approx |l_1(j\omega)| \end{aligned}$$

Thus

$$\begin{aligned} (6.31) &\implies |t_2(j\omega)| < |t_1(j\omega)| \\ &\implies |w_2 t_2| + |w_1 s_2| < |w_2 t_1| + |w_1 s_1| \\ &\implies \inf_{d>0} \bar{\sigma}\left[\tilde{M}_{22}(d)\right] < \inf_{d>0} \bar{\sigma}\left[\tilde{M}_{11}(d)\right] \end{aligned}$$

This corresponds to case (c) in Figure 6.8 and $\mu_{\tilde{\Delta}}(M) = \inf_{d>0} \bar{\sigma}\left[\tilde{M}_{11}(d)\right]$.

The structured singular value μ, has therefore been shown to be determined at low frequencies by the low gain g_2 in the lower loop. At high frequencies μ is dependent on the higher gain g_1 in the upper loop. This is not too surprising since robust performance requires high gains at low frequencies and robust stability demands low gains at high frequencies. Thus there exists no coupling between the upper and lower loops due to Δ_{ij} and δ_{ij} with $i \neq j$ at low and high frequencies. However a coupling effect does occur at intermediate frequencies for case (b), the transitional stage of the curves between case (a) and case (c).

6.5 Plant-Inverting Controllers

As multivariable control theory has developed there has been (particularly in the early days) a keen interest in controllers which aim to invert the plant. Consider therefore what happens when the single-loop controllers are chosen as

$$k_1(s) = \beta(s)g_1(s)^{-1}, \quad \text{and} \tag{6.38}$$

$$k_2(s) = \beta(s)g_2(s)^{-1} \tag{6.39}$$

where $\beta(s)$ is a scalar loop transfer function which makes $k_1(s)$ and $k_2(s)$ proper and ensures stability of the closed-loop system. We will calculate the structured singular value to evaluate the corresponding performance levels. For k_1 and k_2 given by (6.38) and (6.39), we have

$$t_1(s) = t_2(s) = \frac{\beta(s)}{1+\beta(s)} =: t(s), \quad \text{and} \tag{6.40}$$

$$s_1(s) = s_2(s) = \frac{1}{1+\beta(s)} =: s(s) \tag{6.41}$$

from which (6.36) becomes

$$\tilde{M}(d) = \left[\begin{array}{cc|cc} -w_2t & -w_2tg_1^{-1}d^{-1} & 0 & 0 \\ w_1sg_1d & w_1s & 0 & 0 \\ \hline 0 & 0 & -w_2t & -w_2tg_2^{-1}d^{-1} \\ 0 & 0 & w_1sg_2d & w_1s \end{array}\right] \tag{6.42}$$

The following results are useful:

- $\min_{d>0} \bar{\sigma}\left[\tilde{M}_{11}(d)\right] = |w_2t| + |w_1s|$, when

$$d = \sqrt{\left|\frac{w_2tg_1^{-1}}{w_1sg_1}\right|} =: d_1 \tag{6.43}$$

- $\min_{d>0} \bar{\sigma}\left[\tilde{M}_{22}(d)\right] = |w_2t| + |w_1s|$, when

$$d = \sqrt{\left|\frac{w_2tg_2^{-1}}{w_1sg_2}\right|} =: d_2 \tag{6.44}$$

- $\frac{d_1}{d_2} = \frac{|g_2|}{|g_1|} \ll 1$, since $|g_1| \gg |g_2|$
- $d_1 < d_2$ and $\min_{d>0} \bar{\sigma}\left[\tilde{M}_{11}(d)\right] = \min_{d>0} \bar{\sigma}\left[\tilde{M}_{22}(d)\right]$ imply

$$\begin{aligned} \bar{\sigma}\left[\tilde{M}_{22}(d_1)\right] &> \bar{\sigma}\left[\tilde{M}_{11}(d_1)\right], \text{ and} \qquad (6.45)\\ \bar{\sigma}\left[\tilde{M}_{11}(d_2)\right] &> \bar{\sigma}\left[\tilde{M}_{22}(d_2)\right] \qquad (6.46)\end{aligned}$$

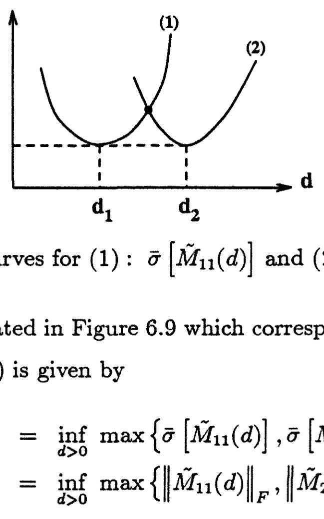

Figure 6.9: Curves for $(1): \bar{\sigma}\left[\tilde{M}_{11}(d)\right]$ and $(2): \bar{\sigma}\left[\tilde{M}_{22}(d)\right]$.

The latter are illustrated in Figure 6.9 which corresponds to case (b) in Figure 6.8. The value of $\mu_{\tilde{\Delta}}(M)$ is given by

$$\begin{aligned} \mu_{\tilde{\Delta}}(M) &= \inf_{d>0} \max\left\{\bar{\sigma}\left[\tilde{M}_{11}(d)\right], \bar{\sigma}\left[\tilde{M}_{22}(d)\right]\right\} \\ &= \inf_{d>0} \max\left\{\left\|\tilde{M}_{11}(d)\right\|_F, \left\|\tilde{M}_{22}(d)\right\|_F\right\} \qquad (6.47)\end{aligned}$$

and the optimal value $\hat{d}$ of (6.47) is

$$\begin{aligned} \hat{d} &= \arg \inf_{d>0} \max\left\{\left\|\tilde{M}_{11}(d)\right\|_F, \left\|\tilde{M}_{22}(d)\right\|_F\right\} \\ &= \arg\left\{d : \left\|\tilde{M}_{11}(d)\right\|_F = \left\|\tilde{M}_{22}(d)\right\|_F\right\} \\ &= \arg\left\{d : \left\|\tilde{M}_{11}(d)\right\|_F^2 = \left\|\tilde{M}_{22}(d)\right\|_F^2\right\} \\ &= \sqrt{\frac{|w_2 t|}{|w_1 s|} \cdot \frac{1}{|g_1 g_2|}} \qquad (6.48)\end{aligned}$$

This last equality follows directly from

$$\begin{aligned} \left\|\tilde{M}_{11}(d)\right\|_F^2 &= |w_2 t|^2 + |w_1 s|^2 + |w_1 s g_1 d|^2 + |w_2 t g_1^{-1} d^{-1}|^2, \text{ and} \qquad (6.49)\\ \left\|\tilde{M}_{22}(d)\right\|_F^2 &= |w_2 t|^2 + |w_1 s|^2 + |w_1 s g_2 d|^2 + |w_2 t g_2^{-1} d^{-1}|^2 \qquad (6.50)\end{aligned}$$

and thus

$$\begin{aligned}
\mu_{\tilde{\Delta}}(M)^2 &= |w_1 s|^2 + |w_2 t|^2 + |w_1 s| \cdot |w_2 t| \cdot \left[\frac{|g_1|}{|g_2|} + \frac{|g_2|}{|g_1|}\right] \\
&= |w_1 s|^2 + |w_2 t|^2 + |w_1 s| \cdot |w_2 t| \cdot \left[\mathrm{cond}\,(G_0) + \frac{1}{\mathrm{cond}\,(G_0)}\right] \quad (6.51)
\end{aligned}$$

Moreover, if the plant is ill-conditioned, $\mathrm{cond}(G_0) \gg 1$, and then (6.51) shows that $\mu_{\tilde{\Delta}}(M)$ achieved by the plant-inverting controller is proportional to the square root of the condition number of the plant, with constant of proportionality equal to the geometric mean of the nominal performance and robust stability functions, that is

$$\mu_{\tilde{\Delta}}(M) \approx \sqrt{|w_1 s| \cdot |w_2 t| \cdot \mathrm{cond}\,(G_0)} \quad (6.52)$$

For scalar plant, $\mathrm{cond}(G_0) = 1$, and (6.51) gives

$$\mu_{\tilde{\Delta}}(M) = |w_1 s| + |w_2 t| \quad (6.53)$$

6.6 A Design Strategy

From our analysis and the expectation that the optimal μ will be constant, at least over the frequencies of interest, we desire

$$\begin{aligned}
\mu_{\tilde{\Delta}}(M) &= |w_1 s_2| + |w_2 t_2| = c, \quad \text{in the low frequency range, and} \quad (6.54) \\
\mu_{\tilde{\Delta}}(M) &= |w_1 s_1| + |w_2 t_1| = c, \quad \text{in the high frequency range} \quad (6.55)
\end{aligned}$$

where c is a frequency independent constant. Furthermore, we can establish the following properties/guidelines for the optimal loop gains.

∘ In the low frequency range: $|l_2(j\omega)| \gg 1 \Longrightarrow |t_2(j\omega)| \approx 1$ and $|s_2(j\omega)| \approx |1/l_2(j\omega)|$. Assume that $|w_2(j\omega)|$ is constant in the low frequencies, then (6.54) implies

$$\left|w_1(j\omega)\frac{1}{l_2(j\omega)}\right| \approx |w_1(j\omega)s_2(j\omega)| = c - |w_2(j\omega)t_2(j\omega)| \approx c - |w_2(j\omega)| = \text{constant}$$

and hence

the loop gain $|l_2(j\omega)|$ // $|w_1(j\omega)|$ at low frequencies where a // b denotes that a is parallel to b.

• In the high frequency range: $|l_1(j\omega)| \ll 1 \Longrightarrow |t_1(j\omega)| \approx |l_1(j\omega)|$ and $|s_1(j\omega)| \approx 1$. Assume that $|w_1(j\omega)|$ is constant in the high frequencies, then (6.55) implies

$$|w_2(j\omega)l_1(j\omega)| \approx |w_2(j\omega)t_1(j\omega)| = c - |w_1(j\omega)s_1(j\omega)| \approx c - |w_1(j\omega)| = \text{constant}$$

and hence

$$\text{the loop gain } |l_1(j\omega)| \;//\; |w_2(j\omega)|^{-1} \text{ at high frequencies}$$

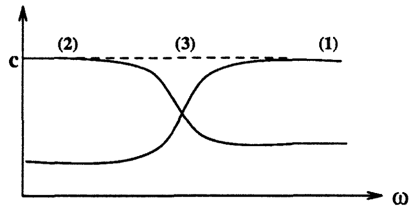

Figure 6.10: Curves of $(1): \; |w_1s_1| + |w_2t_1|$, $(2): \; |w_1s_2| + |w_2t_2|$ and $(3): \; \mu_{\tilde{\Delta}}(M)$.

But what should happen to $|l_2(j\omega)|$ at high frequencies and $|l_1(j\omega)|$ at low frequencies? The open-loop gains $|l_1(j\omega)|$ and $|l_2(j\omega)|$ should be shaped to reduce the coupling effect between the loops in the intermediate frequency range corresponding to case (b) in Figure 6.8. Note that in (6.27)

$$\mu_{\tilde{\Delta}}(M) \geq \sqrt{|w_1s_1| \cdot |w_2t_2| \cdot \left|\frac{g_1}{g_2}\right|}$$

which reveals the coupling effect of the simultaneous perturbations, Δ_{12} and δ_{21}, between the upper and lower loops.

It is very difficult to determine the optimal value c of $\mu_{\tilde{\Delta}}(M)$ and to properly shape the loop gains for optimality. Fortunately, we can use $\mu - K$ iteration as will be demonstrated in the next section.

6.7 Distillation Column Example

In this section a μ-optimal controller for an ill-conditioned plant is designed by $\mu-K$ iteration [LPG91]. The plant we consider is a simplified model of a high purity distillation column (LV-configuration) which was originally studied by Skogestad et al. [SMD88]. For more details of the process see [SMD88]. We will compare our results with those reported by Freudenberg [Fre89b] using a loop shaping method and by Skogestad et al. [SMD88] using Doyle's $D-K$ iteration methodology [Doy85].

The transfer function of the nominal plant is

$$G_0(s) = \frac{1}{75s+1}\begin{bmatrix} 0.878 & -0.864 \\ 1.082 & -1.096 \end{bmatrix} \tag{6.56}$$

and it is assumed that all the uncertainties can be represented by a normalized multiplicative input perturbation Δ, $\|\Delta\|_\infty \leq 1$, with error bounding function

$$W_2(s) = w_2 I = 2\,\frac{s+0.2}{s+2}\,I_2 \tag{6.57}$$

Performance is characterized by the performance weighting function

$$W_1(s) = w_1 I = \frac{1}{2}\,\frac{s+0.1}{s}\,I_2 \tag{6.58}$$

The singular value decomposition of $G_0(s)$ is given by

$$G_0(s) = U\Sigma_0(s)V^* \tag{6.59}$$

where

$$U = \begin{bmatrix} 0.6246 & 0.7809 \\ 0.7809 & -0.6246 \end{bmatrix}, \quad V = \begin{bmatrix} 0.7066 & 0.7077 \\ -0.7077 & 0.7066 \end{bmatrix} \tag{6.60}$$

and

$$\Sigma_0(s) = \text{diag}\left\{\frac{1.972}{75s+1}, \frac{0.01391}{75s+1}\right\} \tag{6.61}$$

Note that the singular subspaces do not vary with frequency and the condition number is constant

$$\text{cond}\,[G_0(j\omega)] = 141.7 \quad \forall\omega \in \mathcal{R} \tag{6.62}$$

The controller $K(s)$ is assumed, as in [Fre89b], to be

$$K(s) = V\Gamma(s)U^* \tag{6.63}$$

with

$$\Gamma(s) := \text{diag}\,\{k_1(s), k_2(s)\} \tag{6.64}$$

In the sequel, we will use "$\mu - K$" iteration to design a diagonal μ-optimal controller $\Gamma := \text{diag}\,\{k_1(s), k_2(s)\}$ for the nominal diagonal plant $\Sigma_0 = \text{diag}\,\left\{\frac{1.972}{75s+1}, \frac{0.01391}{75s+1}\right\}$.

The interconnection matrix $M(s)$ shown in (6.32) can be rearranged into the more compact form:

$$\begin{aligned}
\hat{M} &:= PMP^{-1} \\
&= \left[\begin{array}{cc|cc}
-w_2t_1 & -w_2t_1g_1^{-1} & 0 & 0 \\
w_1s_1g_1 & w_1s_1 & 0 & 0 \\
\hline
0 & 0 & -w_2t_2 & -w_2t_2g_2^{-1} \\
0 & 0 & w_1s_2g_2 & w_1s_2
\end{array}\right] \\
&=: \text{diag}\,\left\{\hat{M}_{11},\ \hat{M}_{22}\right\}
\end{aligned} \tag{6.65}$$

by use of a permutation matrix P as in (6.35).

Because of the special structure of $\hat{M}$ and K, we can solve for k_1 and k_2 separately. To see this consider the first stage of $\mu - K$ iteration, which in this case is the following $\mathcal{H}^\infty$-optimization:

$$\begin{aligned}
\inf_{k_1,k_2} \sup_{\omega}\ \bar{\sigma}\left[M(j\omega)\right] &= \inf_{k_1,k_2} \sup_{\omega}\ \bar{\sigma}\left[\hat{M}(j\omega)\right] \\
&= \max\left\{\inf_{k_1} \left\|\hat{M}_{11}\right\|_\infty, \inf_{k_2} \left\|\hat{M}_{22}\right\|_\infty\right\}
\end{aligned} \tag{6.66}$$

The above expression reveals that the optimal controllers $k_1(s)$ and $k_2(s)$ can be obtained separately from each loop, without loop coupling. It also demonstrates a benefit of super-optimal $\mathcal{H}^\infty$-optimization over standard $\mathcal{H}^\infty$-optimization. A problem with (6.66) is that $k_2(s)$ is hard to find by $\mathcal{H}^\infty$-optimization because

$$\left\|\hat{M}_{22}\right\|_\infty = \left\|\begin{array}{cc} -w_2t_2 & -w_2t_2g_2^{-1} \\ w_1s_2g_2 & w_1s_2 \end{array}\right\|_\infty \approx \left\|w_2t_2g_2^{-1}\right\|_\infty \tag{6.67}$$

due to the fact that $|g_2^{-1}|$ is very large and dominates all of the other terms. A remedy for this problem is to scale $\hat{M}_{22}$ without changing the value of $\mu_{\tilde{\Delta}}(M)$. Let the scaling matrix $D := \text{diag}\,\{I_2,\ dI_2\}$, $d > 0$, then

- $\mu_{\tilde{\Delta}}\left(DMD^{-1}\right) = \mu_{\tilde{\Delta}}(M)$
- $\bar{\sigma}\left(DMD^{-1}\right) = \bar{\sigma}\left(PDMD^{-1}P^{-1}\right)$

where $(PDMD^{-1}P^{-1})$ is as shown in (6.36) and the nasty property of $g_2(s)$ has been modified by the scaling factor d. In this example, d is chosen to be 141.7, i.e. $d = \text{cond}(G_0)$. $\mu - K$ iteration can now be applied directly to DMD^{-1} instead of M. After five $\mu - K$ iterations the μ-curve is reasonably flat and its maximum value is less than was obtained by [Fre89b] and [SMD88]. Note that the curve fitting for $\tilde{\mu}(j\omega)$, normalized $\mu(j\omega)$, becomes harder as μ gets flatter. The optimal k_1 and k_2 are given by

$$\begin{aligned} k_1(s) &= 2637\,\frac{(s+0.014)(s+0.09)(s^2+5.1s+3.15)(s+10.6)(s+25.5)(s+53.4)}{(s+10^{-5})(s+0.027)(s^2+9.5s+5.3)(s+31.5)(s+79.6)(s+100)} \\ k_2(s) &= 397.6\,\frac{(s+0.014)(s^2+4.5s+3.38)(s+37.16)}{(s+10^{-5})(s+0.27)(s+22.54)(s+84.47)} \end{aligned}$$

Thus the μ-optimal controller is $K(s) = V\Gamma(s)U^*$ with matrices V and U shown in (6.60); and $\Gamma(s) = \text{diag}\,\{k_1(s),\ k_2(s)\}$. All the simulation results are shown in Figures 6.12 to 6.18. Figures 6.12 and 6.13 show the Bode plots of the diagonal subplants $g_1(s)$, $g_2(s)$ and the weightings, respectively. Figure 6.14 shows the μ-values of five $\mu - K$ iterations. Bode plots of the optimal diagonal subcontrollers $k_1(s)$ and $k_2(s)$ and the compensated loop gains are shown in Figures 6.15 and 6.16, respectively. The relationships between $|w_1s_1| + |w_2t_1|$, $|w_1s_2| + |w_2t_2|$ and the "optimal" μ-curve are shown in Figure 6.17. Figure 6.18 shows the comparison of the μ-curve obtained by $\mu - K$ iteration with that proposed by Freudenberg [Fre89b] via a loop shaping method and that by Skogestad et al. [SMD88] via Doyle's $D - K$ iteration methodology.

6.8 Discussion and Summary

The *RSRP* problem of an ill-conditioned plant, in this case a simplified model of a high purity distillation column, has been solved by $\mu - K$ iteration as proposed in Chapter 5. The method was applied to DMD^{-1} instead of M to improve convergence. The example illustrated how the μ-curve becomes flatter when $\mu - K$ iteration is applied.

Because of the inequality $\mu_{\tilde{\Delta}}\,[M(j\omega)] \leq \bar{\sigma}\,[M(j\omega)]$, there are 3 kinds of relationship between $\mu_{\tilde{\Delta}}\,[M(j\omega)]$ and $\bar{\sigma}\,[M(j\omega)]$ as illustrated in Figure 6.11.

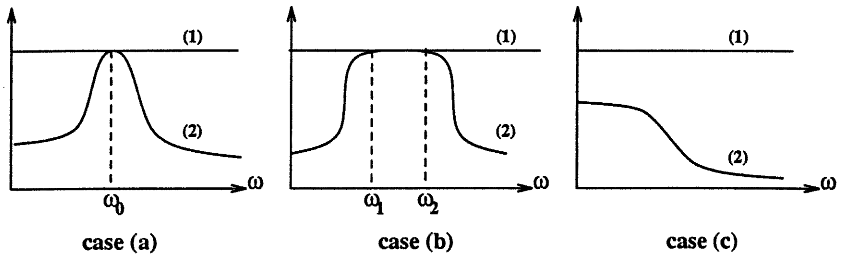

Figure 6.11: Curves of $(1): \bar{\sigma}(M)$ and $(2): \mu(M)$.

- Case (a): $\mu_{\tilde{\Delta}}[M(j\omega)] = \bar{\sigma}[M(j\omega)]$ at some frequency $\omega = \omega_0$

The demo example in the μ-toolbox of MATLAB [BDGPS91] corresponds to this case. This demo example shows how to apply $D-K$ iteration to the pitch axis control for plant HIMAT which was presented in Example 5.5-2.

- Case (b): $\mu_{\tilde{\Delta}}[M(j\omega)] = \bar{\sigma}[M(j\omega)]$ for a frequency band $\omega_1 \le \omega \le \omega_2$

The benchmark example proposed by G. Stein and J.C. Doyle in [StD88] corresponds to this case. The plant is

$$G_0(s) = \begin{bmatrix} \frac{25}{s} & 0 \\ 0 & \frac{1}{25s} \end{bmatrix}, \quad \text{cond}(G_0) = 625 \tag{6.68}$$

with

$$W_1(s) = \frac{0.2(s+1)}{(s+0.001)} I_2, \quad \text{and } W_2(s) = \frac{200(s+1)}{(s+1000)} I_2 \tag{6.69}$$

Without scaling of M, $\mu - K$ iteration can be applied successfully to cases (a) and (b), although the cond(G_0) of case (b) is much larger than the value of 141.7 for the high purity distillation column.

- Case (c): The curve of $\mu_{\tilde{\Delta}}[M(j\omega)]$ does not touch the curve of $\bar{\sigma}[M(j\omega)]$.

The example of the distillation column is like this. It is so nasty that the interconnection matrix M must be scaled before $\mu - K$ iteration can be used effectively to design a μ-optimal controller. But note that not all examples corresponding to case (c) have to be pre-scaled; it depends on the example.

Furthermore recall that the interconnection matrix

$$M = \begin{bmatrix} -W_2T_I & -W_2T_IG_0^{-1} \\ W_1S_OG_0 & W_1S_O \end{bmatrix} \tag{6.70}$$

and the weightings are given by

$$W_1(s) = w_1(s)I_2 = \frac{1}{2}\,\frac{s+0.1}{s}\,I_2, \quad W_2(s) = w_2(s)I_2 = 2\,\frac{s+0.2}{s+2}\,I_2 \tag{6.71}$$

A little thought reveals that

$$M(\infty) = \begin{bmatrix} 0 & -2K(\infty) \\ 0 & 0.5I_2 \end{bmatrix}, \quad \text{and} \quad \mu\left[M(\infty)\right] = 0.5$$

Therefore the optimal solution to this problem does not give a flat μ-curve over all frequencies, but drops down in the high frequencies, as shown in Figure 6.14. Therefore the control requirement for the $RSRP$ problem is to flatten the μ-curve over a frequency range greater than the closed-loop bandwidth.

Finally it is worth emphasizing the interesting results obtained in Section 4; see Figure 6.17:

- At low frequencies:

$$\mu_{\tilde{\Delta}}(M) = |w_2t_2| + |w_1s_2| \tag{6.72}$$

  Thus "robust performance" is effectively determined by the "lower gain" subplant $g_2(s)$.

- At high frequencies:

$$\mu_{\tilde{\Delta}}(M) = |w_2t_1| + |w_1s_1| \tag{6.73}$$

  Thus "robust stability" is effectively determined by the "higher gain" subplant $g_1(s)$.

- At intermediate frequencies:

$$\mu_{\tilde{\Delta}}(M) > \max\left\{|w_2t_1| + |w_1s_1|, |w_2t_2| + |w_1s_2|\right\} \tag{6.74}$$

  Thus a "coupling effect" occurs between the upper and lower loops in Figure 6.4 in this frequency range.

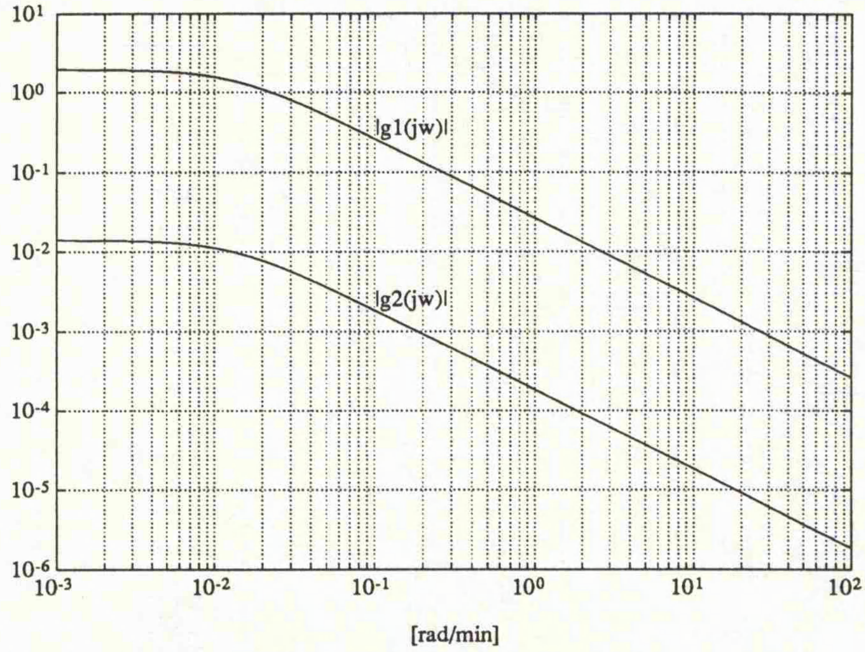

Figure 6.12: Bode plots of the diagonal subplants $g_1(s)$ and $g_2(s)$.

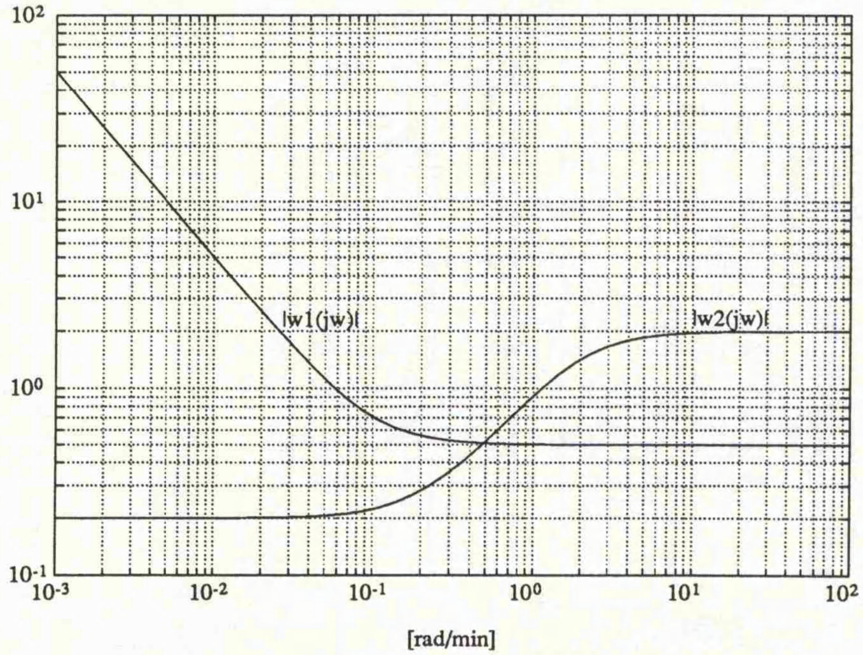

Figure 6.13: Bode plots of the weightings $w_1(s)$ and $w_2(s)$.

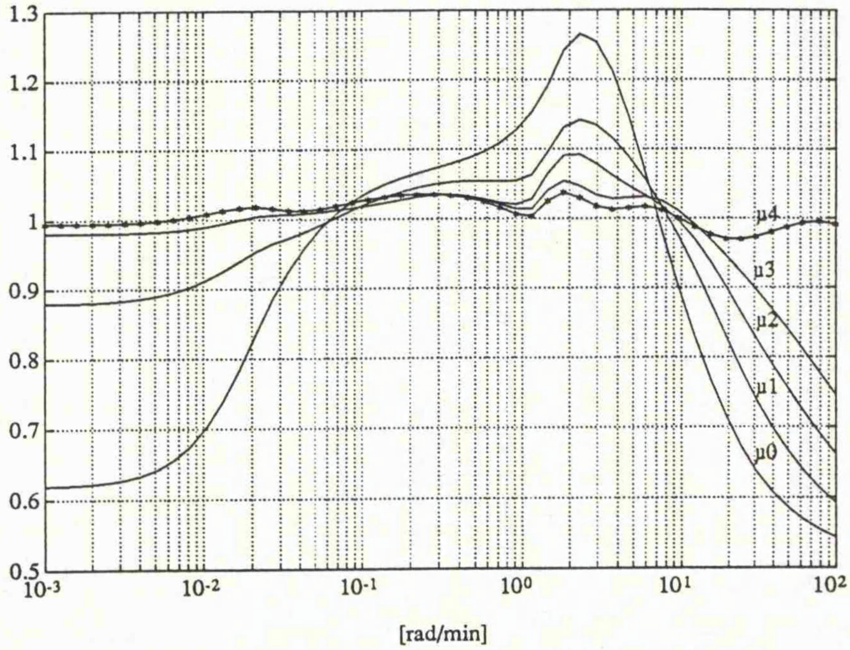

Figure 6.14: μ-values of five $\mu - K$ iterations.

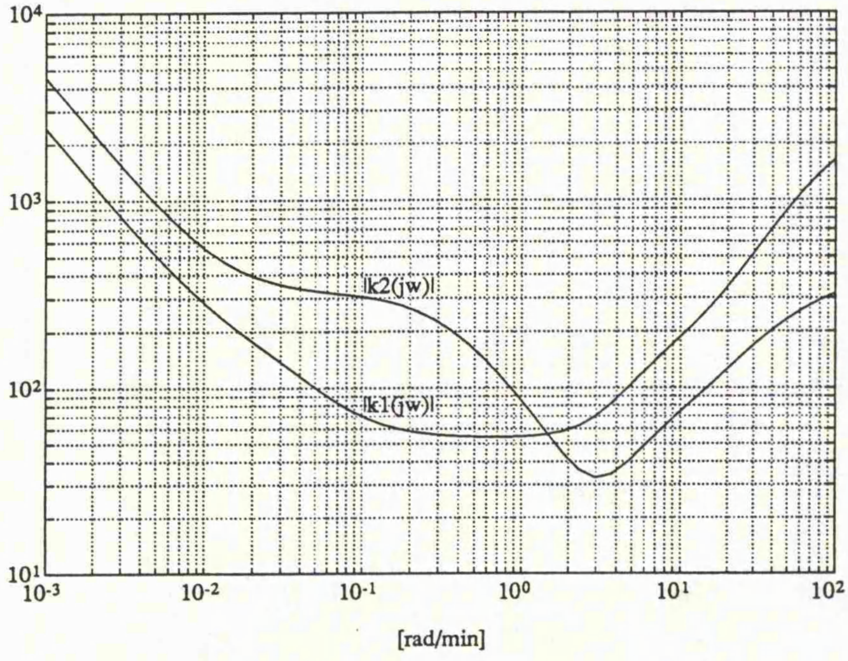

Figure 6.15: Bode plots of optimal diagonal subcontrollers $k_1(s)$ and $k_2(s)$.

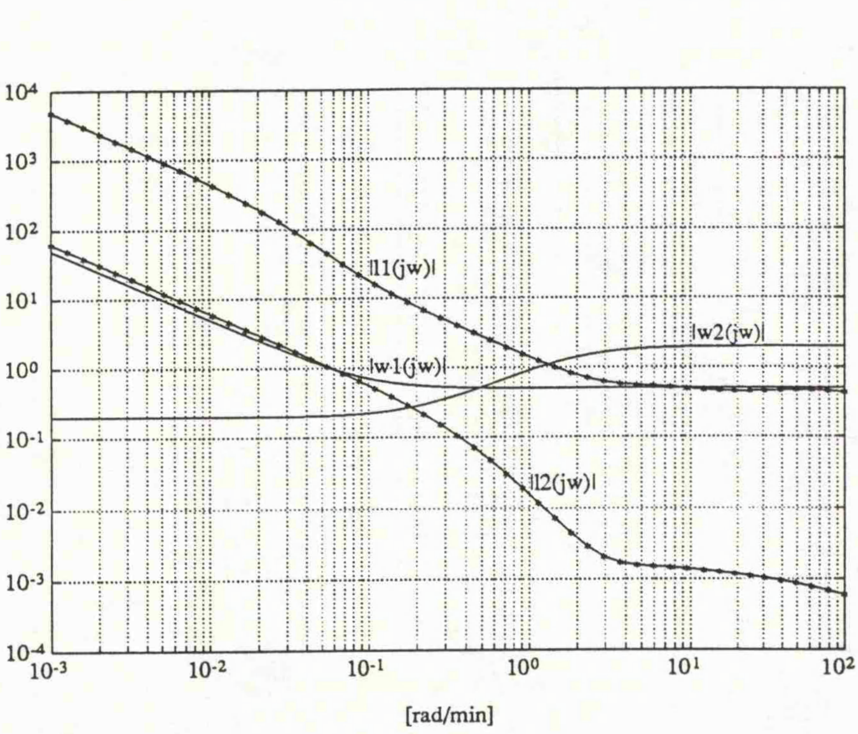

Figure 6.16: Bode plots of loop gains $l_1(s)$ and $l_2(s)$.

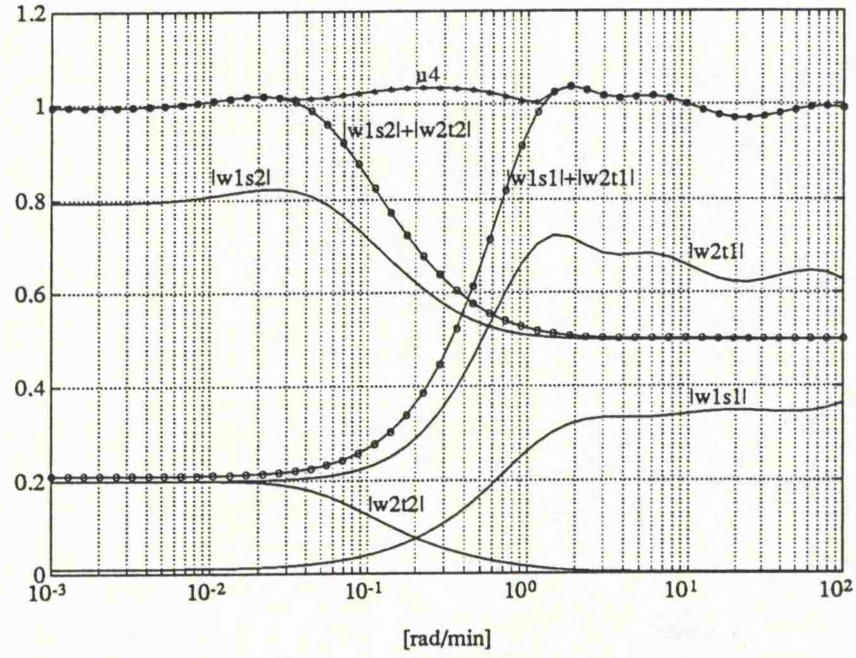

Figure 6.17: Bode plots of $|w_1 s_1| + |w_2 t_1|$, $|w_1 s_2| + |w_2 t_2|$ and optimal μ-curve.

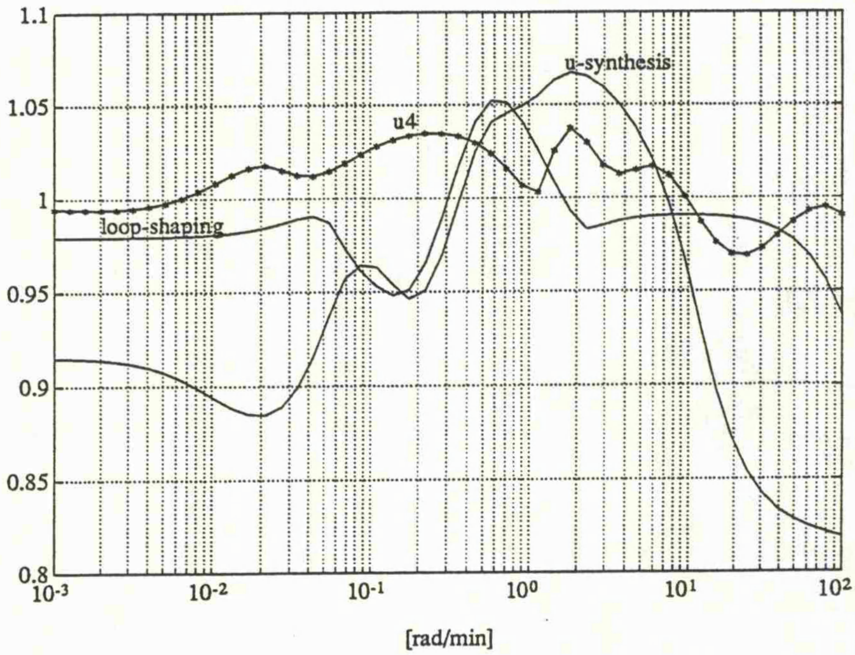

Figure 6.18: Comparison of μ-curves: (1) μ_4 by $\mu - K$ iteration, (2) loop shaping by Freudenberg and (3) μ-synthesis by Skogestad et al.

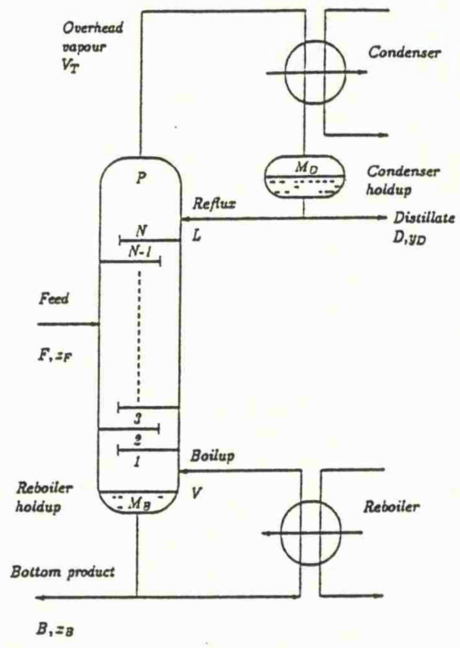

Figure 6.19: The distillation column system.

Chapter 7

μ-OPTIMAL CONTROLLER DESIGN FOR REAL UNCERTAINTY BY $\mu - K$ ITERATION

7.1 Introduction

For a $SISO$, linear and time-invariant plant with one real parameter uncertainty and one complex fictitious perturbation representing performance uncertainty, the structured singular value, $\mu_{\hat{\Delta}}(M)$, is calculated in this chapter. Then $\mu - K$ iteration is used to design a μ-optimal controller for a simple example. The results are compared with those obtained for the same system with the real parameter modelled as a complex perturbation. This illustrates the conservatism that can be introduced by treating real uncertainty as complex uncertainty.

Feedback is mainly motivated by the incompleteness of the knowledge of the system to be controlled. A nominal plant is a simplified, ideal, mathematical model which is used to design a controller which will be robust against the modelling uncertainties and exogenous disturbance signals. Generally speaking, a plant has two kinds of uncertainties:

- uncertain real parameters (real uncertainties) which are produced, for example, by the variations of parameters with different operating points and typically affect low frequency behaviour.

- unmodelled dynamics (complex uncertainties) at high frequencies.

For real-parameter variations, complex-μ analysis, as proposed by Doyle [Doy82], can give arbitrarily conservative results.

For μ-synthesis, recall from the discussion in Section 3.10 that the $D-K$ iteration proposed by Doyle [Doy85] is based on

$$\mu_{\hat{\Delta}}(M) \approx \inf_{D \in \mathbf{D}} \bar{\sigma}\left(DMD^{-1}\right) \tag{7.1}$$

for non-repeated *complex* uncertainty blocks. Expression (1.1) does not hold when *real* uncertainty blocks are present, and hence in this case $D-K$ iteration would fail to find the μ-optimal controller by $\mathcal{H}^{\infty}$-optimization. However, the ability of $\mu-K$ iteration to flatten μ still works. Thus $\mu-K$ iteration has an advantage over $D-K$ iteration when real uncertainty is present.

This chapter is organized as follows. In Section 7.2, some properties of bilinear mappings are presented which are useful for calculating complex-μ [1] and real-μ [2] in the later sections. In Section 7.3, as an alternative to the conventional method of calculating complex-μ by $\mu_{\hat{\Delta}}(M) = \inf_{D \in \mathbf{D}} \bar{\sigma}(DMD^{-1})$, with $M \in \mathcal{C}^{2\times 2}$, a closed form method is derived using a geometric approach. Building on this, in Section 7.4, a method for calculating real-μ is given when there is one real modelling uncertainty and one complex fictitious performance uncertainty. The section ends with a simple algorithm for finding real-μ. In Section 7.5, a μ-optimal controller is obtained by $\mu-K$ iteration for a *SISO* example with real modelling uncertainty. The results are compared with those obtained by treating the real uncertainty as complex. Concluding remarks are given in Section 7.6.

[1]complex $\mu := \mu$ when all the uncertainty blocks are complex.

[2]real $\mu := \mu$ when at least one of the uncertainty blocks is real.

7.2 Properties of LFTs

Let $\mathcal{C}$ denote the set of complex numbers. The equation of a circle in the complex z-plane centred at c_0 with radius r_0 is

$$\begin{aligned} |z - c_0| = r_0, \quad z \in \mathcal{C} &\iff z\bar{z} - \bar{c}_0 z - c_0 \bar{z} + c_0 \bar{c}_0 = r_0^2 \\ &\iff [\bar{z} \quad 1] \begin{bmatrix} 1 & -c_0 \\ -\bar{c}_0 & c_0\bar{c}_0 - r_0^2 \end{bmatrix} \begin{bmatrix} z \\ 1 \end{bmatrix} = 0 \end{aligned} \tag{7.2}$$

Now consider the following equation

$$[\bar{z} \quad 1] M_z \begin{bmatrix} z \\ 1 \end{bmatrix} = 0 \tag{7.3}$$

in the complex z-plane with

$$M_z := \begin{bmatrix} a & b \\ \bar{b} & d \end{bmatrix}, \quad a, d \in \mathcal{R}, \ b \in \mathcal{C} \tag{7.4}$$

where $\mathcal{R}$ denotes the set of real numbers. It is obvious that $M_z = M_z^*$ and if $a = 0$, then (7.3) gives

$$\bar{b}z + b\bar{z} + d = 0 \tag{7.5}$$

This is an equation of a straight line in the complex z-plane. Furthermore, if $a \neq 0$, then (7.3) yields

$$[\bar{z} \quad 1] \begin{bmatrix} 1 & \frac{b}{a} \\ \frac{\bar{b}}{a} & \frac{d}{a} \end{bmatrix} \begin{bmatrix} z \\ 1 \end{bmatrix} = 0 \tag{7.6}$$

Comparing (7.6) with (7.2), it is clear that (7.6) represents a circle in the z-plane with

$$\text{centre} \quad c_0 = -\frac{b}{a} \tag{7.7}$$

$$\text{radius} \quad r_0 = \frac{\sqrt{-\det M_z}}{|a|} \tag{7.8}$$

$$\text{and} \quad |c_0|^2 - r_0^2 = \frac{d}{a} \tag{7.9}$$

(7.9) implies that the circle does not contain the origin if $\frac{d}{a} > 0$.

Geometrically, the straight line of (7.5) is the degenerate case of a circle with infinite radius.

To recap

$$\text{if} \quad M_z^* = M_z \tag{7.10}$$

$$\text{then} \quad [\,\bar{z} \quad 1\,]\, M_z \begin{bmatrix} z \\ 1 \end{bmatrix} = 0 \tag{7.11}$$

is an equation of a circle in the complex z-plane.

Let us now consider a bilinear mapping from the z-plane to the ξ-plane, defined by

$$\xi = \frac{\tilde{r}z + \tilde{s}}{\tilde{p}z + \tilde{q}}\,, \quad \tilde{r}\tilde{q} - \tilde{p}\tilde{s} \neq 0 \tag{7.12}$$

which can be rewritten to describe the inverse mapping as

$$z = \frac{r\xi + s}{p\xi + q}\,, \quad rq - ps \neq 0 \tag{7.13}$$

where

$$\begin{bmatrix} r & s \\ p & q \end{bmatrix} = \begin{bmatrix} \tilde{q} & -\tilde{s} \\ -\tilde{p} & \tilde{r} \end{bmatrix} =: R \tag{7.14}$$

Then the circle defined by (7.10) and (7.11) in the z-plane will be mapped to the ξ-plane by the following equations:

$$\begin{aligned}
[\,\bar{z} \quad 1\,]\, M_z \begin{bmatrix} z \\ 1 \end{bmatrix} = 0 \iff & [\,\tfrac{\bar{r}\bar{\xi}+\bar{s}}{\bar{p}\bar{\xi}+\bar{q}} \quad 1\,]\, M_z \begin{bmatrix} \frac{r\xi+s}{p\xi+q} \\ 1 \end{bmatrix} = 0 \\
\iff & [\,\bar{r}\bar{\xi} + \bar{s} \quad \bar{p}\bar{\xi} + \bar{q}\,]\, M_z \begin{bmatrix} r\xi + s \\ p\xi + q \end{bmatrix} = 0 \\
\iff & [\,\bar{\xi} \quad 1\,] \begin{bmatrix} \bar{r} & \bar{p} \\ \bar{s} & \bar{q} \end{bmatrix} M_z \begin{bmatrix} r & s \\ p & q \end{bmatrix} \begin{bmatrix} \xi \\ 1 \end{bmatrix} = 0 \\
\iff & [\,\bar{\xi} \quad 1\,]\, M_\xi \begin{bmatrix} \xi \\ 1 \end{bmatrix} = 0
\end{aligned} \tag{7.15}$$

where

$$M_\xi := R^* M_z R \tag{7.16}$$

Therefore

$$M_z^* = M_z \Longrightarrow M_\xi^* = M_\xi \tag{7.17}$$

The consequences are summarized in the following theorem (e.g. [StT83]):

Theorem 7.2-1 (Bilinear Mapping): Under a bilinear transformation (or LFT) the image of any circle is again a circle. ■

In this theorem, straight lines are treated as generalized circles. Moreover, the centre and radius of the mapped circle in the ξ-plane can easily be obtained by (7.7) and (7.8). Note that a bilinear transformation is a linear fractional transformation as described in Chapter 3.

7.3 Complex-μ

In 1982, Doyle [Doy82], motivated by the conservativeness of singular values in robustness analysis and design, proposed and developed the concept of the structured singular value (SSV). By introducing a fictitious bounded (in the unit disk) uncertainty Δ_p to represent performance requirements, robust performance can be guaranteed against uncertainty Δ if and only if a robust stability test is satisfied as described in Theorem 3.9-2. The problem is illustrated in Figure 7.1 below, where $\tilde{\Delta} = \mathrm{diag}\{\Delta, \Delta_p\}$.

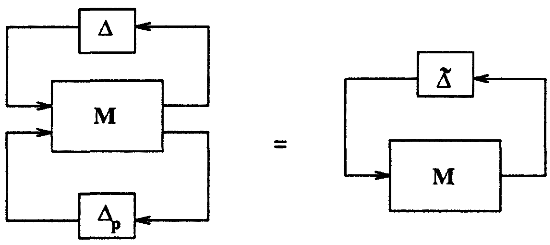

Figure 7.1: $M - \tilde{\Delta}$ structure.

If $\mu_{\tilde{\Delta}}(M)$ is to be determined algebraically, as in Example 3.8-5, using the identity $\mu_{\tilde{\Delta}}(M) = \inf_{D \in \mathbf{D}} \bar{\sigma}(DMD^{-1})$ with $M \in \mathcal{C}^{2\times 2}$, then it must be assumed that the uncertainty blocks Δ and Δ_p are complex. However, as we will show a geometric approach can be derived using the properties described in the preceding section when $M \in \mathcal{C}^{2\times 2}$ and Δ is "complex" or "real". In this section, we will develop the approach first for complex Δ. Needless to say, the fictitious performance uncertainty Δ_p must be complex.

In Figure 7.1, the transfer function "seen" by Δ is $F_l(M, \Delta_p)$ using the notation introduced in Chapter 3 for linear fractional transformations. Suppose

$$M = \begin{bmatrix} a & b \\ c & d \end{bmatrix} \in C^{2\times 2} \tag{7.18}$$

then

$$F_l(M, \Delta_p) = a + \frac{bc\Delta_p}{1 - d\Delta_p} = \frac{a - \delta\Delta_p}{1 - d\Delta_p} \tag{7.19}$$

where $\delta := \det(M)$ and we assume $1 - d\Delta_p \neq 0$. Then $\det(I - M\tilde{\Delta}) = 0$ implies, and is implied by,

$$1 - \Delta \cdot F_l(M, \Delta_p) = 0 \tag{7.20}$$

In which case

$$\Delta = [F_l(M, \Delta_p)]^{-1} = \frac{d\Delta_p - 1}{\delta\Delta_p - a}, \quad \delta\Delta_p - a \neq 0 \tag{7.21}$$

Clearly, Δ is then a bilinear mapping of Δ_p and vice versa. And, if there is a circle with radius r centred at the origin in the Δ_p-plane, then both (7.14) and (7.16) imply that

$$\begin{aligned} M_\Delta = R^* M_{\Delta_p} R &= \begin{bmatrix} -a & 1 \\ -\delta & d \end{bmatrix}^* \begin{bmatrix} 1 & 0 \\ 0 & -r^2 \end{bmatrix} \begin{bmatrix} -a & 1 \\ -\delta & d \end{bmatrix} \\ &= \begin{bmatrix} |a|^2 - |\delta|^2 r^2 & -\bar{a} + \bar{\delta} d r^2 \\ -a + \delta \bar{d} r^2 & 1 - |d|^2 r^2 \end{bmatrix} \end{aligned} \tag{7.22}$$

and by (7.7) and (7.8), the circle in the Δ_p-plane is mapped into a circle in the Δ-plane with

$$\text{centre} \quad c_0 = -\frac{-\bar{a} + \bar{\delta} d r^2}{|a|^2 - |\delta|^2 r^2} \tag{7.23}$$

$$\text{radius} \quad r_0 = \frac{|bc| r}{\left| |a|^2 - |\delta|^2 r^2 \right|} \tag{7.24}$$

Note that the circle degenerates to a straight line when $r = \frac{|a|}{|\delta|}$.

Then according to the definition of the SSV, it follows that

$$
\begin{aligned}
\mu_{\tilde{\Delta}}^{-1}(M) &= \min_{\Delta \in \tilde{\Delta}} \left\{ \bar{\sigma}(\tilde{\Delta}) : \det(I - M\tilde{\Delta}) = 0, \quad \Delta \in \mathcal{C}, \ \Delta_p \in \mathcal{C} \right\} \\
&= \min_{\Delta \in \mathcal{C}, \ \Delta_p \in \mathcal{C}} \left\{ \max\left\{|\Delta|, |\Delta_p|\right\} : 1 - \Delta \cdot F_l(M, \Delta_p) = 0 \right\} \\
&= \min_{\Delta \in \mathcal{C}, \ \Delta_p \in \mathcal{C}} \left\{ \max\left\{|\Delta|, |\Delta_p|\right\} : \Delta = \left[F_l(M, \Delta_p)\right]^{-1} =: f(\Delta_p) \right\} \\
&= \min_{\Delta_p \in \mathcal{C}} \left\{ \max\left\{|f(\Delta_p)|, |\Delta_p|\right\} : f(\Delta_p) = \frac{d\Delta_p - 1}{\delta\Delta_p - a} \right\} \\
&= \min_{\Delta_p = re^{j\theta}} \left\{ \max\left\{|f(\Delta_p)|, |\Delta_p|\right\} \right\} \\
&= \min_{r>0} \min_{0 \le \theta < 2\pi} \left\{ \max\left\{\left|f\left(re^{j\theta}\right)\right|, \left|re^{j\theta}\right|\right\} \right\} \\
&= \min_{r>0} \min_{0 \le \theta < 2\pi} \left\{ \max\left\{\left|f\left(re^{j\theta}\right)\right|, r\right\} \right\} \\
&= \min_{r>0} \left\{ \max\left\{ \min_{0 \le \theta < 2\pi} \left|f\left(re^{j\theta}\right)\right|, r \right\} \right\} \\
&=: \min_{r>0} \left\{ \max\left\{ g_C(r), r \right\} \right\} \qquad (7.25)
\end{aligned}
$$

where

$$g_C(r) := \min_{0 \le \theta < 2\pi} \left|f\left(re^{j\theta}\right)\right| \qquad (7.26)$$

All the steps in (7.25) are straightforward except the interchange of max and min. The latter can be seen to be valid by considering separately what happens (i) if $\left|f\left(re^{j\theta}\right)\right| < r$ at some θ, (ii) if $\left|f\left(re^{j\theta}\right)\right| > r \ \ \forall\theta$, and (iii) if $\left|f\left(re^{j\theta}\right)\right| < r \ \ \forall\theta$. This is left to the reader.

Let

- $C_p :=$ the circle with radius r and centred at the origin in the Δ_p-plane.
- $C_m :=$ the mapped circle of $f(\Delta_p)$ in the Δ-plane.
- $r_t :=$ the radius of circle C_p when circles C_m and C_p are tangent.
- $O :=$ the origin of the complex plane.
- $\mathrm{dist}(P, Q) :=$ the distance between points P and Q.

It is obvious that $g_C(r)$ is the minimum distance between the circle C_m and the origin in the Δ-plane when the radius of circle C_p is r. There are three cases which need to be considered as r increases gradually from zero to some appropriately large value; these are illustrated in Figure 7.2 below.

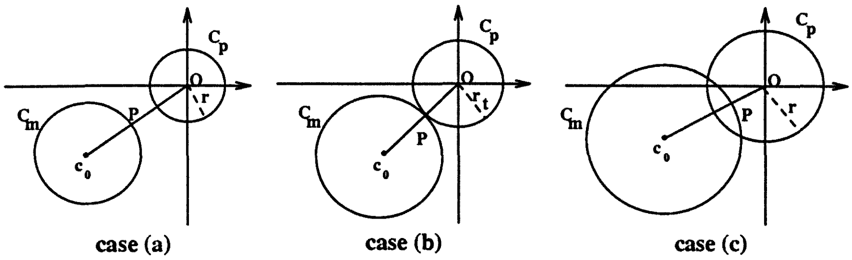

Figure 7.2: Relationships between circles C_m and C_p.

- case (a): $0 \le r < r_t$ (C_m and C_p are disjoint)
  $\max\{g_C(r), r\} = \max\{\text{dist}(P,O), r\} = \text{dist}(P,O)$; see case (a) in Figure 7.2.
- case (b): $r = r_t$ (C_m and C_p are tangent)
  $\max\{g_C(r), r\} = \max\{r_t, r_t\} = r_t$; see case (b) in Figure 7.2.
- case (c): $r > r_t$ (C_m and C_p intersect)
  $\max\{g_C(r), r\} = \max\{\text{dist}(P,O), r\} = r > r_t$; see case (c) in Figure 7.2.

Furthermore, the following theorem is necessary to guarantee that dist$(P,O) > r_t$, when $0 \le r < r_t$.

Theorem 7.3-1:

(1) $\frac{dg_C(r)}{dr} \le 0$, for $0 \le r < \frac{1}{|d|}$, and

(2) $\frac{dg_C(r)}{dr} \ge 0$, for $r > \frac{1}{|d|}$

Proof: It is obvious that

(i) if $|c_0| > r_0$, C_m does not contain the origin, then $g_C(r) = |c_0| - r_0$

(ii) if $|c_0| < r_0$, C_m contains the origin, then $g_C(r) = r_0 - |c_0|$

and hence

$$g_C(r) = \Big||c_0| - r_0\Big| = \left|\frac{\left|-\bar{a} + \bar{\delta} d r^2\right| - |bc|r}{|a|^2 - |\delta|^2 r^2}\right|$$

by (7.23) and (7.24).

From (7.9), (7.22), (7.23) and (7.24) we have the following identity:

$$\left|-\bar{a} + \bar{\delta} d r^2\right| = \sqrt{|bc|^2 r^2 + (1 - |d|^2 r^2)(|a|^2 - |\delta|^2 r^2)} \tag{7.27}$$

Differentiating the term on the right hand side of (1.27) with respect to r yields

$$\frac{\mathrm{d}}{\mathrm{d}r}\left\{\left|-\bar{a}+\bar{\delta}dr^2\right|\right\} = \frac{\left(|bc|^2-|ad|^2-|\delta|^2\right)r + 2|d\delta|^2 r^3}{\left|-\bar{a}+\bar{\delta}dr^2\right|}$$

which is useful in finding $\frac{\mathrm{d}gc(r)}{\mathrm{d}r}$. Furthermore it follows directly from identity (1.27) that

$$gc(r) = \frac{\left|1-|d|^2r^2\right|}{\left|-\bar{a}+\bar{\delta}dr^2\right| + |bc|r} \tag{7.28}$$

∘ In the range $0 \leq r < \frac{1}{|d|}$: we have

$$gc(r) = \frac{1-|d|^2r^2}{\left|-\bar{a}+\bar{\delta}dr^2\right| + |bc|r} \tag{7.29}$$

Mathematical manipulation then yields

$$\begin{aligned}
\frac{\mathrm{d}gc(r)}{\mathrm{d}r} &= \frac{1}{\left(\left|-\bar{a}+\bar{\delta}dr^2\right| + |bc|r\right)^2 \cdot \left|-\bar{a}+\bar{\delta}dr^2\right|} \cdot \\
&\quad \Big\{-\left(|d|^2r^2+1\right)|bc| \cdot \left|-\bar{a}+\bar{\delta}dr^2\right| - \left(|bc|^2+|ad|^2-|\delta|^2\right)r \\
&\quad - \left(|bc|^2-|ad|^2+|\delta|^2\right)|d|^2r^3\Big\}
\end{aligned} \tag{7.30}$$

The last two terms in the numerator can be simplified to

$$\begin{aligned}
\left(|bc|^2+|ad|^2-|\delta|^2\right) r &= \left(ad\bar{b}\bar{c}+\bar{a}\bar{d}bc\right) r, \quad \text{and} \\
\left(|bc|^2-|ad|^2+|\delta|^2\right)|d|^2r^3 &= -\left(\bar{b}\bar{c}\delta+bc\bar{\delta}\right)|d|^2r^3
\end{aligned}$$

It follows that

$$\left(|bc|^2+|ad|^2-|\delta|^2\right) r + \left(|bc|^2-|ad|^2+|\delta|^2\right)|d|^2r^3 = 2\Re e\left[bc\bar{d}r\left(\bar{a}-d\bar{\delta}r^2\right)\right]$$

where $\Re e(\circ)$ denotes the real part of $(\circ)$, and

$$\begin{aligned}
-2\Re e\left[bc\bar{d}r\left(\bar{a}-d\bar{\delta}r^2\right)\right] &\leq \left|2bc\bar{d}r\left(\bar{a}-d\bar{\delta}r^2\right)\right| \\
&= 2|bc| \cdot |d|r \cdot \left|\bar{a}-d\bar{\delta}r^2\right|
\end{aligned}$$

Thus the numerator of $dgc(r)/dr$ is equal to

$$\begin{aligned}
&-\left(|d|^2r^2+1\right)|bc| \cdot \left|-\bar{a}+\bar{\delta}dr^2\right| - 2\Re e\left[bc\bar{d}r\left(\bar{a}-d\bar{\delta}r^2\right)\right] \\
&\leq -\left(|d|^2r^2+1\right)|bc| \cdot \left|-\bar{a}+\bar{\delta}dr^2\right| + 2|bc| \cdot |d|r \cdot \left|\bar{a}-d\bar{\delta}r^2\right| \\
&= -\left(|d|r-1\right)^2|bc| \cdot \left|-\bar{a}+\bar{\delta}dr^2\right| \\
&\leq 0
\end{aligned}$$

Therefore $dg_C(r)/dr \le 0$ in the range $0 \le r < \frac{1}{|d|}$.

• <u>In the range $r > \frac{1}{|d|}$:</u> (7.28) gives that

$$g_C(r) = -\frac{1 - |d|^2 r^2}{\left|-\bar{a} + \bar{\delta} d r^2\right| + |bc| r}$$

which is of opposite sign to (7.29) and hence $dg_C(r)/dr \ge 0$. This completes the proof. ∎

Straightforward substitution into (7.28) reveals that $g_C(0) = \frac{1}{|a|}$, $g_C(\frac{1}{|d|}) = 0$ and $g_C(\infty) = \frac{|d|}{|\delta|}$. Furthermore, it follows directly from (7.30) that if r approaches $\frac{1}{|d|}$ from below, then $dg_C(r)/dr = -\frac{|d|^2}{|bc|}$; on the other hand $dg_C(r)/dr = \frac{|d|^2}{|bc|}$, if r approaches $\frac{1}{|d|}$ from above. Therefore $g_C(r)$ is continuous, but not differentiable at $r = \frac{1}{|d|}$ when $d \ne 0$.

The consequence of the three situations in Figure 7.2 and Theorem 7.3-1 is illustrated in Figure 7.3. By (7.25), it is clear that

$$\begin{aligned}
\mu_{\tilde{\Delta}}^{-1}(M) &= \min_{r>0} \left\{ \max\left\{ g_C(r), r \right\} \right\} \\
&= \min_{r>0} \left\{ r : g_C(r) = r \right\} \\
&= \min_{r>0} \left\{ r : |c_0| - r_0 = r \right\}
\end{aligned}$$

Hence

$$\mu_{\tilde{\Delta}}(M) = \max_{r>0} \left\{ \frac{1}{r} : |c_0| - r_0 = r \right\} \tag{7.31}$$

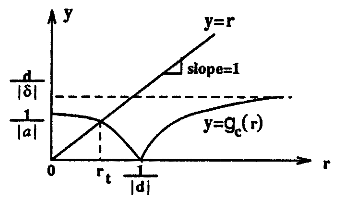

Figure 7.3: Curves show: $\mu_{\tilde{\Delta}}(M) = 1/r_t$.

By (7.23) and (7.24), the equation $|c_0| - r_0 = r$ is equivalent to the following equation

$$\frac{\left|-\bar{a} + \bar{\delta} d r^2\right|}{|a|^2 - |\delta|^2 r^2} - \frac{|bc| r}{|a|^2 - |\delta|^2 r^2} = r$$

The second term on the left hand side of the above equation can be shifted to the right hand side, then squaring both sides yields

$$|\delta|^2 r^4 - \left(|a|^2 + |d|^2 + 2|bc|\right) r^2 + 1 = 0$$

Equivalently, this can be written as

$$\left(\frac{1}{r}\right)^4 - \left(|a|^2 + |d|^2 + 2|bc|\right)\left(\frac{1}{r}\right)^2 + |\delta|^2 = 0$$

so that

$$\frac{1}{r^2} = \frac{(|a|^2 + |d|^2 + 2|bc|) \pm \sqrt{(|a|^2 + |d|^2 + 2|bc|)^2 - 4|\delta|^2}}{2}$$

Hence from (7.31)

$$\mu_{\tilde{\Delta}}(M) = \left[\frac{(|a|^2 + |d|^2 + 2|bc|) + \sqrt{(|a|^2 + |d|^2 + 2|bc|)^2 - 4|\delta|^2}}{2}\right]^{1/2}$$

This coincides with the formula obtained in (3.91).

7.4 Real-μ

In the preceding section, the SSV for complex modelling uncertainty Δ and complex performance uncertainty Δ_p was derived. We will now consider the SSV for a real parameter uncertainty Δ and a complex Δ_p.

Similar to the development in (7.25) we have

$$\begin{aligned}
\mu_{\tilde{\Delta}}^{-1}(M) &= \min_{\Delta \in \tilde{\Delta}} \left\{ \bar{\sigma}(\tilde{\Delta}) : \det(I - M\tilde{\Delta}) = 0, \quad \Delta \in \mathcal{R}, \ \Delta_p \in \mathcal{C} \right\} \\
&= \min_{\Delta \in \mathcal{R}, \ \Delta_p \in \mathcal{C}} \left\{ \max\{|\Delta|, |\Delta_p|\} : \Delta = \left[F_l(M, \Delta_p)\right]^{-1} =: f(\Delta_p) \right\} \\
&= \min_{\Delta_p \in \mathcal{C}} \left\{ \max\{|f(\Delta_p) \cap \mathcal{R}|, |\Delta_p|\} : f(\Delta_p) = \frac{d\Delta_p - 1}{\delta\Delta_p - a} \right\} \\
&= \min_{\Delta_p = re^{j\theta}} \left\{ \max\left\{\left|f\left(re^{j\theta}\right) \cap \mathcal{R}\right|, r\right\} \right\} \\
&= \min_{r>0} \left\{ \max\left\{ \min_{0 \le \theta < 2\pi} \left|f\left(re^{j\theta}\right) \cap \mathcal{R}\right|, r \right\} \right\} \\
&=: \min_{r>0} \left\{ \max\left\{\tilde{g}_{\mathcal{R}}(r), r\right\} \right\} \qquad (7.32)
\end{aligned}$$

where

$$\tilde{g}_{\mathcal{R}}(r) := \min_{0 \leq \theta < 2\pi} \left| f\left(re^{j\theta}\right) \cap \mathcal{R} \right| \tag{7.33}$$

and $\cap$ denotes the intersection between two sets.

Therefore, $\tilde{g}_{\mathcal{R}}(r)$ denotes the minimum distance between the origin and the crossover points of the circle C_m on the real-axis in the Δ-plane. Let L be any straight line passing through the origin in the Δ-plane, (we will later let $L = \mathcal{R}$). It is obvious that there exists one or two crossover points between the circle C_m and the line L if C_m and L are not disjoint. Let $\tilde{g}_L(r)$ denote the minimum distance between the crossover points and the origin. Mathematically, we have

$$\tilde{g}_L(r) := \min_{0 \leq \theta < 2\pi} \left| f\left(re^{j\theta}\right) \cap L \right| \tag{7.34}$$

Then the following lemma can be established.

Lemma 7.4-1: If $C_m \cap L \neq \phi$, then $\tilde{g}_L(r)$ decreases with r in the range $0 \leq r \leq \frac{1}{|d|}$, where ϕ denotes the empty set.

Proof: The bilinear transformation of

$$\Delta = f(\Delta_p) = \frac{d\Delta_p - 1}{\delta\Delta_p - a}$$

is a conformal mapping from the Δ_p-plane to the Δ-plane, if $bc \neq 0$. Thus two nontouching circles, C_1 and C_2, centred at the origin, are mapped into two nontouching circles, $\tilde{C}_1$ and $\tilde{C}_2$, as is illustrated in Figure 7.4. It is clear that $\operatorname{dist}(P_2, O) < \operatorname{dist}(P_1, O)$ if C_m increases with r, and P_1, P_2 are as shown in Figure 7.4.

Recall that the circle C_m passes through the origin when $r = \frac{1}{|d|}$ and degenerates to a straight line when $r = \frac{|a|}{|\delta|}$. This determines the following two cases for special consideration:

<u>case 1</u>: $\frac{1}{|d|} \leq \frac{|a|}{|\delta|}$, then

$$\circ\ 0 \leq r \leq \frac{1}{|d|} \Longrightarrow r_0 = \frac{|bc|r}{|a|^2 - |\delta|^2 r^2} \Longrightarrow \left\{ \begin{array}{l} C_m \text{ does not contain the origin} \\ r_0 \text{ increases with } r \end{array} \right.$$
$$\Longrightarrow \tilde{g}_L(r) \text{ decreases with } r$$

<u>case 2</u>: $\frac{1}{|d|} \geq \frac{|a|}{|\delta|}$, then

- $0 \leq r < \frac{|a|}{|\delta|} \implies r_0 = \frac{|bc|r}{|a|^2-|\delta|^2r^2} \implies \begin{cases} C_m \text{ does not contain the origin} \\ r_0 \text{ increases with } r \end{cases}$

  $\implies \tilde{g}_L(r)$ decreases with r
- $r = \frac{|a|}{|\delta|} \implies C_m$ degenerates to a straight line
- $\frac{|a|}{|\delta|} < r \leq \frac{1}{|d|} \implies r_0 = \frac{-|bc|r}{|a|^2-|\delta|^2r^2} \implies \begin{cases} C_m \text{ contains the origin} \\ r_0 \text{ decreases with } r \end{cases}$

  $\implies \tilde{g}_L(r)$ decreases with r

Therefore $\tilde{g}_L(r)$ decreases with r in the range $0 \leq r \leq \frac{1}{|d|}$, which completes the proof. ■

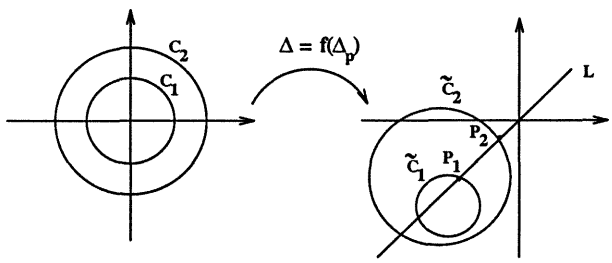

Figure 7.4: Mapping from Δ_p-plane to Δ-plane.

If we choose line L to be the real-axis in the Δ-plane, then the following theorem is established.

Theorem 7.4-1: If $C_m \cap \mathcal{R} \neq \phi$, then $\tilde{g}_{\mathcal{R}}(r)$ decreases with r in the range $0 \leq r \leq \frac{1}{|d|}$, where ϕ denotes the empty set. ■

Now let us consider (7.33). Firstly, define
$\tilde{r}_t :=$ the radius of circle C_p when the circle C_m is tangent to the real-axis.
There are many cases which need to be considered in detail when the radius r of Δ_p increases gradually from zero to a sufficiently large value.

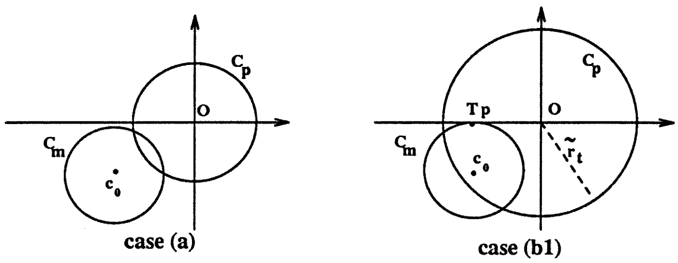

Figure 7.5: Relationships between circles C_m and C_p: case (a) and case (b1).

- case (a): $0 \leq r < \tilde{r}_t$ (C_m does not touch the real-axis)
  Then $\det(I - M\tilde{\Delta}) \neq 0$
  Define $\max\left\{\tilde{g}_{\mathcal{R}}(r), r\right\} = \infty$; see case (a) in Figure 7.5.

- case (b): $r = \tilde{r}_t$ (C_m is tangent to the real-axis)
  This prompts us to consider the following two situations:

(b1): *if circle C_p contains the tangent point T_p*, as shown in case (b1) of Figure 7.5, then

$$\max_{r=\tilde{r}_t} \left\{\tilde{g}_{\mathcal{R}}(r), r\right\} = \max_{r=\tilde{r}_t} \left\{\text{dist}\,(T_p, O), \tilde{r}_t\right\} = \tilde{r}_t$$

Geometrically, if r increases and becomes greater than $\tilde{r}_t$, then Theorem 7.4-1 implies

$$\tilde{g}_{\mathcal{R}}(r) < \text{dist}\,(T_p, O)$$

Thus

$$\max_{r>\tilde{r}_t} \left\{\tilde{g}_{\mathcal{R}}(r), r\right\} = r > \tilde{r}_t$$

Hence (7.32) gives

$$\mu_{\tilde{\Delta}}^{-1}(M) = \tilde{r}_t \tag{7.35}$$

(b2): *if circle C_p does not contain the tangent point T_p*, as shown in case (b21) of Figure 7.6, then

$$\max_{r=\tilde{r}_t} \left\{\tilde{g}_{\mathcal{R}}(r), r\right\} = \text{dist}\,(T_p, O)$$

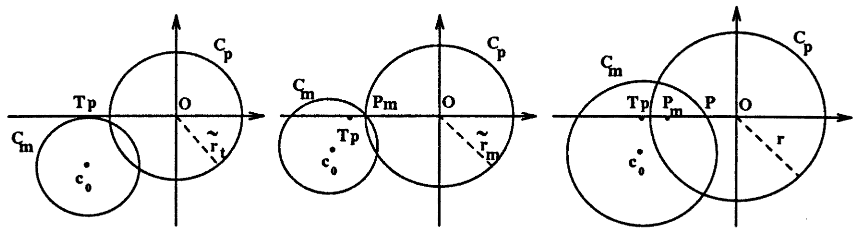

Figure 7.6: Relationships between circles C_m and C_p: case (b2).

Geometrically, if r increases above $\tilde{r}_t$, Theorem 7.4-1 implies

$$\tilde{g}_{\mathcal{R}}(r) < \text{dist}\,(T_p, O)$$

Thus with $\tilde{r}_m$ and P_m defined as shown in case (b22) of Figure 1.6, it is clear that

$$\max_{\tilde{r}_m > r > \tilde{r}_t} \left\{\tilde{g}_{\mathcal{R}}(r), r\right\} < \text{dist}\,(T_p, O)$$

Therefore, increasing r in the range $\tilde{r}_m > r > \tilde{r}_t$ will decrease the value of $\max\{\tilde{g}_{\mathcal{R}}(r), r\}$. The case (b22) in Figure 1.6 illustrates the situation where one of the crossover points between C_m and C_p just appears on the real-axis for some proper value of r, called $\tilde{r}_m$. Then

$$\max_{r=\tilde{r}_m} \left\{\tilde{g}_{\mathcal{R}}(r), r\right\} = \tilde{r}_m = \text{dist}\,(P_m, O)$$

If r increases further without exceeding $\frac{1}{|d|}$ as shown in case (b23) of Figure 1.6, then Theorem 7.4-1 gives

$$\text{dist}\,(P, O) < \text{dist}\,(P_m, O) = \tilde{r}_m$$

and

$$\max_{r > \tilde{r}_m} \left\{\tilde{g}_{\mathcal{R}}(r), r\right\} = r > \tilde{r}_m$$

To recap, in case (b2), the minimum value of

$$\max_{r \geq \tilde{r}_t} \left\{\tilde{g}_{\mathcal{R}}(r), r\right\}$$

occurs in the case of (b22) in Figure 7.6, and hence (7.32) gives

$$\mu_{\tilde{\Delta}}^{-1}(M) = \tilde{r}_m \tag{7.36}$$

To summarize, cases (b1) and (b2) are illustrated in Figure 7.7. Comparing with the complex-μ derived in the preceding section, the real-μ in (7.35) or (7.36) can be arbitrarily smaller.

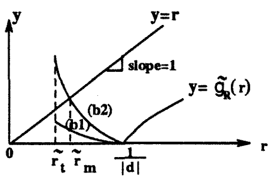

Figure 7.7: Curves show: $\mu_{\tilde{\Delta}}(M) = 1/\tilde{r}_t$ or $\mu_{\tilde{\Delta}}(M) = 1/\tilde{r}_m$.

Let us now consider finding $\tilde{r}_t$ in (7.35) , and then $\tilde{r}_m$ in (7.36). Since the circle C_m in the case (b1) of Figure 7.5 is tangent to the real-axis, we have

$$|\mathcal{I}_m(c_0)| = r_0 \tag{7.37}$$

where $\mathcal{I}_m(c_0)$ denotes the imaginary-part of c_0. Substituting c_0 and r_0 from (7.23) and (7.24) into (7.37) yields

$$\left|\mathcal{I}_m\left(\bar{a} - \bar{\delta} d r^2\right)\right| = |bc| r$$

Straightforward manipulation and squaring both sides of the above equation shows that

$$\left[\mathcal{I}_m\left(\bar{\delta} d\right)\right]^2 r^4 - \left[|bc|^2 + 2\mathcal{I}_m(\bar{a}) \cdot \mathcal{I}_m\left(\bar{\delta} d\right)\right] r^2 + \left[\mathcal{I}_m(\bar{a})\right]^2 = 0 \tag{7.38}$$

and $\tilde{r}_t$ is the minimum positive root of this equation.

Now to find $\tilde{r}_m$. The case (b22) of Figure 7.6 is redrawn in Figure 7.8. Geometrically, it follows that

$$|\Re e(c_0)| - \sqrt{r_0^2 - |\mathcal{I}_m(c_0)|^2} = r \tag{7.39}$$

Shifting the term $|\Re e(c_0)|$ to the right hand side of the above equation, substituting for c_0 and r_0, squaring both sides and a little manipulation shows that

$$|\delta|^2 r^4 + \left(|d|^2 - |a|^2\right) r^2 + 1 = -2\left|\Re e(a) - \Re e\left(\bar{\delta} d\right) r^2\right| r$$

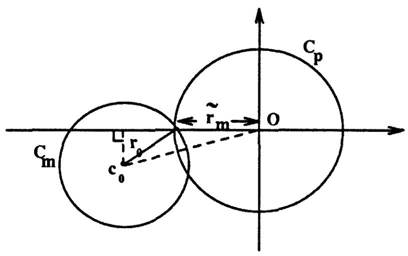

Figure 7.8: To find $\tilde{r}_m$.

Squaring both sides again gives

$$\begin{aligned} |\delta|^4 r^8 &+ \left\{2|\delta|^2\left(|d|^2-|a|^2\right)-4\left[\Re e\left(\bar{\delta}d\right)\right]^2\right\}r^6 \\ &+ \left\{\left(|d|^2-|a|^2\right)^2-2|\delta|^2+8\Re e(a)\cdot\Re e\left(\bar{\delta}d\right)\right\}r^4 \\ &- \left\{2\left(|d|^2-|a|^2\right)+4\left[\Re e(a)\right]^2\right\}r^2+1=0 \end{aligned} \tag{7.40}$$

and $\tilde{r}_m$ is the minimum positive real root of this equation. The roots of equations (7.38) and (7.40) can easily be found using MATLAB, for example. The real-μ computation can be summarized as follows:

Step 1: Solve (7.38) for $\tilde{r}_t$, then obtain c_0 and r_0 by substituting $r = \tilde{r}_t$ into (7.23) and (7.24).
Step 2: If $\tilde{r}_t \geq |\Re e(c_0)|$, then $\mu_{\tilde{\Delta}}(M) = \tilde{r}_t^{-1}$, stop; otherwise, do Step 3.
Step 3: Solve (7.40) for $\tilde{r}_m$, then $\mu_{\tilde{\Delta}}(M) = \tilde{r}_m^{-1}$, stop.

The above algorithm has been coded into a Matlab m-file in which some additional routines have been included to avoid the extra roots resulting from the squaring process in equations (7.38) and (7.40).

7.5 A Simulation Example

This simulation example is given to illustrate the application of $\mu - K$ iteration in the design of a μ-optimal controller for a plant with real parameter uncertainty. The control system shown in Figure 7.9 is the same as Example 5.5-1, except that the modelling uncertainty Δ is real. It is a $SISO$ plant with an additive perturbation $\Delta \in \mathcal{R}$ and fictitious performance uncertainty $\Delta_p \in \mathcal{C}$. The nominal plant and weighting functions are

$$\begin{aligned} G_0(s) &= \frac{0.5(1-s)}{(s+2)(s+0.5)} \\ W_1(s) &= 50\frac{1+\frac{s}{1.245}}{1+\frac{s}{0.007}} \\ W_2(s) &= 0.1256\frac{1+\frac{s}{0.502}}{1+\frac{s}{2}} \end{aligned}$$

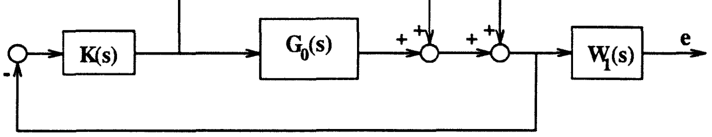

Figure 7.9: System with additive real parameter uncertainty.

The simulation results are shown in Figures 7.10 through 7.14. 3 iterations were required to find the "optimal" complex-μ controller and 8 iterations were required to find the "optimal" real-μ controller. By "optimal" we mean a reasonably flat μ. Figure 7.10 illustrates the characteristics of the optimal controllers: $\mathcal{H}^\infty$, complex-μ and real-μ. Note that real-μ is less than complex-μ. The curves of $\bar{\sigma}(M)$, $\mu_{\mathcal{C}}(M)$ and $\mu_{\mathcal{R}}(M)$ for $\mathcal{H}^\infty$, complex-μ and real-μ optimal controllers are shown in Figures 7.11, 7.12 and 7.13, respectively. Bode plots for the compensated open-loop transfer functions and the weightings for complex-μ and real-μ optimal controllers are also shown in Figure 7.14. Figure 7.15 illustrates the real-μ optimal controller characteristics: before and after model reduction of the optimal controller. The μ-optimal controller after balanced model reduction is

$$K(s) = 1.844\frac{(s+0.498)(s+2.057)}{(s+0.007)(s+2.639)} \tag{7.41}$$

It is interesting to note that the controller $K(s)$ is a cascade combination of a phase lead and a phase lag network, it is stable and has only 2 states compared with 2 for the nominal plant $G_0(s)$. The curves $\bar{\sigma}(M)$ and $\mu_{\mathcal{R}}(M)$, before and after the reduction of the controller, are shown in Figure 7.15, and illustrate little change in using the reduced order controller.

7.6 Discussion

It is natural for a plant model to suffer from real parametric uncertainty at low frequencies. On the other hand, complex uncertainty is typically present at high frequencies because of unmodelled dynamics. However, in robust control it frequently happens that real parametric uncertainty is modelled as a norm bounded complex perturbation. This chapter has illustrated the conservatism that can be introduced by this practice. The chapter has also shown how $\mu - K$ iteration can be used to design a μ-optimal controller for the case of real modelling uncertainty mixed with a complex fictitious perturbation representing uncertainty. Doyle's $D - K$ iteration fails in this case because $\mu_{\hat{\Delta}}(M)$ cannot be expressed as a linear fractional transformation of the controller $K(s)$.

The simulation results in Figure 7.12 show that $\mu_{\mathcal{R}}(M)$ coincides with $\mu_{\mathcal{C}}(M)$ in both low and high frequency ranges. Geometrically this corresponds to the case that both circles C_m and C_p are tangent to each other with the tangent point just on the real-axis. However, $\mu_{\mathcal{R}}(M)$ and $\mu_{\mathcal{C}}(M)$ are quite different in the intermediate frequencies. The complex-μ optimal controller therefore gives a more conservative design.

We have shown that the circle-invariant property of a bilinear mapping is useful in determining the SSV. But if the number of uncertainties increase, the situation becomes more complicated. The problem of calculating the SSV is known to be difficult and only a few papers are available on the subject. An "exact" method is given in [Ack85] but this is simply a brute force global search over a grid of parameter values. It involves an exponential growth in computation time as a function of the number of parameters, and taking fewer grid points to avoid this results in loss of exactness. Gaston and Safonov presented a method [DeS88] to reduce the computational burden using the mapping of $\det(I - kM\Delta)$ from a hypercube of Δ to the complex plane with k as a parameter. The minimum value of k such that $\det(I - kM\Delta) = 0$ was defined as the stability margin which is the inverse of $\mu_{\hat{\Delta}}(M)$. In 1991 Fan et al. presented a paper [FTD91] to calculate μ in the presence of mixed parametric uncertainty and unmodelled dynamics. It is computationally attractive, but potentially inexact. The main idea is to get upper and lower bounds using local search methods which are computationally inexpensive, but it may fail to find the global solution.

It is interesting to note that whatever kinds of uncertainties are present in the system, if a computational method for calculating $\mu_{\hat{\Delta}}(M)$ is available for a given controller, then $\mu - K$ iteration will be applicable for designing a μ-optimal controller. Therefore $\mu - K$ iteration is potentially useful for practical control system design.

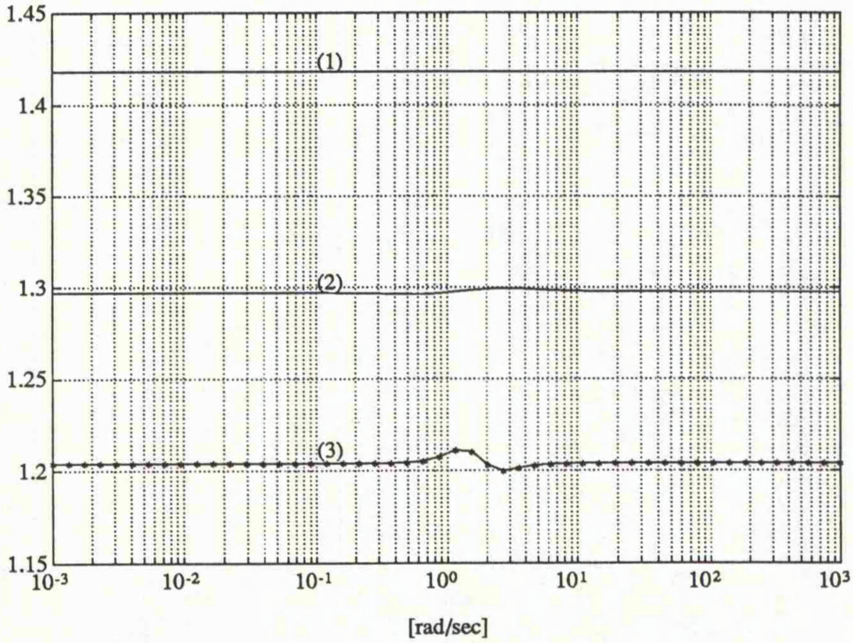

Figure 7.10: Characteristics of the optimal controllers:

(1): $\bar{\sigma}(M)$ for $\mathcal{H}^\infty$ optimal controller; (2): $\mu_{\mathcal{C}}(M)$ for the complex-μ optimal controller; and (3): $\mu_{\mathcal{R}}(M)$ for the real-μ optimal controller.

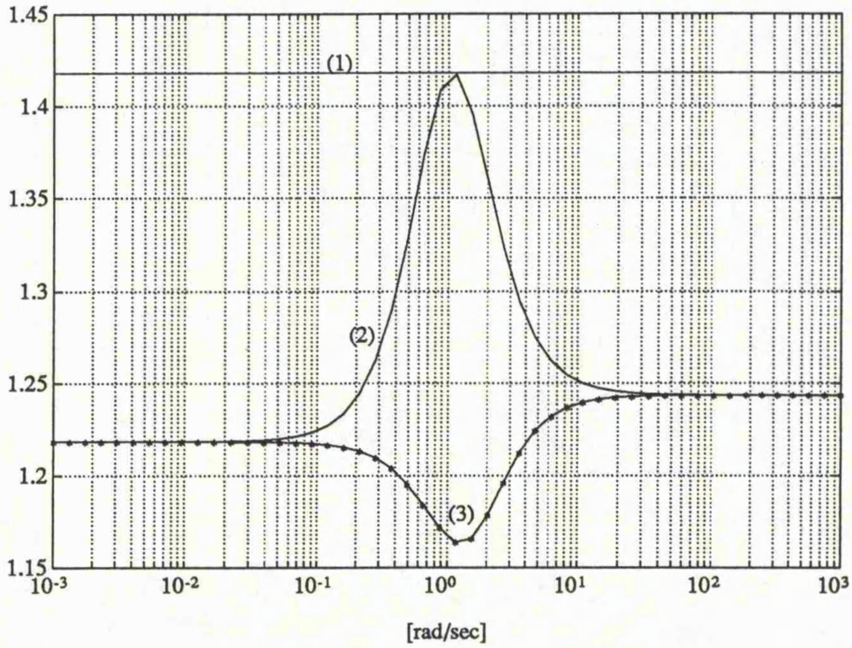

Figure 7.11: $\mathcal{H}^\infty$ optimal controller characteristics:

(1) $\bar{\sigma}(M)$; (2) $\mu_{\mathcal{C}}(M)$; and (3) $\mu_{\mathcal{R}}(M)$.

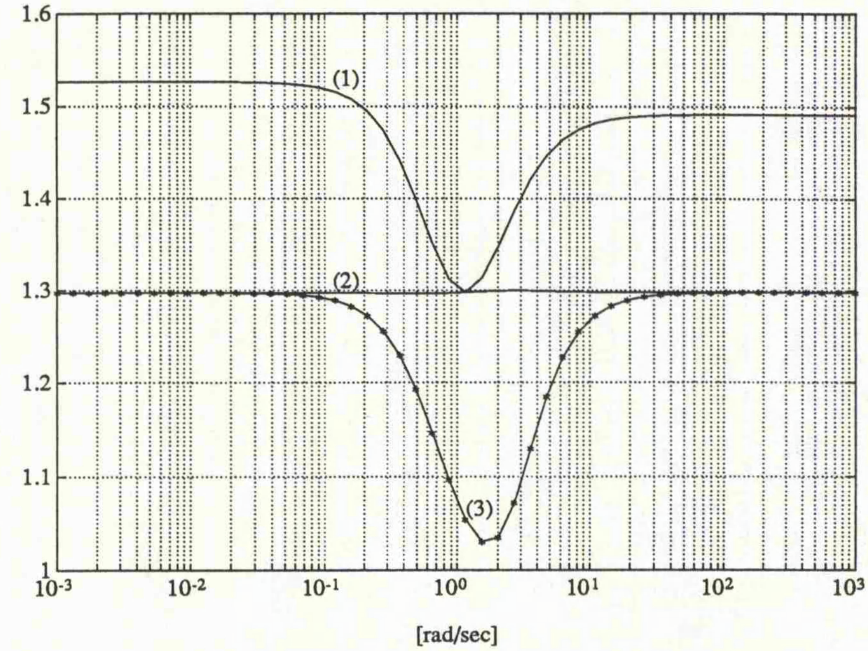

Figure 7.12: Complex-μ optimal controller characteristics:
(1) $\bar{\sigma}(M)$; (2) $\mu_{\mathcal{C}}(M)$; and (3) $\mu_{\mathcal{R}}(M)$.

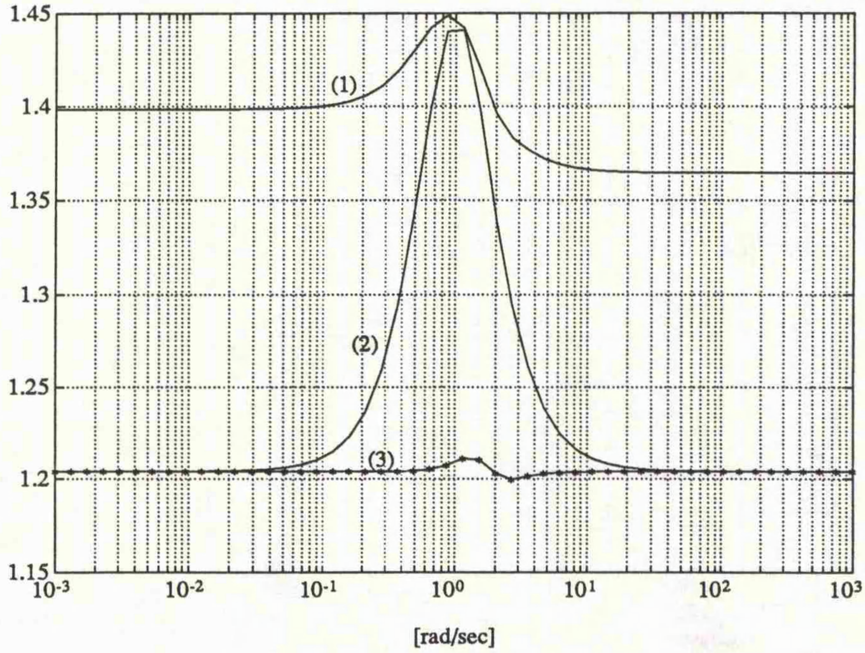

Figure 7.13: Real-μ optimal controller characteristics:
(1) $\bar{\sigma}(M)$; (2) $\mu_{\mathcal{C}}(M)$; and (3) $\mu_{\mathcal{R}}(M)$.

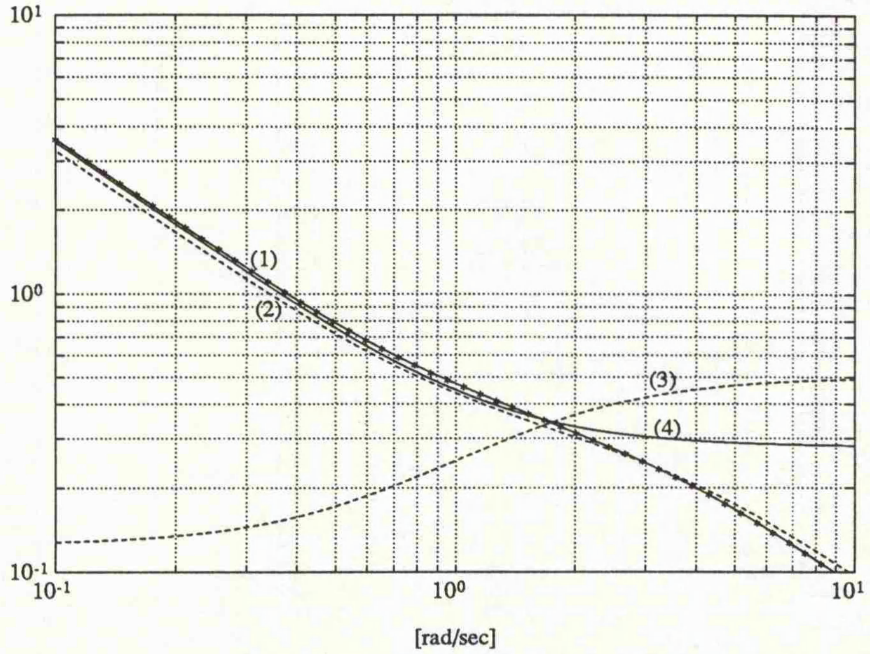

Figure 7.14: Bode-plots for the compensated open-loop transfer functions and the weightings: (1) $|l_{\mathcal{R}}(j\omega)|$; (2) $|l_{\mathcal{C}}(j\omega)|$; (3) $|W_2(j\omega)|$, and (4) $|W_1(j\omega)|$.

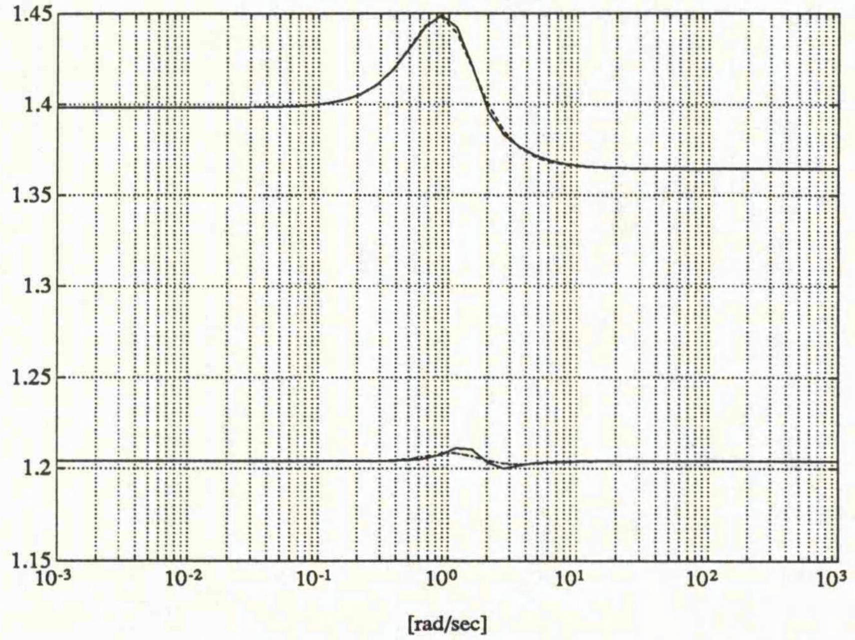

Figure 7.15: Real μ optimal controller characteristics, $\bar{\sigma}(M)$ and $\mu_{\mathcal{R}}(M)$.
upper curves: $\bar{\sigma}(M)$; lower curves: $\mu_{\mathcal{R}}(M)$;
solid lines: before reduction; dashed lines: after reduction.

Chapter 8

CONCLUSIONS AND FURTHER WORK

8.1 Summary

This thesis has studied the robust stability and robust performance ($RSRP$) problem which is central to control system design. A new design algorithm for the $RSRP$ problem has been presented for multivariable feedback control systems in Chapter 5. We have confined ourselves to the treatment of finite dimensional linear time-invariant models with modelling uncertainties because these are the most commonly used models in practical design. It is argued that the $\mu - K$ iteration algorithm can be used to design μ-optimal controllers for the $RSRP$ problem when the plant has real and/or complex modelling uncertainties. The idea is motivated from an engineering point of view and takes advantage of $\mathcal{H}^\infty$-optimization. $\mu - K$ iteration is therefore seen as a potentially useful tool for practical control system design.

A loop shaping approach to robust performance design for $SISO$ systems was also presented in Chapter 4. Although it is not easy to extend this approach to multivariable systems, it reveals an interesting and useful relationship between a mixed sensitivity $\mathcal{H}^\infty$-optimization problem and classical loop shaping. The insight provided by this relationship led to the development of the loop shaping approach for minimizing the structured singular value for robust performance.

In Chapter 6, an ill-conditioned 2-input 2-output high purity distillation column was analyzed. The plant has a large value of condition number which implies that the gain of the system has strong directionality as well as frequency dependence, and is detrimental to robust stability and robust performance. Although the large condition number causes controller design problems, it does have a nice "separation property": robust performance depends only on the low plant gain in the low frequencies and robust stability depends only on the high plant gain in the high frequencies. A μ-synthesis design is carried out for the distillation column using $\mu - K$ iteration algorithm, and comparisons are made with results in [SMD88] and [Fre89b].

In Chapter 7, based on the circle-invariant property of a linear fractional transformation, a geometric approach for calculating the real and/or complex structured singular value was proposed. This is useful because the method of $\mu - K$ iteration is strongly dependent on the precision of the μ-computation.

8.2 Recommendations for Further Work

Suggestions for further research include:

(1) The loop shaping approach to robust performance is particularly useful for $SISO$ systems. The extension of this approach to $MIMO$ systems needs to be investigated.

(2) The optimization problem given in Section 4.2 is to find a stabilizing controller $K(s)$ which satisfies

$$\inf_{K(s)} \sup_{\omega \in \mathcal{R}} \left\{ |r_1(j\omega)s(j\omega)| + |r_2(j\omega)t(j\omega)| \right\}$$

This problem does not yet have an analytical solution.

(3) As in Doyle's $D - K$ iteration algorithm, there is no *a priori* guarantee that the $\mu - K$ iteration algorithm will converge to a global minimum. The

modification of $\mu - K$ iteration to obtain a globally optimal controller is an important area of study.

(4) The high purity distillation column design example presented in this thesis, and previously discussed by Skogestad et al. [SMD88] and Freudenberg [Fre89b] is not very practical because no amplitude and bandwidth constraints are placed on the controller. The choice of weighting function to improve the bandwidth of the control energy is not obvious. The relationship between the μ-curve and this bandwidth is critical to the synthesis problem and deserves more study. A more detailed performance specification for this example was given at the 1991 IEEE Conference on Decision and Control, Brighton and could form the basis of further study.

(5) The geometric approach presented in Chapter 7 is useful for computing the structured singular value with respect to real and/or complex uncertainties. The question remaining is, to what extent, the geometric approach used here can be extended if the number of uncertainties increases.

Bibliography

[Ack85] Ackermann, J., *Sampled-Data Control Systems*, London: Springer-Verlag, 1985.

[AmH58] Amir-Móez, A.R. and A. Horn, "Singular value of a matrix," *Amer. Math. Monthly*, pp. 742-748, Dec. 1958.

[ÅNG86] Åström, K.J., L. Neumann and P.O. Gutman, "A comparison of robust and adaptive control," *Contr. and Signal Processing*, Lund, Sweden, 1986.

[BaD89] Balas, G.J. and J.C. Doyle, "Identification of a flexible structure for use in μ-synthesis control design," Submitted for publication in *AIAA Journal of Guidance, Control and Dynamics*, May, 1989.

[Bar66] Bartle, R.G., *The Elements of Real Analysis*, New York: John Wiley & Sons, 1966.

[BCD89] Balas, G.J., C.C. Chu and J.C. Doyle, "Vibration damping and robust control of the JPL/AFAL experiment using μ-synthesis," *In Proc. 28th IEEE Conf. on Decision and Control*, Tampa, Florida, pp. 2689-2694, 1989.

[BDGPS91] Balas, G.J., J.C. Doyle, K. Glover, A. Packard and R. Smith, *μ-Analysis and Synthesis Toolbox*, by MUSYN Inc. and the MathWorks, Inc., 1991.

[Cam90] Cambridge Control, *Lecture Notes for μ and $\mathcal{H}_\infty$: A short course*, Cambridge University Engineering Department and Delft University of Technology, 1990.

[CaD91] Callier, F.M. and C.A. Desoer, *Linear System Theory*, New York: Springer-Verlag, 1991.

[ChD82] Chen, M.J. and C.A. Desoer, "Necessary and sufficient condition for robust stability of linear distributed feedback systems," *Int. J. Control*, vol. 35, No. 2, pp. 255-267, 1982.

[Che84] Chen, C.T., *Linear System Theory and Design*, New York: Holt, Rinehart & Winston, 1984.

[Dai90] Dailey, R.L., "A new algorithm for the real structured singular value," *American Control Conference*, San Diego, California, pp. 3036-3040, 1990.

[DeS88] de Gaston, R.R.E. and M.G. Safonov, "Exact Calculation of the multiloop stability margin," *IEEE Trans. Auto. Control*, AC-33, No. 2, pp. 156-171, 1988.

[DeV75] Desoer, C.A. and M. Vidyasagar, *Feedback Systems: Input-Output Properties*, New York: Academic Press, 1975.

[DFT92] Doyle, J.C., B.A. Francis and A.R. Tannenbaum, *Feedback Control Theory*, New York: Macmillan, 1992.

[DKL86] Daniel, R.W., B. Kouvaritakis and H. Latchman, "Principal direction alignment: a geometric framework for the complete solution to the μ-problem," *IEE Proc., Part D*, vol. 133, No. 2, pp. 45-56, 1986.

[DLP87] Doyle, J.C., K. Lenz and A. Packard, "Design example using μ-synthesis: space shuttle lateral axis FCS during re-entry," *NATO ASI Series, v. F34: Modelling, Robustness and Sensitivity Reduction in Control Systems*, edited by Ruth Curtain, pp. 126-154, 1987.

[Doy82] Doyle, J.C., "Analysis of control systems with structured uncertainties," *IEE Proc., Part D*, vol. 129, pp. 242-250, 1982.

[Doy84] Doyle, J.C., *Lecture Notes for ONR/Honeywell workshop on advances in multivariable control*, Minneapolis, Minnesota, 1984.

[Doy85] Doyle, J.C., "Structured uncertainty in control system design," *In Proc. 24th IEEE Conf. on Decision and Control*, Ft. Lauderdale, pp. 260-265, 1985.

[Doy87] Doyle, J.C., "A review of μ for case studies in robust control," *IFAC 10th World Congress on Automatic Control*, Munich, vol. 8, pp. 395-402, 1987.

[DWS82] Doyle, J.C., J.E. Wall and G. Stein, "Performance and robustness analysis for structured uncertainty," *In Proc. IEEE Conf. on Decision and Control*, Orlando FL, pp. 629-636, 1982.

[Enn87] Enns, D.F., "Multivariable flight control for an attack helicopter," *IEEE Control System Magazine*, pp. 34-38, 1987.

[FaT88] Fan, M.K.H. and A.L. Tits, "M-form numerical range and the computation of the structured singular value," *IEEE Trans. Auto. Control*, AC-33, pp. 284-289, 1988.

[Foo85] Foo, Y.K., "Robustness of multivariable feedback systems: analysis and optimal design," Report No. OUEL 1601/85, Oxford University, 1985.

[FoP88] Foo, Y.K. and I. Postlethwaite, "Extensions of the small-μ test for robust stability," *IEEE Trans. Auto. Control*, AC-33, No. 2, pp. 172-176, 1988.

[Fra87] Francis, B.A., *A course in $\mathcal{H}_\infty$ Control Theory*, Lecture Notes in Control and Information Sciences, vol. 88. Berlin: Springer-Verlag, 1987.

[Fre89a] Freudenberg, J.S., "Analysis and design for ill-conditioned plants: Part 1. Lower bounds on the structured singular value," *Int. J. Control*, vol. 49, No. 3, pp. 851-871, 1989.

[Fre89b] Freudenberg, J.S., "Analysis and design for ill-conditioned plants: Part 2. Directionally uniform weightings and an example," *Int. J. Control*, vol. 49, No. 3, pp. 873-903, 1989.

[Fre90] Freudenberg, J.S., "Plant directionality, coupling and multivariable loop-shaping," *Int. J. Control*, vol. 51, No. 2, pp. 365-390, 1990.

[FrL87] Freudenberg, J.S. and D.P. Looze, *Frequency Domain Properties of Scalar and Multivariable Feedback Systems*, Berlin: Springer-Verlag, 1987.

[FTD91] Fan, M.K.H., A.L. Tits and J.C. Doyle, "Robustness in the presence of mixed parametric uncertainty and unmodelled dynamics," *IEEE Trans. Auto. Control*, AC-36, No. 1, pp. 25-38, 1991.

[Gan59] Gantmacher, F.R., *The Theory of Matrices*, vol.1 and vol.2, New York: Chelsea, 1959.

[Hel85] Helton, J.W., "Worst case analysis in the frequency domain: the H^∞ approach to control," *IEEE Trans. Auto. Control*, AC-30, No. 12, pp. 1154-1170, 1985.

[Hel88] Helton, J.W., "A numerical method for computing the structured singular value," *System and Control Letters*, vol. 10, pp. 21-26, 1988.

[HHL91] Hoyle, D.J., R.A. Hyde and D.J.N. Limebeer, "An $\mathcal{H}_\infty$ approach to two degree of freedom design," *In Proc. 30th IEEE Conf. on Decision and Control*, Brighton, England, pp. 1581-1585, 1991.

[Kai80] Kailath, T., *Linear Systems*, Englewood Cliffs NJ: Prentice-Hall, 1980.

[Kre78] Kreyszig, E., *Introductory Functional Analysis with Applications*, New York: John, Wiley & Sons, 1978.

[LaT85] Lancester, P. and M. Tismenetsky, *The Theory of Matrices with Applications*, 2nd Ed., New York: Academic Press, 1985.

[Lim91] Limebeer, D.J.N., "The specification and purpose of a controller design case study," *In Proc. 30th IEEE Conf. on Decision and Control*, Brighton, England, pp. 1579-1580, 1991.

[LPG91] Lin, J.-L., I. Postlethwaite and D.-W. Gu, "$\mu - K$ iteration: A new algorithm for μ-synthesis," Accepted for publication in *Automatica Special Issue on Robust Control*, Report 91-14 June 1991, Engineering Dept., Leicester Uni., 1991.

[Lun84] Lunz, J., "Robustness tests for feedback control systems using multidimensional uncertainty bounds," *System & Control Letter*, vol. 4, pp. 85-89, 1984.

[Lun89] Lunz, J., *Robust Multivariable Feedback Control*, London: Prentice Hall, 1989.

[Mac89] Maciejowski, J.M., *Multivariable Feedback Design*, England: Addison-Wesley, 1989.

[MAVS88] Milich, D.A., M. Athans, L. Valavani and G. Stein, "A method for designing robust multivariable feedback systems," *Proceedings of the 27th Conference on Decision and Control*, Austin, Texas, pp. 2150-2156, 1988.

[McG90] McFarlane, D. and K. Glover, *Robust Controller Design using Normalized Coprime Factor Plant Descriptions*, Lecture notes in Control and Information Sciences series, Springer-Verlag, 1990.

[MoZ89] Morari, M. and E. Zafiriou, *Robust Process Control*, London: Prentice-Hall, 1989.

[OHÅP88] O'Young, S.D., J. Hope, K.J. Åström and I. Postlethwaite, "A comparative study and performance assessment on H^∞ control designs," Oxford University, internal report, 1988.

[OPG89] O'Young, S.D., I. Postlethwaite and D.W. Gu, "A treatment of model matching zero in the optimal H^2 and H^∞ control design," *IEEE Trans. Auto. Control*, AC-34, No.5, pp. 551-553, 1989.

[OrL91] O'Reilly, J. and W.E. Leithead, "Multivariable control by 'individual channel design'," *Int. J. Control*, vol. 54, No. 1, pp. 1-46, 1991.

[Osb60] Osborne, E.E., "On pre-conditioning of matrices," *Journal of the ACM*, vol. 7, pp. 338-345, 1960.

[Pac88] Packard, A.K., *What's new with μ: structured uncertainty in multivariable control*, Ph.D. Thesis, UC Berkeley, 1988.

[PaD88] Packard, A.K. and J.C. Doyle, "Structured singular value with repeated scalar blocks," *Proc. ACC*, Atlanta, GA,, pp. 1213-1218, 1988.

[PFD88] Packard, A.K., M.K.H. Fan and J.C. Doyle, "A power method for the structured singular value," *Conf. on Decision and Control*, Austin, Texas, pp. 2132-3137, 1988.

[PLG91a] Postlethwaite, I., J.-L. Lin and D.-W. Gu, "A loop-shaping approach to robust performance for SISO systems," *Trans. Inst. MC.*, vol. 13, No. 5, pp. 262-268, 1991.

[PLG91b] Postlethwaite, I., J.-L. Lin and D.-W. Gu, "Robust control of a high purity distillation column using $\mu - K$ iteration," *In Proc. 30th IEEE Conf. on Decision and Control*, Brighton, England, pp. 1586-1590, 1991.

[PoF85] Postlethwaite, I. and Y.K. Foo, "Robustness with simultaneous pole and zero movement across the $j\omega$-axis," *Automatica*, vol. 21, No. 4, pp. 433-443, 1985.

[Pos88] Postlethwaite, I., "Application of H^∞ design," *SERC vacation school on self-tuning and robust control design*, Oxford, 1988.

[Red50] Redheffer, R.M., "Remarks on the basis of network theory," *J. Math. Phys.* , 28, pp. 237-258, 1950.

[Red60] Redheffer, R.M., "On a certain linear fractional transformation," *Journal of MATHS. and physics*, pp. 269-286, 1960.

[Saf82] Safonov, M.G., "Stability margins of diagonally perturbed multivariable feedback systems," *IEE Proc., Part D*, pp. 251-256, 1982.

[SeO90] Sezginer, R.S. and M.L. Overton, "The largest singular value of $e^X A_0 e^{-X}$ is convex on convex sets of commuting matrices," *IEEE Trans. Auto. Control*, AC-35, No. 2, pp. 229-230, 1990.

[SkM86] Skogestad, S. and M. Morari, "Control of ill-conditioned plants: high purity distillation," *AIChE Annual Meeting*, Miami Beach, Florida, November 1986.

[SkM88] Skogestad, S. and M. Morari, "Some new properties of the structured singular value," *IEEE Trans. Auto. Control*, AC-33, No.12, pp. 1151-1154, 1988.

[SMD88] Skogestad, S., M. Morari and J.C. Doyle, "Robust control of ill-conditioned plants: high purity distillation," *IEEE Trans. Auto. Control*, AC-33, No.12, pp. 1092-1105, 1988.

[STBS90] Steinbuch, M., J.C. Terlouw, O.H. Bosgra and S.G. Smit, "Multivariable application of μ-synthesis to servo system design in the consumer electronics industry," *IEE, Computing and Control Division Colloquium*, London, pp. 8/1-8/3, 1990.

[StD85] Stein, G. and J.C. Doyle, "Beyond singular values and loop shapes," *Notes ONR/Honeywell workshop, report No. LIDS-P-1504*, MIT, Cambridge, Massachusetts, 1985.

[StD88] Stein, G. and J.C. Doyle, "Beyond singular values and loop shapes," *AIAA Journal of Guidance, Control and Dynamics*, 1988.

[Ste73] Stewart, G.W., *Introduction to Matrix Computations*, New York: Academic Press, 1973.

[Ste85] Stein, G., "Beyond singular values and loop shapes," *24th Conf. on Decision and Control*, Ft. Lauderdale, FL., 1985.

[Ste89] Steinbuch, M., *Dynamic Modelling and Robust Control of a Wind Energy Conversion System*, Dissertation, Delft University of Technology, 1989.

[StT83] Stewart, I. and D. Tall, *Complex Analysis*, Cambridge: Cambridge University Press, 1983.

[Vid85] Vidyasagar, M., *Control System Synthesis: A Factorization Approach*, Boston MA: MIT Press, 1985.

[YaH91] Yaniv, O. and I. Horowitz, "Ill conditioned plants: a case study," *In Proc. 30th IEEE Conf. on Decision and Control*, Brighton, England, pp. 1596-1600, 1991.

[YJB76] Youla, D.C., H.A. Jabr and J.J. Bongiorno, "Modern Wiener-Hopf design of optimal controllers, part II: The multivariable case," *IEEE Trans. Auto. Control*, AC-21, pp. 319-338, 1976.

[ZhK91] Zhou, T. and H. Kimura, "Controller design of an ill-conditioned plant using robust stability degree assignment," *In Proc. 30th IEEE Conf. on Decision and Control*, Brighton, England, pp. 1591-1595, 1991.